UNIVERSITY OF BIRMINGHAM

DESIGN AND EVALUATION OF DEVICES FOR

THE TREATMENT OF INTERVERTEBRAL DISC DISORDERS

by

ALICJA JOANNA KUBIAK

A thesis submitted to

The University of Birmingham

For the degree of

DOCTOR OF PHILOSOPHY

School of Engineering

Department of Mechanical Engineering

University of Birmingham

April 2018

UNIVERSITYOF
BIRMINGHAM

University of Birmingham Research Archive

e-theses repository

Abstract

The aim of this thesis was to design and evaluate implants used in the treatment of intervertebral disc disorders.

For this purpose, a new cervical PEEK-on-PEEK disc device, combining a ball-on-socket mechanism with an elastomeric core, was designed. To find a material for the core, quasi-static compression tests were performed; on the basis of which an elastomer MED 4780 was selected for further testing. Finite element analysis (FEA) was used to investigate the maximum stresses in the device during static compression. The results showed that maximum stresses did not exceed PEEK's compressive or fatigue strength.

The evaluation and comparison of the mechanical properties of pedicle screws (cylindrical and dual-core), used as an integral part of the posterior lumbar stabilisation system, was also performed. The screws were tested in axial pullout, quasi-static and dynamic bending, as well as subjected to the static bending, using FEA. The results of the pullout tests, performed using three polyurethane foams (0.16, 0.32 and 0.64 g/cm^3) showed no significant difference between pullout strength values. However, dual-core screws had significantly higher bending strength and a longer fatigue life. The FEA showed lower stress values for the dual-core screw. Furthermore, a critical assessment of explanted screws has shown that fatigue bending was the main cause of failure *in vivo*.

Acknowledgements

Table of Contents

List of Figures

List of Tables

Acronyms

ACDF……………………………………………….anterior cervical discectomy and fusion

AF…………………………………………………………………………...annulus fibrosus

ASD……………………………………………………………..adjacent segment disease

ASTM…………………………………………….…American society for testing materials

BFus 2……………………………………………………….…..cylindrical pedicle screw

BFus 2+………………………………………………………...dual-core pedicle screw

CDA……………………………………………………………….cervical disc arthroplasty

CDR………………………………………………………….cervical disc replacement

CDyn………………………………………………...….cervical dynamic disc device

CE…………………………………………………………...European conformity

COR…………………………………………………………………...centre of rotation

CT…………………………………………………………….computed tomography

El$_e$…………………………………………………………….structural stiffness

FDA……………………………………………………...food and drugs administration

FE……………………………………………………………...…….finite element

FEA……………………………………………………………...finite element analysis

FMEA…………………………………………………...…….failure mode and effect analysis

FOA……………………………………………………………………..flank overlap area

FSU…………………………………………………………………….functional spinal unit

I…………………………………………………………………….area moment of inertia

ID………………………………………………………………………...inner diameter

IVD……………………………………………………………...intervertebral disc

MA…………………………………………………………………………...monoaxial

MRI………………………………………………………….magnetic resonance imaging

NP……………………………………………………………………...nucleus pulposus

OM……………………………………………………………………….optical microscope

PA………………………………………………………………………….......polyaxial

PCU…………………………………………………………………….polycarbonate urethane

PDS………………………………………………………………….posterior dynamic stabilisation

PE…………………………………………………………………………….polyethylene

PEEK…………………………………………………………………polyether-ether-ketone

PG……………………………………………………………………..proteoglycans

PS…………………………………………………………………...pedicle screws

PU……………………………………………………………………polyurethane

ROM…………………………………………………………….....range of motion

RP1…………………………………………………………rapid prototype 1

RP2…………………………………………………………rapid prototype 2

S…………………………………………………………………….shape factor

SD……………………………………………………………....standard deviation

TDA…………………………………………………………total disc arthroplasty

TDR…………………………………………………………total disc replacement

TRIZ…………………………………………………... theory of inventive problem solving

UHMWPE……………………………………………...ultra-high molecular weight polyethylene

Z……………………………………………………………………. section modulus

1   Introduction

Intervertebral disc degeneration is the main source of neck and lower back pain and in the case of severe degeneration and herniation, surgical intervention is inevitable (Williams and Sambrook, 2011; Todd, 2011). For many years spinal fusion was the gold standard, however, it can alter the biomechanics of the spine and more specifically the load transfer patterns of both treated and adjacent spinal segments and may lead to symptomatic adjacent segment disease (ASD) (Kurtz, 2006; Grupp et al., 2010). Therefore, new motion-preservation technologies have been developed including artificial disc replacement devices and pedicle-screw-based posterior dynamic stabilisation systems.

There are currently many different designs of cervical disc replacements (CDR) available on the market, either based on the ball-on-socket mechanism or a compliant elastomer cushion. However, most of the devices either do not fully mimic the functionality of the natural disc exposing the treated segment to further degeneration, or can experience complications associated with the material used as well as subsidence and device migration (Skeppholm et al., 2015; Hallab, 2014; Vicars et al., 2011; Kurtz et al., 2006; Wagner et al., 2016). Therefore, a new design solution is needed to surpass these limitations and better mimic the functionality of a natural disc.

Pedicle-screw-based posterior stabilisation systems are mostly used to treat the lumbar spine, with limitations associated with the pedicle screws including screw breakage and loosening/pullout. Many different designs of pedicle screws have been proposed in order to surpass these shortcomings.

The aims of this thesis were to design and evaluate implants used in the treatment of the intervertebral disc disorders. For this purpose, a new dynamic solution for the device to replace the degenerated intervertebral disc in the cervical spine was proposed.

This thesis has also described an assessment and comparison of mechanical properties of two pedicle screw designs, which are part of a posterior lumbar stabilisation system. The specific objectives of this thesis were to:

- Develop new dynamic design of cervical disc replacement device.

- Analyse the new disc design using the finite element method.

- Perform mechanical tests in order to evaluate and compare mechanical properties of different pedicle screw designs.

- Analyse both screw designs using the finite element method.

- Critically analyse failed, explanted pedicle screws in order to determine the likely causes of failure and to refer them to the results obtained during mechanical testing.

Chapter 2 outlines the relevant background information needed in order to understand each individual chapter in this thesis. The chapter begins with a description of the spinal anatomy, including the intervertebral disc. It continues by describing disc ageing and degeneration phenomenon as well as the general treatments. The chapter introduces cervical disc arthroplasty (CDA), followed by a description of the design characteristics and reasons for the failure of CDAs as well as examples of the available cervical disc devices. The second part of this chapter contains information concerning pedicle screws. It focuses on pedicle screw characteristics, types and reasons for failure.

Chapter 3 describes the design process, prototyping and finite element analysis (FEA) of a novel PEEK-on-PEEK dynamic cervical disc implant (CDyn). The evolution of the device concept and final design is presented and discussed. This chapter also outlines the quasi-static compression tests of the potential compliant materials for use as a deformable core.

Chapter 4 presents mechanical tests, finite element analysis and visual assessment of two pedicle screw designs with different geometries. Also included in this chapter is a critical assessment of failed, explanted screws carried out to identify the reasons for failure and refer them to the results obtained during mechanical testing.

Chapter 5 provides the overall discussion and conclusions of the study undertaken in this thesis and outlines potential areas of the future investigations concerning the CDyn device.

Appendix A contains engineering drawings of the individual elements of the CDyn implant.

2   Background

Chapter Overview

The purpose of this chapter is to provide the background information necessary to understand the following chapters in this thesis. Section 2.1 describes the relevant anatomy of the spine and its elements such as vertebrae and the intervertebral disc. The nature of intervertebral disc ageing and degeneration and its consequences are presented in section 2.2. Section 2.3 describes general methods used to treat the degenerated disc. Total cervical disc arthroplasty along with the potential problems that can affect implants and examples of available devices are presented in section 2.4. Information regarding characteristics, types and complications associated with pedicle screws are presented in section 2.5. Finally, the chapter summary can be found in section 2.6.

2.1   Spine Anatomy and Biomechanics

2.1.1   Regions of the Spine

The spine is a flexible column that is divided into five regions, starting from the head: 7 cervical vertebrae (C1-C7), 12 thoracic vertebrae (T1-T12), 5 lumbar vertebrae (L1-L5), 5 fused sacral vertebrae (S1-S5) and 3 to 4 coccygeal vertebrae.

The main role of the spinal column is to maintain stability and an upright position as well as providing mobility at the segmental level and protecting the spinal cord and cauda equina (lower back). Looking at the spine from the front, it is straight and symmetrical; however, in the sagittal (side) plane, the main spinal regions create special curvatures. The cervical and lumbar levels are characterized by an anteriorly convex curve (lordosis), while the thoracic and sacral regions are characterized by a posteriorly convex curve (kyphosis) (Figure 2.1).

This S-shaped curvature gives increased flexibility to the spine and allows for load bearing and shock absorption.
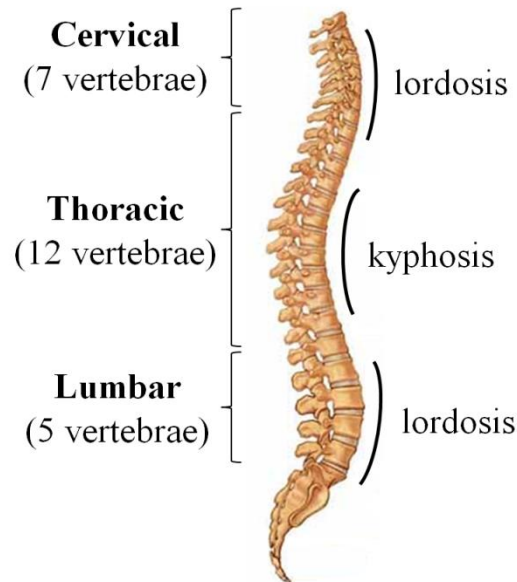
Figure 2.1 - Main segments and curves of the spine

(Adapted from www.spineuniverse.com/anatomy).

The cervical region supports the head and is characterized by the highest flexibility and range of motion. The thoracic segment is the longest part of the spine, however, each vertebra is connected to the rib, making this part the least mobile. The lumbar segment contains the largest and strongest vertebral bodies as it has to withstand the highest loads and moments of the spine. For comparison, in the case of the cervical spine, the weight of the body segment carried above is only 1/9th of the load carried by the lumbar spine. For example, in a cervical region for a 70 kg person, the load amounts to approximately 50 N, whereas in the lumbar region the load is 450 N (Panjabi et al., 1998).

2.1.2   Spinal Motion

Figure 2.2 presents the main motions of the spine. Flexion and extension is when a body bends forward (anteriorly) or backward (posteriorly), respectively.

5

Bending sideways is known as lateral bending whereas axial torsion (axial rotation) is when a body rotates along its longitudinal axis. The axial displacement of the spine due to tensile load or muscle forces is called traction (Kurtz and Edidin, 2006).
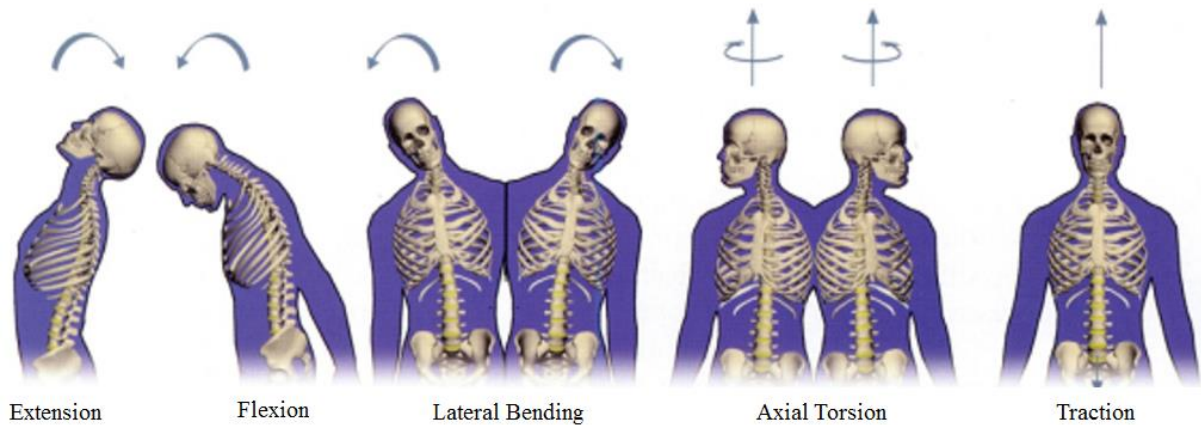
Figure 2.2 - Main spinal motions (Adapted from Kurtz and Edidin, 2006).

2.1.3   The Vertebra

The vertebrae, along with other structures, create the spinal column, protect the spinal cord and cauda equina and transfer load. Figure 2.3 shows a typical vertebra along with its characteristic components. Though the size and shape of the vertebrae vary with the spinal segment, each vertebra is made of two main parts: anterior vertebral body and a posterior vertebral arch. The vertebral body serves as a support and bears most of the compressive loading. It is made of a cancellous bone surrounded by a cortical shell. The posterior arch consists of pedicles, lamina, and processes (articular, transverse and spinous). The pedicles and lamina serve as the protection of the spinal cord (cervical and thoracic regions) or cauda equina (below the level of L1). Elements such as the spinous, transverse and articular processes, serve the function of motion by attaching muscles and ligaments and possessing articular facets (articular processes).
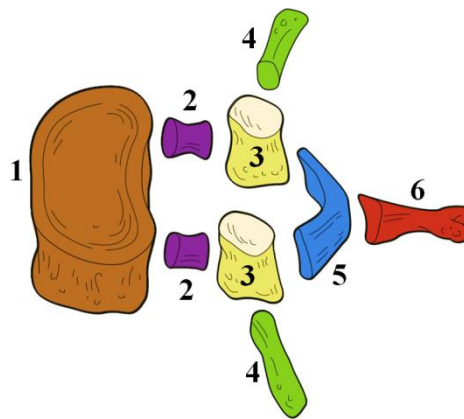
Figure 2.3 - Components of typical vertebra: 1 - The vertebral body; 2 - The pedicles; 3 - Articular processes (zygapophyses); 4 - Transverse processes; 5 - Lamina; 6 - The spinous process. (Adapted from Cramer and Darby, 2013).

2.1.4   Intervertebral Disc

Adjacent vertebrae are separated by a structure called the intervertebral disc (IVD), a sort of viscoelastic cushion, which allows for 6 degrees of freedom (Cramer and Darby, 2013). The discs are connected to the vertebrae by cartilaginous endplates. Two adjacent vertebrae along with the intervertebral disc create the functional spinal unit (FSU), the smallest physiological motion segment of the spine, which represents biomechanical characteristics similar to those of the entire spine. Though the range of motion (ROM) between two adjacent discs is minor, the collective effect of multiple vertebrae and discs results in significant flexibility to the whole skeletal column.

While the size and shape of each IVD vary with the spinal region (enlarges in a caudal direction), the structure remains consistent. Each IVD consists of two main components: annulus fibrosus (AF) and nucleus pulposus (NP) (Figure 2.4a).

The annulus fibrosus is a durable outer part of the intervertebral disc, consisting of several layers (lamellae) of highly organized fibrocartilage (Kurtz and Edidin, 2006).

7

It encapsulates the nucleus pulposus and prevents it from protruding out. The water content of the annulus fibrosus is 60-70%, the proteoglycans-content 20% dry weight and the collagen content is 50-60% dry weight (Bogduk, 2005; Smith and Fazzalari, 2009). Fibres in a given layer of the annulus are orientated parallel and run in the same direction (approximately 30° to the disc plane) but in the opposite direction in the adjacent layers (Figure 2.4b) (Cramer and Darby, 2013; White and Panjabi, 1990). Such organized, multi-layered structure of the AF is ideal for withstanding large and complex loads in multiple directions. Under compressive loading of the intervertebral disc, the inner annulus fibrosus is exposed to axial compressive stresses, and outward nucleus pulposus bulging causes radial compressive and circumferential tensile stresses in the outer annulus fibrosus (Hickey and Hukins, 1980). Therefore, the AF is the major load-bearing component of the intervertebral disc.

a)   b)
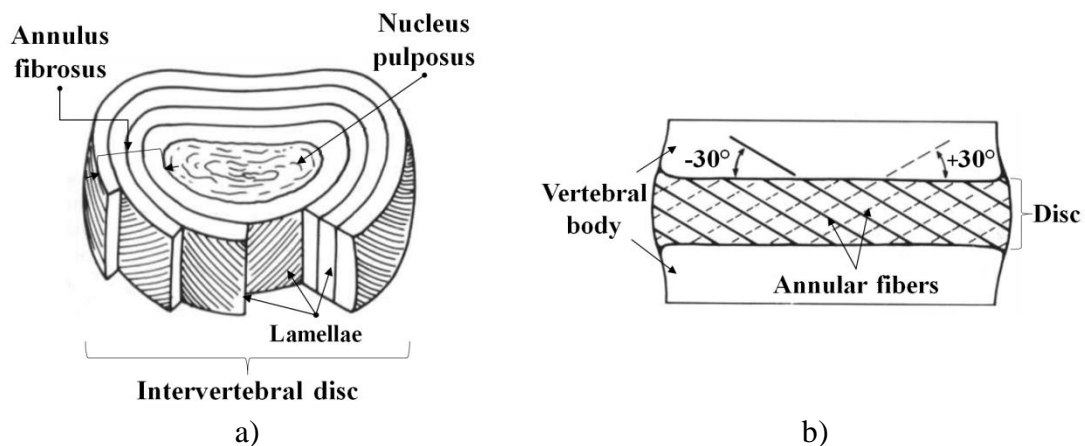
Figure 2.4 - Intervertebral disc (Adapted from White and Panjabi, 1990).

The nucleus pulposus is a central transparent, jelly-like component of the intervertebral disc. It is a viscoelastic structure and thus has properties dependant on the rate of change of load. It consists of a loose meshwork of randomly distributed collagen fibrils suspended in a mucoprotein gel, containing hydrophilic proteins called proteoglycans (PG) (Kurtz and Edidin, 2006). The PG-content is 60-65% dry weight; the collagen content is 30% dry weight

(Bogduk, 2005). The NP water content ranges between 70% and 90% and is the highest at birth and tends to decrease with age (White and Panjabi, 1990). The NP is avascular; thus it must be hydrated by absorbing water and nutrients from surrounding tissue. This is provided by cartilaginous endplates, which form a barrier between intervertebral disc and vertebrae, through which water and nutrients can easily pass through. The main function of the nucleus pulposus is translating the compressive load to a radial pressure contained by the AF. To achieve this, it uses the water-binding abilities of proteoglycans, which provide hydration and swelling pressure to the host tissue, enabling it to withstand compressional forces (Hukins et al., 1999; Yanagishita, 1993).

2.2   Disc Ageing and Degeneration

Intervertebral disc degeneration is the main cause of neck and back pain (Williams and Sambrook, 2011; Todd, 2011; Hughes et al., 2012). It is said to affect approximately 60-85% of the general population (Vicars et al., 2011). The gradual degeneration of the intervertebral disc occurs through: natural ageing processes, genetic predisposition, micro/macro traumas as a result of abnormal loading conditions and the loss of nutrition to the disc (Morishita, 2008; Stokes and Iatridis, 2004).

A healthy disc plays a very important role, as it transfers loads directly from the vertebral bodies and is responsible for the flexibility and mobility of individual spinal segments (White and Panjabi, 1990). The inner nucleus pulposus acts as a pillow filled with fluid that swells under pressure. The components of the disc interact similarly to a thick-walled pressure vessel, which enables the intervertebral disc to absorb and transfer the loads experienced by the spine (Hukins and Meakin, 2000).

However, like most biological structures, the intervertebral disc changes/loses its properties with age and through normal, daily use. The main mechanism responsible for this is the gradual loss of water-binding capacity, the content of which drops from about 90% to 70% with age (Kurtz, 2006). With the loss of water, the disc loses its height and flexibility. As a result of the changes in the internal structure resulting from degeneration, the biomechanical properties of the disc are altered (Morishita, 2008). The dehydrated disc becomes stiffer, which leads to the transfer of the compressive load directly to the annulus fibrosus, making the disc more prone to mechanical injury and further degeneration. The degenerated annulus may experience radial tears, cracks and fissures under increased and unevenly transmitted pressure (Adams et al., 2000). Discs are avascular structures, which mean that they do not have their own blood supply. Therefore, they are not able to regenerate and painful symptoms may quickly become chronic.

In the most advanced stage of degeneration, the structure of the nucleus pulposus is almost completely replaced by the structures of the annulus fibrosus, which makes them practically impossible to distinguish. The progression of tears in the weakened annulus fibrosus, allows the nucleus to penetrate into the defect. Tears that extend through the outer annulus produce ingrowth of granulation tissue and accelerate the degenerative process. Advanced degeneration can lead to a gas formation or calcification within the disc.

Continuing subsidence of the intervertebral disc leads to change in the load transfer and distribution. The loads are now largely transmitted by the facet joints and other neighbouring structures, which leads to their gradual degeneration, resulting in pain and possibly arthritis (Pollintine et al., 2004). It was observed that the cervical discs are dehydrating much faster than the other parts of the spine, which results in their narrowing and increased load on the Zygapophysial joints (Cramer and Darby, 2013).

An intervertebral disc weakened by ageing and degeneration is also prone to disc herniation. A herniated disc occurs when the annulus fibrosus tears causing the nucleus pulposus to bulge. The inner portion of the disc that extrudes can then irritate or compress nearby nerves and be the cause of pain. A herniated disc can cause a variety of painful neurological symptoms. The majority of herniated discs occur in the cervical and lumbar part of the spine. It is due to the fact that these regions are characterized by the highest mobility and loading and therefore are more prone to degeneration and injury. In the lumbar region, disc herniation can cause pain, numbness, tingling or weakness radiating down the legs, which is also known as lumbar radiculopathy. When disc herniation takes place in the cervical spine, the pinched nerves cause the pain to radiate down the shoulders into the arms and fingers causing numbness as well as causing neurological symptoms (cervical radiculopathy). Overall, disc degeneration seems to be mostly a natural process that happens to every individual. The treatment of the degenerative disc includes both non-invasive (non-surgical) treatments such as bed rest, physical exercises or pharmacological treatment as well as invasive treatments involving surgical intervention.

2.3   General Treatment of Degenerative Disc Disease

To treat intervertebral disc degeneration, non-invasive methods such as physiotherapy or pharmacological treatment (pain relievers and anti-inflammatory medications) are attempted first (Iyer et al., 2016). However, in cases of severe degeneration and herniation, non-invasive methods usually do not bring the expected results and do not improve the patient's condition. In the case of severe disability and pain, surgical intervention is inevitable.

There are generally two main types of surgical options available for the treatment of degenerative disc pathology for both cervical and lumbar spine: spinal fusion and motion-preservation technologies.

2.3.1 Spinal Fusion

A spinal fusion (arthrodesis) consists of the complete removal of the degenerated disc and replacing it with a bone graft to fuse vertebrae, thus eliminating the motion at the treated spinal segment. In order to have higher union rates, additional fixation like screws, rods, plates or fusion cages are used, while the graft fuses the vertebrae. There are many types of spinal fusion techniques, which vary depending on the level of the spine and the location of the compressed spinal cord/nerves. In the case of the cervical spine, fusion is performed mostly through the anterior (front) approach called the anterior cervical discectomy and fusion (ACDF) (Iyer et al., 2016). For the lumbar spine, the fusion procedure is performed either through the anterior (front), posterior (back) or both sides of the spine. The goals of spinal fusion are to relieve patients from the pain (decompression) and to restore spinal column alignment and stability. It is considered to be the gold standard of spinal surgery, presenting high fusion rates of over 95% (Galbusera et al., 2008). However, by immobilizing the functional spinal unit, fusion alters the biomechanics and load transfer patterns of both treated and adjacent vertebral segments. Therefore, it can be a potential source of the symptomatic adjacent segment disease (ASD) (Kurtz, 2006; Grupp et al., 2010; Gillet, 2003). Though it is unclear whether the ASD is a direct result of fusion, it is generally believed that it may accelerate degeneration at adjacent levels.

Another drawback that has been reported in some cases, is the lack of fusion after surgery, also known as pseudoarthrosis (Vaccaro et al., 1998; Wang et al., 2000).

It can be very dangerous to the patient as it may lead to bone graft loosening, breakage or even pullout, and might require revision surgery.

2.3.2   Motion-preservation Technologies

Motion-preservation technologies aim to maintain the motion at the treated functional spinal unit and thus surpass the shortcomings of spinal fusion. They include total disc arthroplasty (cervical and lumbar region) and posterior dynamic stabilisation (PDS) based on the pedicle screw/rod system (lumbar region).

Total disc arthroplasty (TDA) surgery is usually performed for the cervical and lumbar spine levels. This method involves complete removal of the degenerated disc and replacing it with a prosthesis. This treatment is meant to provide nerve decompression and restore motion and biomechanics of the functional spinal unit affected by the degeneration.

Posterior dynamic stabilisation is a motion-sparing technique that is meant to provide controlled motion at the disc level without replacing it entirely. This technique is mainly applied in the lumbar region because the posterior approach seems to be the most convenient in this segment. It can be used separately or as adjuncts to fusion, when additional spinal stabilisation is needed (Khoueir et al., 2007; Serhan et al., 2011). The devices usually consist of metallic rods connected with a pedicle screw head and damper elements incorporated into the longitudinal components (Figure 2.5).
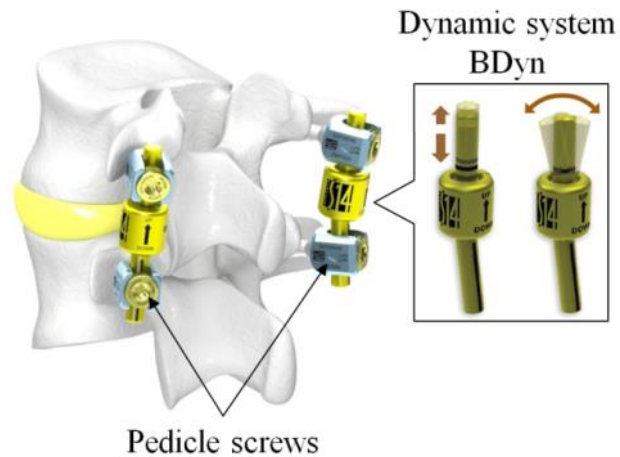
Figure 2.5 - Photograph showing BDyn (S14 Spinal Implants, France), an example of

pedicle-screw-based posterior dynamic stabilisation system (Adapted from S14 Implants).

2.4   Cervical Disc Arthroplasty (CDA)

Cervical disc arthroplasty (CDA) is a surgical procedure aimed at the treatment of degenerative cervical disc disorders such as radiculopathy, myelopathy and disc herniation. During this procedure, the degenerated disc is completely removed and substituted with an artificial device (Figure 2.6). CDA has emerged as an alternative to ACDF and is intended to bypass its limitations and shortcomings (Anderson and Rouleau, 2004). Cervical disc arthroplasty is aimed at relieving patients from pain, preserving the affected segment's mobility, preventing overload of the adjacent disc levels and any further degeneration. It may be particularly suited to young patients who may benefit the greatest from its theoretical advantages.

Figure 2.6 - Flexion (left) and extension (right) views of a Prestige ST implant (Wu et al., 2012).

In order to receive cervical disc replacement (CDR), patients have to meet certain requirements including:

- Cervical radiculopathy and/or myelopathy (Auerbach et al., 2008).

- Herniated disc.

- Osteophyte formation (Traynelis, 2006).

- History of a neck and/or arm pain and/or a functional/neurological deficit associated with the cervical level to be treated.

- Failed at least 6 weeks of non-operative treatment prior to surgery.

- Good bone quality.
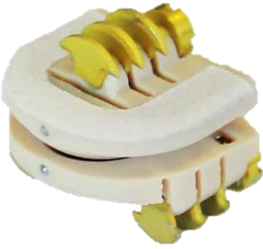
In the last two decades, the interest in cervical disc arthroplasty has gradually increased. Many new cervical disc replacement devices have appeared on the European and US market, receiving CE (European conformity) mark and FDA (food and drugs administration) approval. Though different designs of CDR are currently available, the ball-on-socket based designs are the most commonly used, whether consisting of a simple ball and socket or including a mobile core (Alvin et al., 2014; Alvin and Mroz, 2014; Peng et al., 2011). However, the next generation of devices based on elastomers is gradually being introduced.
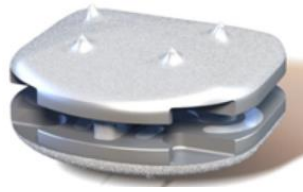
Examples of cervical devices that are currently available on the market are presented in Table 2.1.

Table 2.1 - Examples of CDRs and their main features.

Device	Features
ProDisc-C (Synthes Spine, West Chester, PA. USA) *Source: (Traynelis, 2006)*	• Ball-on-socket device • 3 components • Constrained • Two cobalt-chromium-molybdenum (titanium) alloy endplates and a polyethylene (UHMWPE) inlay element • Primary and long-term fixation: keels, titanium textured coating • Received a CE mark in 2002 • FDA approved in 2007
Prestige LP (Medtronic Sofamor Danek, Memphis, TN, USA) *Source: (Traynelis, 2006)*	• Ball-on-socket device • 2 components • Semi-constrained • The device is made of titanium carbide. The reciprocating socket is placed on the inferior endplate, which apart from the flexion/extension and lateral bending and rotation allows a small degree of translation • Primary and long-term fixation: keels, screws, titanium textured coating • Received a CE mark in 2002 • FDA approved for 1-level surgery in July 2014 and 2-level in 2016
SeCure-C (Globus Medical, Audubon, PA, USA) *Source: (Vaccaro et al., 2013)*	• Ball-on-socket device • 3 components • Semi-constrained • Two cobalt-chromium-molybdenum alloy endplates and a plastic (UHMWPE) inlay. The inlay creates a spherical and cylindrical interface with upper and lower endplate, respectively • Primary and long-term fixation: keels, titanium textured coating • FDA approved in 2012

PCM (NuVasive, Cervitech, Rockaway, NJ, USA) *Source: (Traynelis, 2006)*	• Ball-on-socket device • 3 components • Semi-constrained/ broad radius • Two cobalt-chromium-molybdenum alloy endplates and a UHMWPE spacer, with a large radius, attached to the lower endplate • Primary and long-term fixation: ridges, surface replacement, calcium phosphate/titanium coating • Received a CE mark in 2005 • FDA approved in 2012
Mobi-C (LDR Spine, Austin, TX, USA) *Source: (Baltimore et al., 2013)*	• Ball-on-socket device • 3 components • Semi-constrained • Two cobalt-chromium-molybdenum alloy endplates and a polyethylene mobile core (UHMWPE). The upper surface of the lower endplate is flat and is characterized by two stops, which restrain the translational movement of the core • Primary and long-term fixation: teeth, titanium and hydroxyapatite • Received a CE mark in 2004 • FDA approved for 1 and 2-level implantation in 2013
Kineflex|C (Spinal Motion, Inc., Mountainview, CA, USA) *Source: (Traynelis, 2006)*	• Ball-on-socket device • 3 components • Semi-constrained • Two cobalt-chromium-molybdenum endplates and a mobile core • Primary and long-term fixation: keels, titanium textured coating • Received a CE mark in 2012
Discover (DePuy Spine, Raynham, MA, USA) *Source: (Du et al., 2011)*	• Ball-on-socket device • 3 components • Constrained • Two titanium alloy endplates and a central ultra-high molecular weight polyethylene (UHMWPE) articulating core • Primary and long-term fixation: teeth, titanium and hydroxyapatite • Received a CE mark in 2006

NuNec (Pioneer® Surgical Technology, Marquette, Michigan, USA) *Source: (Xin et al., 2013)*	• Ball-on-socket device • 5 components • Constrained • Bearing Surface material: PEEK-on-PEEK • The device made of medical grade PEEK-OPTIMA (polyether-ether-ketone) • Primary and long-term fixation: screw locking mechanism, hydroxyapatite • Received a CE mark in 2008
Baguera-C (Spineart, Geneva, Switzerland) *Source:(Benmekhbi et al., 2008)*	• Ball-on-socket device • 3 components • Semi-constrained • A high-density polyethylene (PE) nucleus that articulates between two titanium endplates. The interior surfaces of the endplates are coated with Diamolith, a diamond-like carbon titanium coating • Primary and long-term fixation: teeth/fins, porous coating • Received a CE mark in 2007
Simplify Disc (Simplify Medical, Inc. Mountainview, California, USA) *Source:(www.simplifymedical.com)*	• Ball-on-socket device • 3 components • Semi-constrained • Two PEEK endplates and a ceramic articulating core • Primary and long-term fixation: teeth/fins, titanium textured coating • Received a CE mark in 2015
Bryan (Medtronic Sofamor Danek, Memphis, TN, USA) *Source: (Traynelis, 2006)*	• 3 components • Unconstrained (elastomeric ball-on-socket) • Two titanium alloy endplates, a polycarbonate polyurethane nucleus and a polyether polyurethane sheath. The sheath surrounds the nucleus and is attached to endplates by titanium retaining wires, creating a capsule. The device is an elastomeric ball-on-socket articulation; with a nucleus specially shaped to fit in between the two dome-shaped shells • Primary and long-term fixation: milled vertebral endplates, titanium textured coating • Received a CE mark in 2000 • FDA approved in 2009

M6-C (Spinal Kinetics, Sunnyvale, California, USA) *Source: (Reyes-Sanchez et al. 2010)*	• 5 components • Unconstrained • Two titanium outer plates, a core made of polycarbonate urethane (artificial nucleus), polyethylene (UHMWPE) woven-fibre construct (artificial annulus) and a polymer sheath • Primary and long-term fixation: keels, titanium textured coating • Received a CE mark in 2005
Freedom (AxioMed Spine Corporation, Cleveland, Ohio, USA) *Source: (www.axiomed.com)*	• 3 components • Unconstrained • The device consisting of an elastomeric core made of CarboSil™ TSPU (a silicone polycarbonate urethane thermoplastic elastomer) bonded to a titanium retaining endplate using AxioLock™, a proprietary polymer-metal bonding technology • Primary and long-term fixation: teeth/fins, titanium textured coating • Received a CE mark in 2012
RHINE Disc (K2M Group Holdings, Inc) *Source: (K2M Group Holdings, Inc)*	• 3 components • Unconstrained • Compressible polymer core design with dome-shaped, plasma-coated endplates • Primary and long-term fixation: keels, titanium textured coating • Received a CE mark in 2016
CP ESP (FH ORTHOPEDICS, France) *Source:(Lazennec et al., 2016)*	• 3 components • Unconstrained • The deformable implant including a central core made of polycarbonate urethane (PCU) securely fixed to titanium endplates • Primary and long-term fixation: teeth, spikes, titanium and hydroxyapatite • Received a CE mark in 2012
Cadisc-C (Ranier Technology Limited, Cambridge, UK) *Source: (Holsgrove, 2012)*	• 1 component • Unconstrained • A one-piece device manufactured from a polyurethane-polycarbonate polymer with a graduated Young's modulus that is lowest at the centre, and highest at the outskirts • Primary and long-term fixation: spikes, macro- and micro-texture with a CaPO4 coating

2.4.1   CDRs Design Characteristics

The main task of the artificial intervertebral disc is to maintain the anatomical range of motion of the FSU while simultaneously transferring the axial loads to the neighbouring vertebrae. Currently, many design solutions for cervical disc implants are used. They can be classified according to various criteria, such as articulation and kinematics (the type of motion they provide), materials (friction couples), and the fixation methods (Leven et al., 2017; Sekhon and Ball, 2005).

Articulation and kinematics

The functional spinal unit is characterized by an instantaneous centre of rotation (COR). This feature varies between spine levels but is generally situated posteriorly with respect to the endplate centre, on the surface of the inferior vertebral body. In order to preserve the motion of the functional spinal unit, the CDRs usually operate based on a ball-on-socket, a flexible core or a combination of both. Depending on the degrees of freedom allowed by the specific design, the bearing surfaces of CDRs can be classified as constrained, semi-constrained and unconstrained (Sekhon and Ball, 2005; Leven et al., 2017; Vicars et al., 2011).

<u>Constrained</u> designs are characterized by a fixed COR and 3 degrees of freedom (Galbusera et al., 2008). They provide more stability to an operated joint but require a more precise placement to replicate the natural axis of rotation, and stronger anchorage as they put more strain to an implant-bone interface, compared to less constrained designs (Vital et al., 2014; Leven et al., 2017).

<u>Semi-constrained</u> devices are usually characterized by a spherical interface and possess 4-5 degrees of freedom with a mobile nucleus. These types of designs are stable since translation is employed within the nucleus, increasing along with its radius (Vital and Boissière, 2014).

Unconstrained designs feature a non-conformal ball-on-socket, two different articulating pairings or a deformable core (Galbusera et al., 2008). They have 6 degrees of freedom and a mobile COR that can adjust to the natural instantaneous centre of rotation of the functional spinal unit. Unlike constrained designs, they do not require perfect positioning but may inflict greater stress on the posterior joints (Vital et al., 2014; Kurtz and Edidin, 2006).

Materials

When choosing materials for the TDR both the articulating conditions (the type of frictional couples) and the influence on the surrounding environment, have to be taken into consideration. Various materials are currently being used in TDR designs including medical grade metal alloys (stainless steel, titanium and cobalt-chromium alloys); medical grade ceramics and polymers (ultra-high molecular weight polyethylene (UHMWPE), poly-ether-ether-ketone (PEEK), polyurethane) (Taksali et al., 2004). As mentioned previously, most CDRs designs use a ball-on-socket connection to provide motion, therefore, the materials used have to effectively minimize friction. The most common CDRs bearing types are either metal-on-metal or metal-on-polymer designs. However, lately, the use of alternative bearing materials has been observed, which include PEEK and elastomers (Kurtz and Edidin, 2006).

Medical grade PEEK is considered a promising material for all-polymer artificial discs due to a favourable combination of manufacturability, radiolucency, biocompatibility, mechanical strength and wear resistance. PEEK can be processed using conventional techniques including injection moulding, extrusion or machining. Moreover, PEEK's Young's modulus is significantly lower compared to other popular implantable metal alloys and closer to the modulus of cortical bone (Table 2.2). It is an important property that may reduce the incidence of stress-shielding and thus provide a stable implant-bone interface.

Table 2.2 - Relative Young's modulus of PEEK-OPTIMA and implantable metals

(Patel and Gohil, 2012; Xin et al., 2012).

	Co-Cr Alloy	Stainless Steel 316L	Titanium 6Al 4V	PEEK (Optima)	Cortical Bone
Young's Modulus (GPa)	210 - 253	190	120	3.7	15 - 30

Brown and Bao (2012) have investigated and compared the wear performance of a PEEK-on-PEEK cervical TDR NuNec to previous experimentally established rates of wear for other TDR devices. The results of their study indicated comparable or improved wear performance of self-mating PEEK in cervical arthroplasty. Furthermore, implantable PEEK has the ability to be sterilized with gamma and electron beam radiation without suffering any degradation in mechanical properties (Xin et al., 2013; Kurtz and Devine, 2007). However, fixation to the bone is a major issue regarding the use of PEEK, as the untreated surfaces of PEEK implants are bioinert and do not induce osseointegration. This can be achieved by applying a titanium or/and hydroxyapatite to a surface of the implant, making it more hydrophilic and bioactive (Johansson et al., 2014; Robotti and Zappini, 2011).

The artificial disc devices based on elastomeric cores are emerging as a new generation of total disc replacements (Figure 2.7). Elastomers (rubbers) are viscoelastic polymers that can undergo varying degrees of deformation under stress without rupture, and recover to their original state when the stress is removed. The intervertebral discs perform their required function because of the elastomeric nature of the collagen and fluids of which they are made of. The intervertebral disc is essentially a deforming fibrocartilaginous joint. Therefore, elastomers are seen as potential materials that may closely mimic the behaviour of a natural disc in a way that a conventional ball-on-socket device cannot.

Figure 2.7 - Examples of artificial cervical discs based on elastomers.

The main elastomers that are used in disc arthroplasty include polyurethanes (PU) and polycarbonate-urethanes (PCU) (Table 2.3) (Chen et al., 2013). Some of the disc devices such as the Freedom and M6-C use polycarbonate urethane elastomers in conjunction with metallic components; other devices such as the Cadisc - C are one-piece polyurethane-polycarbonate polymer devices.

Table 2.3 - Typical properties of PCU materials used in spinal devices (John, 2014).

Materials	Flexural modulus (MPa)	Tensile strength (MPa)	Hardness scale	Hardness	Elongation to break (%)
PCU (80A)	28	45	Shore A	80A	525
PCU (90A)	42	55	Shore A	90A	400
PCU (55D)	48	60	Shore D	55D	360

Initial and long-term fixation

The strength of the implant-bone union is an important aspect that has to be considered, as it has a major influence on the proper functioning of the device. In general, the fixation systems of the TDR usually divide into initial/primary and long-term.

Initial fixation is based on some form of mechanical constraint, which includes: keels, teeth, spikes, ridges and screws.

In order to provide the long-term union between implant and bone (osseointegration), specialized coatings of plasma-sprayed titanium, aluminium oxide, hydroxyapatite and calcium phosphate are applied.

2.4.2   Failure of CDRs

CDA is a relatively new technique that derives largely from the achievements and experience acquired in lumbar disc arthroplasty, therefore, it struggles with similar complications (Van Ooij et al., 2003; Kurtz et al., 2006), which includes:

- **Complications related to the bearing type:**

Ball-on-socket type of bearings tend to be axially rigid, therefore, it does not provide the resistance to an axial loading (compliance) and does not accurately reproduce FSU mobility. This leads to an abnormal loading and compressive stresses put on the facet joints, ligaments and vertebral bodies, which may lead to their degeneration.

Less constrained bearing types such as the ones with mobile COR are supposed to provide more physiological motion. However, they also exhibit little shear stability, which means that the facet joints may be overloaded, which may again lead to degeneration.

On the other hand, the unconstrained implants based on elastomers, though providing axial compression, may not provide sufficient mobility; they, therefore, may not demonstrate superior clinical outcomes compared to ACDF (Skeppholm et al., 2015).

- **Complications related to the materials used**

As the majority of available CDR designs are based on ball-on-socket articulation, the wear particles are considered as a major problem (Veruva et al., 2014; Kurtz et al., 2012; Taksali et al., 2004; David, 2005; Kurtz et al., 2007).

Among all types of CDRs, metal-on-metal and metal-on-polymer are the most popular material combinations. Metal-on-metal articulating pairs have good tribological properties but tend to release a lot of small-sized reactive ions and wear particles shaped as fibres, both of which provoke inflammatory reactions (Hallab, 2014). In their study on the Prestige device (metal-on-metal), Anderson et al. (2006) observed a chronic inflammatory response as a result of metallic wear debris. An inflammatory response may then further lead to bone loss (osteolysis) and as a consequence implant loosening. The same problem applies to metal-on-polymer devices as the most commonly used UHMWPE releases large-sized wear particles that provoke an inflammatory response (Golish and Anderson, 2012). Moreover, metal-on-polymer frictional pairs tend to wear at faster rates yielding more volume loss.

Ceramic-on-ceramic couples have good wear properties, but are brittle materials compared with metals, making failures sudden and catastrophic, rather than gradual (Taksali et al., 2004).

Another important aspect is the possibility of precise post-operative imaging of the implanted devices. Metals, especially stainless steel, are a source of artefacts during MRI and CT imaging, whereas ceramics and polymers such as PEEK are best adapted to MRI.

Designs based on the elastomeric core may also suffer from complications. Elastomers usually work in combination with metal parts, therefore, ensuring a lasting connection between these elements requires special techniques, for example, vulcanizing the elastomeric polymer to the metal endplates. What is more, the continuous occurrence of micro-motions at the interface of the elastomer and the material with a different elastic modulus, can lead to the formation of wear debris and, as a result, to failure (Lee and Goel, 2004). Although a one-piece elastomeric bearing will not produce wear debris due to articulation, material loss is still possible due to other factors such as fatigue, erosion, or third-body damage

(Vicars et al., 2011). Further studies concerning elastomeric devices are needed as there is still little literature describing the wear debris and material longevity.

Another problem concerning the materials used for CDR is related to a mismatch of the mechanical properties between the material and the bone, especially Young's modulus. A high stiffness of the implant compared to bone may lead to a phenomenon known as stress-shielding. In this case, the stresses and loads are mainly carried by an implant which results in resorption of the bone.

- **Subsidence**

The wrong choice of the prosthesis size may lead to a disc sinking down into the vertebral bone (subsidence), which is one of the most common complications of TDR. It is caused by a small contact area at the implant-bone interface (Kurtz et al., 2006). Subsidence may also be caused by interfering in the structure of the bone endplates. The devices characterized by keels, rails or a special external shape, require a special bone preparation before they can be implanted. To accommodate the implant, the bone endplates are often surgically reduced to a flat plane, and a slot is cut to receive the implant keel. This action compromises the strength of the vertebrae's cortical shell and reduces its ability to withstand pressure and can lead to implant subsidence or vertebral body fracture.

- **Device migration**

Misplacement during the implantation or insufficient anchorage of the device may lead to device migration within the vertebral cavity (Wagner et al., 2016). The migration in the anterior direction will eventually lead to device expulsion whereas the posterior migration can increase the risk of spinal cord or spinal nerve root compression leading to neurological problems or even a paralysis.

2.5   Pedicle-screw-based PDS System

The main goal of posterior dynamic stabilisation systems is ensuring a healthy load transfer to the lower spine and pain relief. Depending on a clinical condition, this new spinal technique focuses on maintaining or restoring intervertebral motion in a controlled manner. Although there are many different fixation techniques, the most common involves the use of pedicle screws (PS). A PS is a type of bone screw, which is inserted into the isthmus of the pedicle and used for connecting vertebrae to rods (Figure 2.8) (Silbermann et al., 2011; Verlaan et al., 2013; Pihlajämaki et al., 1997). Pedicle-screw-based dynamic stabilisation systems can be used alone or in conjunction with fusion to treat disc herniation and spinal stenosis (Kurtz et al., 2006).

a)   b)
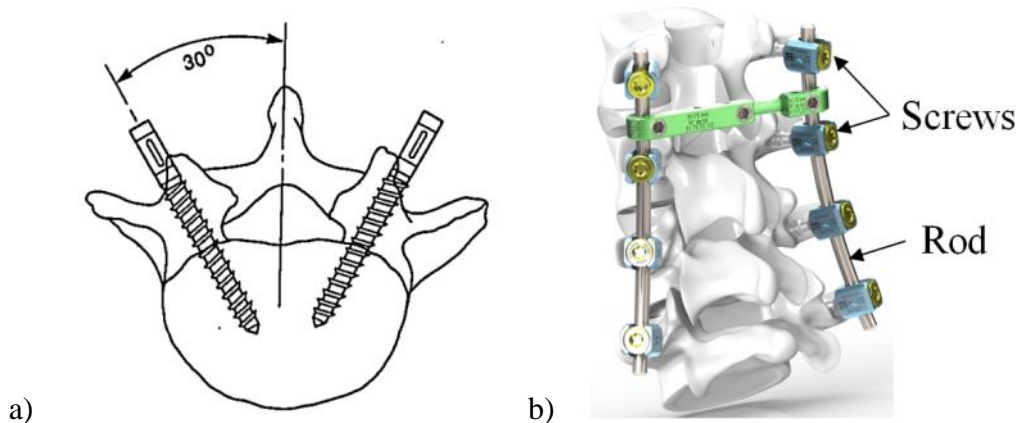
Figure 2.8 - a) Placement of the pedicle screw (Adapted from Barber et al., 1998);

b) Pedicle screw-based dynamic stabilisation system (Adapted from S14 Implants).

2.5.1   Pedicle Screw Characteristics

The pedicle screw comprises a screw head, a threaded shaft (body) and a neck that connects the head and a shaft (Figure 2.9). The threaded shaft consists of a core (also known as an inner or minor diameter), a major (outer) diameter and a thread. The difference between the major and minor diameter is called the thread depth. The pitch of the thread is the distance

between the crests of two adjacent threads. During surgery, the threaded part is inserted into

the vertebra, while the head fixes the rod.
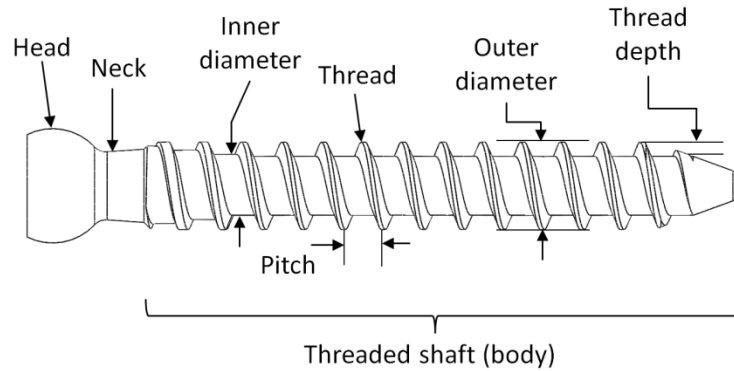
Figure 2.9 - The main parts of a pedicle screw.

2.5.2   Pedicle Screw Types

The main types of pedicle screws available for clinical use can be classified as monoaxial

(MA) and polyaxial (PA) screws (Figure 2.10).

a)   b)
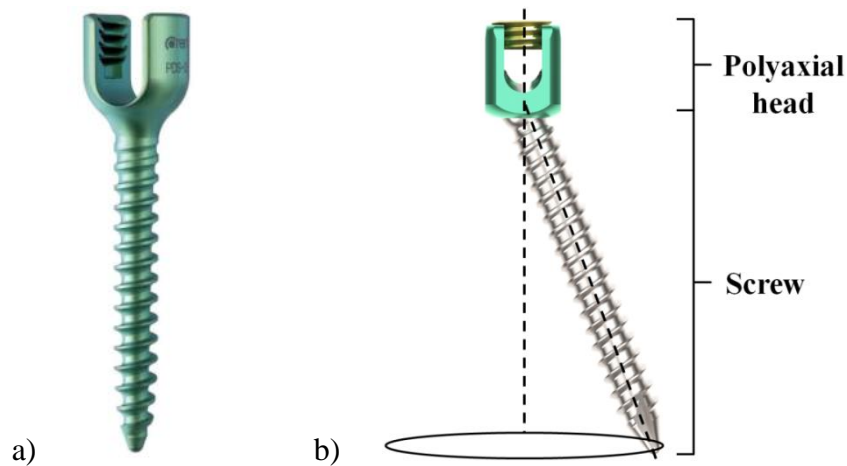
Figure 2.10 - Pedicle screw types: a) Monoaxial screw (Adapted from Corentec);

b) Polyaxial screw (Adapted from S14 Implants).

Monoaxial screws consist of one part, including a specially shaped head that allows for rod

fixation, creating the rigid connection. MA geometry does not allow any flexibility when

connecting the screw to the rod, which makes the rod installation more complicated.

Moreover, a rigid connection between the screw and the rod can cause additional stress in the entire stabilisation system and, as a result, lead to damage (Wang et al., 2011).

To eliminate the restrictions associated with the use of monoaxial screws, a new solution in the form of polyaxial screws was proposed. Polyaxial screws are characterized by a ball joint, formed by a spherical head of the screw enclosed in an additional housing (polyaxial head), thus allowing a range of motion along several different axes relative to the polyaxial head. As a result, it makes the pedicle screw more adjustable to the rod and gives the surgeon some flexibility in placing it, unlike the MA screws. It has been also speculated that the geometry of polyaxial screws may prevent the breakage of the screw shaft or orthopaedic rod, by failing first at the housing/screw head interface (Fogel et al., 2003). Wang et al., (2011) have suggested that flexibility of polyaxial pedicle screws allows for a better control over correction forces and thus may decrease the risk of failure. Therefore, PA screws may be a good option for patients with weak bone quality.

However, despite the advantages associated with easier rod implantation, polyaxial screws exhibit lower mechanical strength compared to monoaxial screws and are particularly vulnerable to fatigue failure (Stanford et al., 2004; Schroerlucke et al., 2014).

Core geometry

There are three main core types: conical (tapered), cylindrical and dual-core (Demir et al., 2015). Cylindrical screws are the most commonly used pedicle screws, characterized by a constant internal diameter along the entire length of the screw. A conical screw is characterized by a tapering of at least the core, with a gradual decrease in diameter in the distal direction. The conical screw was designed to better accommodate the pedicle geometry which has an anteriorly decreasing diameter (Misenhimer et al., 1989). The dual-core design is a new type of pedicle screw that was developed in order to meet both

anatomical and mechanical requirements. A dual-core screw is usually characterized by a cylindrical outer diameter and two cylindrical inner diameters with different dimensions, and a conical transition zone (Figure 2.11). Theoretically, the new design should provide easier insertion due to the small inner diameter of the distal part, while the thicker core in the proximal part should simultaneously provide stability and higher resistance to bending.
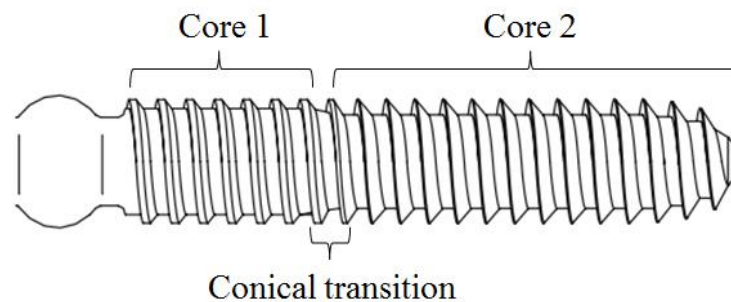
Figure 2.11 - Geometry of a dual-core pedicle screw with a constant outer diameter and two different core diameters (Photograph adapted from Lill et al., 2006).

Thread geometry

Figure 2.12 shows the main three available screw thread shapes: V-shaped, square-shaped and buttress-shaped (Demir et al., 2015). V-shaped screw threads are easy to manufacture and characterized by symmetrical sides inclined at equal angles. V-shaped threads are strong, but they transmit more shear forces to the surrounding bone, comparing to the square-shaped or buttress-shaped threads. The square-shaped thread has symmetrical sides perpendicular to the axis of the screw head and is efficient in transmitting forces in both directions along the axis of the screw thread. The buttress thread is transmitting forces in a single direction along the axis of the screw head as it has an asymmetrical profile characterized by a pressure flank that is nearly perpendicular to the screw axis.

The most common thread shape used for fasteners is the V-shaped type, whereas the other two thread shapes are mostly used in nonmedical applications as power screws as they are efficiently converting rotational motion to linear motion (Shea et al., 2014).

| a) | b) | c) |
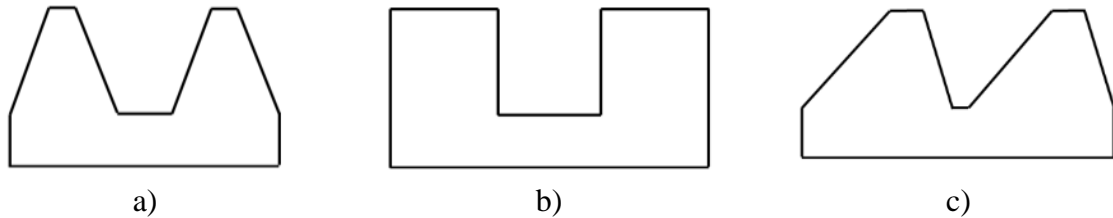
Figure 2.12 - Pedicle screw thread shapes: a) V-shaped; b) square-shaped; c) buttress-shaped.

Some of the pedicle screw designs include a double start thread where there are two parallel, non-crossing threads, spiralling up the length of a screw (Figure 2.13). This type of thread is desired when a faster screw insertion is required, which equals to less operating time.
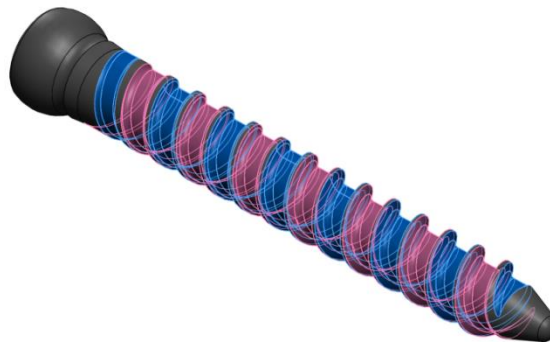
Figure 2.13 - Pedicle screw with a double start thread.

Most of the latest models of pedicle screws are characterized by a varied thread that is adapted to both cortical and cancellous bone. The cortical part of the thread is usually found in the proximal part of the screw shaft and is characterized by closely-spaced, shallow threads in order to grip hard dense cortical bone. The cancellous part of the thread is placed in a distal part of the shaft and is characterized by more deeply cut and more widely spaced threads in order to grip softer less dense cancellous bone.

2.5.3   Failure of Pedicle Screws

Despite the advantages and success associated with the use of pedicle-screw based fixation, failures are still reported. Most pedicle screw failures are very dangerous for patients, as they can result in instability of fixation and may lead to more complicated problems, resulting in corrective surgery (Vanichkachorn et al., 1997). Screw breakage and loosening are the most common causes of failure.

Screw breakage, bending

Pedicle screws are often subjected to bending forces, thus the bending strength of the screws is of major clinical importance. Screw breakage is the most common form of hardware failure and its incidence has been reported to range from 2.6% - 4.9% to 9% - 36% to as high as 60% (Gaines, 2000). Failure is likely to occur due to bending fatigue or due to a loading situation that exceeds the load-bearing capacity of the implant. Given the screw loading conditions, the highest stress concentrations occur in the area where the screw enters the bone. Therefore, it is the point where the screws are the most susceptible to breaking. This is consistent with the *in-vivo* observations, which indicate that the fracture most often occurs at the thread end (Griza et al., 2012; Chen et al., 2005).

However, it is important to understand that not all incidences of screw breakage are directly related to the hardware itself. Many aspects, like screw misplacement and mal-positioning as well as the wrong choice of the screw dimensions, can influence and increase the possibility of screw breakage.

Screw pullout, loosening

The second most common screw hardware failure is screw loosening, which is reported to range from 0.6% - 11% to 21% - 27% (Okuyama et al., 2000; Mohi Eldin et al., 2014).

Though axial pullout tests are very popular in order to evaluate and compare screws, the direct axial pullout failure does not occur clinically. Screw loosening occurs when the continuous bending forces applied to a screw head can cause micro-motions of the distal part of the screw inside the bone, weakening the screw-bone interface, leading to pullout. There are many factors reported in the literature that may affect the loosening of screws, including bone quality, screw dimensions and design, and the screw insertion method (Renner et al., 2004).

Loose screws are a serious clinical problem, as their load transfer function is taken over by other components of the posterior stabilisation system, which are not designed for this. As a result, under the influence of cyclic loading, the entire system is destabilised, which in turn leads to a total system failure and possible reoperation.

2.5.4   Design Factors Affecting Bending Strength

Core geometry

The factor that most affects the pedicle screw bending strength is their inner diameter (ID). The bending strength of a screw is proportional to the section modulus (Z) that is defined as:

$$Z = \pi D^3/32 \tag{2.1}$$

where D is the inner/core diameter. As the section modulus changes by the cube of the change in the core diameter, even a slight change of the inner diameter has a significant impact on the bending strength of the screw. Moreover, as pedicle screws are mainly subjected to cantilever bending moments, the screw neck, or the place where the screw enters the cortical bone, are the most frequent sites of breakage (Yerby et al., 1997). Therefore, to increase the bending strength of the screw, it is necessary to increase its internal diameter as much as possible and reinforce the neck region. An optimal solution to this problem is the conical geometry of the

screws. The studies confirmed that conical screws are more difficult to bend and break than conventional cylindrical screws (Kim et al., 2012).

Thread root radius

Another important factor that may affect the bending strength of the screw is the thread root radius (Figure 2.14). The transition between the inner diameter (ID) and the thread may be a source of undesired stress concentrations that can lead to breakage. It was observed by Griza et al. (2012), that pedicle screws with a small thread root radius should be avoided.
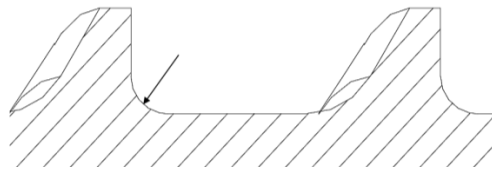
Figure 2.14 - Image illustrating thread root radius.

2.5.5   Design Factors Affecting the Pullout Strength

Previous work has shown that the geometry of the screw shaft and thread has an effect on the pullout strength (Hsu et al., 2005).

Core geometry

The pullout strength is closely associated with a shape of the screw shaft and its internal and external diameter. Each of the three main types of pedicle screw cores (conical, cylindrical, dual) exhibits different pullout strengths. Cylindrical screws are the original version, both the conical and dual-core screws are relatively new solutions and were designed to improve the pullout resistance. Many studies have evaluated and compared the pullout strength of these three screw designs. For instance, the study made by Lill et al., (2006) has shown that the dual-core screw had higher pullout strength compared to the cylindrical design.

Other studies showed that the conical screws are more resistant to loosening, compared with the cylindrical screws (Amaritsakul et al., 2014; Chao et al., 2008). Krenn et al., (2008), reported that conical screws improved pullout strength by increased compression and tightening of the surrounding bone tissue during the insertion.

The difference between the inner and outer diameter determines the amount of bone tissue surrounding the screw, ensuring its stable anchorage. Therefore, decreasing the core diameter while maintaining constant outer diameter, will enlarge the bone material volume between the two diameters, and consequently lead to an increase of the pullout strength. The increase of the outer diameter will provide the same effect, however, its dimension is restricted by the anatomy of the pedicle itself and the risk of a pedicle fracture. It is important to note that the core diameter cannot be too small as it will negatively influence the bending strength of the screw. Therefore, it can be concluded that the factors that increase the pullout strength can simultaneously reduce bending resistance. Thus, screws performing well under bending may not satisfactorily resist loosening (pullout) (Hsu et al., 2005).

Thread design

The pullout strength is proportional to the amount of bone tissue between the thread grooves, which ensures stable screw anchorage. Such factors as the thread shape depth and pitch define the contact area between the thread and the surrounding bone tissue known as flank overlap area (FOA). Increasing the FOA will allow a better distribution of forces and thus increase the pullout strength. Total FOA can be calculated by the following equation 2.2:

$$FOA = [\pi /4 \times (D^2_{outer} - D^2_{inner})] \times l/p \qquad\qquad (2.2)$$

where D_{outer} and D_{inner} are the outer and inner screw diameters, respectively, and l and p, are the shaft length and thread pitch, respectively. Many studies have confirmed a strong

correlation between the FOA and the pullout strength. For instance, Kim et al., (2012) investigated screws with conical and cylindrical inner and outer diameters; and V, square and buttress shaped threads. The results indicated that the V-shaped threads had the highest FOA, and thus the highest pullout strength. In his study Krenn et al., (2008) suggested that a conical core, smaller core diameter, larger FOA and moderately small thread pitch provided the best screw fixation. Additionally, some pedicle screws have two different threads, suitable for both cortical and cancellous bone, which is meant to increase their pullout resistance.

2.5.6   Pedicle Screw Material

While considering an appropriate material for pedicle screws, a few factors are taken into account:

- Mechanical properties

- Biocompatibility

- Ease of osseointegration (direct contact of bone tissues to an implant surface without fibrous membrane)

- Resistance to corrosion and degradation due to body fluids

- Effects on MRI and CT imaging

- Cost and material availability

- Ease of manufacture

The most common materials used to manufacture pedicle screws are 316L stainless steel (SS) and titanium alloy ELI (Ti-6Al-4V) (Christensen et al., 2000).

Titanium alloy is preferred due to its favourable mechanical properties as well as good biocompatibility and resistance to corrosion. Its Young's modulus is around 116 GPa, which is almost half that of other alloys such as stainless steels (Table 2.4).

To obtain good clinical results Young's modulus of the metal and the bone should be similar. If Young's modulus of the metal is much greater than that of bone, the phenomenon known as stress shielding occurs. The load experienced by the bone is reduced and as a result, the bone loses its density. Though titanium-based alloys usually have higher fatigue strength compared to stainless steel, they are vulnerable to any surface flaws. Therefore, any scratch or notch can rapidly accelerate the fatigue failure process. Moreover, implants made from titanium alloy result in fewer artefacts during MRI and CT imaging as opposed to other materials (particularly stainless steel) (Niinomi, 1998; Ebraheim et al., 1994).

Table 2.4 - Mechanical properties (Patel and Gohil, 2012).

Material	Young's modulus (GPa)	Yield strength (MPa)	Tensile strength (MPa)	Fatigue limit (MPa)
Cortical bone	15 - 30	30 - 70	70 - 150	
Ti-6Al-4V ELI	116	896 - 1,034	965 - 1,103	620
Stainless steel	190	221 - 1,213	586 - 1,351	241 - 820

2.6   Chapter Summary

Intervertebral disc degeneration is the main cause of neck and lower back pain and it is said to affect about 60-85% of the general population. Many factors affect the gradual degeneration of the disc, they include natural ageing processes, genetic predisposition, micro and macro injuries due to abnormal load conditions and loss of disc nutrition. In the case of severe degeneration and herniation, surgical intervention is unavoidable. For many years immobilising the functional spinal unit by performing fusion, was considered as the gold standard. However, fusion alters the biomechanics and load transfer patterns of both treated and adjacent vertebral segments and may lead to symptomatic adjacent segment disease

(ASD). The desire to improve the comfort of patients and reduce the costs of treatment and rehabilitation has led to the development of new motion-preservation technologies. These technologies include artificial disc replacement devices and posterior dynamic stabilisation devices. They aim to surpass the limitations of fusion and maintain or restore the motion in a treated segment.

As the discomfort associated with fusion is particularly noticeable in the cervical segment, it is essential that the prosthesis simulates the natural disc and provides a physiological range of motion. There are currently many different designs of cervical disc replacements on the market, in which ball-on-socket constructions dominate. However, most of them either do not entirely mimic the functionality of the natural disc exposing the treated segment to further degeneration, or struggles with complications that prevent them from proper and long functioning. Next generation devices based on elastomers are gradually being introduced, as they are seen as possessing characteristics that may closely mimic the behaviour of a natural disc. However, since this is a new concept, there is still not enough clinical data available to clearly state the superiority of elastomeric devices over other devices.

In the case of the lumbar spine, the most popular dynamic treatment of the degenerated disc involves the use of a posterior pedicle screw/rod system. The main complications associated with this system include fractures and loosening/pullout of pedicle screws. Many different designs of pedicle screws have been proposed over the years in order to surpass these shortcomings and it is important to evaluate their performance prior to clinical use.

The two main objectives of this thesis are to propose a new concept of the dynamic cervical disc and to evaluate the mechanical performance of the novel pedicle screws being an integral part of the posterior dynamic lumbar stabilisation device.

3   A New Design Concept for Dynamic Cervical Disc Replacement

Chapter Overview

This chapter presents the design and development of a new cervical intervertebral disc replacement device (CDyn). In section 3.1 a brief introduction is given. The methodology, which presents the TRIZ tools used during the design process, can be found in section 3.2. Design requirements, according to which the new device has been developed, are presented in section 3.3. The process of design development is described in section 3.4. The final design and design verification are presented in sections 3.5 and 3.6, respectively. Finally, a discussion of the results and chapter summary can be found in sections 3.7 and 3.8.

3.1   Introduction

Cervical radiculopathy is the clinical description of pain and neurological deficit caused by compression of a cervical nerve root. Population-based data from between 1976 and 1990 in Rochester, Minnesota (Radhakrishnan et al., 1994), reports that the incidence of clinically significant cervical radiculopathy is 107 per 100,000 in men and 63.5 per 100,000 in women aged 55-64 years. A more recent study within a closed American population performed by the US military found an incidence of 1.79 per 1000 person-years (Schoenfeld et al., 2011). The most common cause of cervical nerve compression is disc herniation. A herniated disc occurs when the outer portion of an intervertebral disc breaks down and the inner portion extrudes out. The inner portion of the disc that extrudes can then irritate or compress nearby nerves. The negative symptoms that affect patients the most are: radiating neck pain; shoulder stiffness; weakness; lack of coordination in the arm and hand (Caridi et al., 2011).

There are generally two types of surgical options available for the treatment of cervical degenerative pathology: anterior cervical discectomy and fusion (ACDF) and total disc

replacement (TDR). ACDF is still considered to be the gold standard, presenting high fusion rates of over 95% (Galbusera et al., 2008). Although it proves to be a very effective method, fusion alters the biomechanics and load transfer patterns of both treated and adjacent vertebral segments. Thus, it can be a potential source of the symptomatic adjacent segment disease (ASD). However, it is still unclear if the ASD is the direct result of the fusion or just a natural progression of the degenerative disc disease. The alternative method of total disc replacement is a relatively new technology. Cervical TDR is intended to bypass ACDF limitations by preserving the affected segment's mobility, preventing overload of the adjacent disc levels and any further degeneration.

Different designs of TDR are currently available on the market, among which the ball-on-socket design configuration dominates (Alvin et al., 2014; Alvin and Mroz, 2014; Peng et al., 2011). Although these types of devices aim to preserve the range of motion (ROM), they fail to provide compliance to dynamic stresses.

The aim of this chapter is to design a new dynamic artificial intervertebral disc that would ensure more anatomical range of motion, including the compliance to dynamic stresses, and abide the demanding requirements for the medical devices market. A new device should combine three degrees of freedom (flexion-extension; lateral bending; axial rotation) with an additional cushioning effect, achieved by incorporating an elastomeric core. As a result, it may restore both spinal segment kinematics and the viscoelastic properties of the intervertebral disc.

The specific objectives concerning dynamic cervical disc prosthesis, covered in this chapter include:

- Formulating the specific design requirements that the device need to meet.

- Going through the iterative design development process in order to obtain the final satisfactory result, in the form of a new dynamic design, incorporating the elastomeric core.

- Subjecting selected materials for the elastomeric core to quasi-static compression tests, in order to choose the most appropriate one.

- Verifying the design in terms of its intended function by both: producing rapid prototype models and finite element analysis (FEA).

The following sections of this chapter present the development process and a final design of a novel dynamic PEEK-on-PEEK intervertebral disc replacement for the cervical spine (CDyn).

3.2   Methodology - TRIZ

In developing the new device, the Theory of Inventive Problem Solving (TRIZ) methods were applied at various stages of the design process. TRIZ is a methodology developed by the Russian scientist and engineer Genrikh Altshuller (Gadd, 2011; Altshuller, 2004). After years of studying approximately 400,000 proven, successful patents, Altshuller discovered regularities and basic patterns in the process of solving problems, and creating new ideas. In general, TRIZ is based on three pillars: analytical logic, knowledge-based philosophy and a systematic way of thinking (Souchkov, 1999). Over the years Altshuller's approach has been extended with new techniques, tools and methods, which help engineers define, understand and solve future problems, supporting them in a development process.

In general, TRIZ provides very useful tools to help focus on the problems in hand and arrive at solutions quicker and easier than the more traditional methods such as brainstorming. Figure 3.1 shows a simplified flowchart, illustrating how the TRIZ toolkit works.
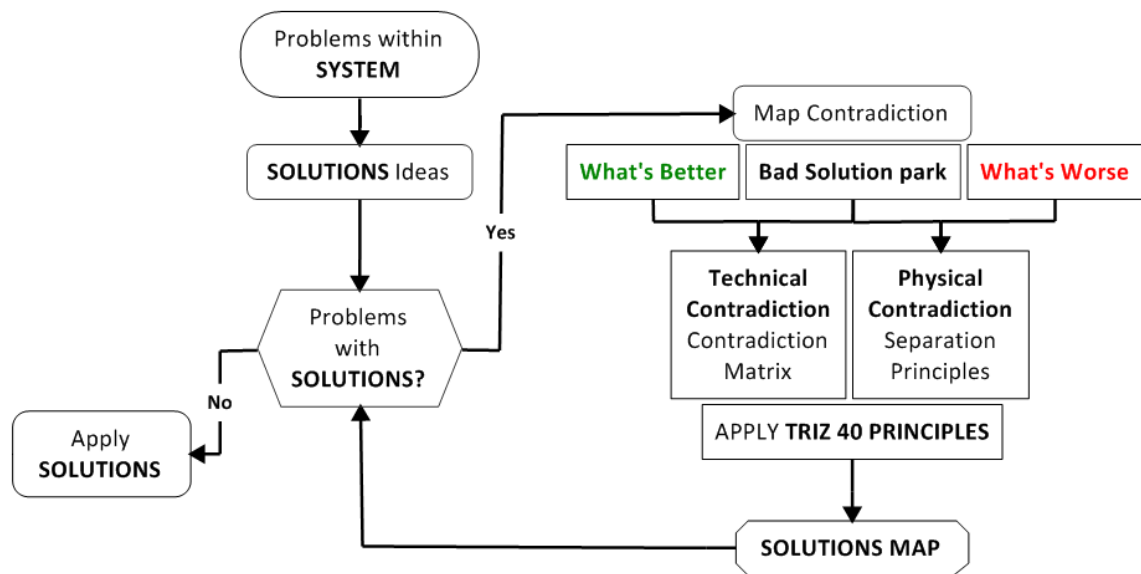
Figure 3.1 - The flowchart representing the TRIZ problem-solving process

(Adapted from Gadd, 2011).

As shown on the flowchart, any occurring problems within system need to be defined first. In case of a CDyn device, in order to provide a cushioning effect and thus better imitate the natural disc, a design based on an elastomeric core, was proposed. The next step in the TRIZ problem-solving process is to establish any problems with the proposed idea and, depending on the result, either the proposed solution is applied or attempts are made to identify contradictions. In general, TRIZ distinguishes two types of contradictions - technical and physical. Technical contradictions occur when by improving certain functions of the system, other functions get worse. Physical contradictions appear when opposite solutions or benefits are desired simultaneously, for example, both hot and cold temperatures. In case of the new device, although the idea of using elastomeric core seemed good, several problems associated with it were quickly discovered. First, the elastomer itself, besides axial compression, did not provide sufficient mobility, characteristic for the cervical spine. Moreover, there was a problem of an unwanted friction between the elastomer and both upper and lower plates of the device. Friction could have both prematurely damage the elastomer and lead to a systematic

loss of material. As a result, an elastomer would lose its viscoelastic properties and the entire device would cease to function as intended. Therefore, the main problem was to simultaneously provide greater mobility, as well as the protection of the elastomer against the adverse effects of friction. This issue has been identified as a physical contradiction, as elastomer is required to be present for the axial compression and absent for the mobility (friction). Physical contradictions can be solved using TRIZ Separation Principles presented in Table 3.1, by separating the solutions in different ways resulting in obtaining both.
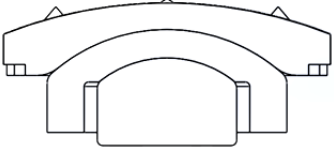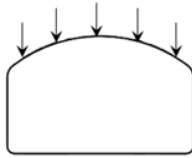
Table 3.1 - Separation Principles - a tool for solving Physical Contradictions.

Separate In Time	One solution at one time, the opposite solution at another
Separate In Space	One solution at one location, the opposite solution at another
Separate On Condition	Opposite solutions in the same place and at the same time ➢ One solution for one element – the opposite for another
Separate By System	Separate by scale (to sub-system or super-system) Switch to inverse system Switch to another system

Each separation principle offers set solution options from the 40 Inventive Principles, which are a list of known solutions and a major TRIZ tool for solving both types of contradictions. They may serve as triggers for solutions and using the experience and knowledge of the user, can then be turned into practical ideas. To identify the right separation principle to apply to the problem, it is important to understand the nature of the opposite demands being placed on the system. Table 3.2 shows the example of solving Physical Contradiction in the context of the CDyn device. While solving the contradiction the Separation in Space principle was used, this then led to a few proposed Inventive Principles. After careful analysis, the Segmentation

principle was applied, allowing the division of the object into more independent parts. As a result, it was possible to combine axial compression with greater mobility, as well as protect the elastomer against unwanted friction.

Table 3.2 - The example of solving Physical Contradiction associated with CDyn device.

Identified Physical Contradiction	Elastomeric core present for axial compression but absent for greater mobility (friction)	
TRIZ Separation Principle	**Separate in Space** (One solution at one location, the opposite solution at another)	
Applying "40 Inventive Principles"	**Suggested Inventive Principles for Separate in Space:** 1 Segmentation* 2 Taking Out 3 Local Quality 4 Asymmetry 7 Nested Doll 13 The Other Way Round 14 Curvature 17 Another Dimension 24 Intermediary 26 Copying 40 Composite Materials *chosen Inventive Principle*	

The process of solving encountered contradiction using TRIZ Separation Principles and 40 Inventive Principles is also mentioned in section 3.4.5.

3.3   Design Requirements

The design requirements for a dynamic intervertebral disc replacement for cervical spine were

formulated in accordance with BS EN ISO 14630 (2012) and are presented in Table 3.3.

Table 3.3 - Design requirements for a dynamic intervertebral disc replacement for cervical spine.

	Design Requirement	Justification
Geometry	Match a rectangular footprint of the average lower vertebrae	To satisfy anatomical requirements. Explained in detail in section 3.4.2.
	Minimum disc height of 5 mm	According to surgeon, it is an average height of the smallest intervertebral disc that should be preserved by the device.
	Lordosis of 5°	To satisfy anatomical requirements.
	Scalable for future development	Industrial viewpoint - to satisfy individual anatomical requirements.
Biomechanics	Maintain segmental stabilisation following discectomy	To stabilize the treated level and improve patient's well-being.
	Preserve range of motion of approximately 10^0 in lateral bending and flexion-extension	To maintain the mobility of the natural disc (Panjabi et al., 2001), as contrary to fusion. In this case, this will be ensured by using the ball-on-socket connection.
	Withstand compression forces of up to a maximum of 1200 N	According to literature the load in cervical segment can in some cases (contact sport, heavy lifting) reach up to a maximum of 1200 N (Vicars et al., 2011). Therefore, it is treated as a worst case loading scenario, which the device should withstand.
	Provide axial compression	To maintain the mobility of the natural disc, with the use of an elastomer in this particular case.
	Produce minimal debris	To not release too many particles into the body of the patient, which may pose a health risk and to ensure long durability.

Material	Manufactured from biocompatible materials	To do not induce the inflammatory response and pose a risk for a patient. Therefore, PEEK and elastomers were chosen as they meet the demanding quality and biocompatibility requirement.
Surgical procedure	Not increase surgery time (~100 min)	To not cause an additional trauma for the patient (Ghori et al., 2016).
	Allow for easy implantation - Not highly invasive (small incision, low bone resection) - Anterior approach - Implantable as a one-piece	The process of implantation should not be more invasive than a fusion procedure, and at the same time comfortable to surgeons.
	Allow revision surgery	To enable safe removal of the device, when necessary (Mcafee, 2005).
	X-ray compatible	Important during implantation procedure and later follow-up, to enable post-operative observation.
	Have efficacy and complication profiles equal to or better than ACDF	Industrial viewpoint - to quicken patient's recovery and reduce the health costs.
Fixation to the vertebra	Provide primary anchorage	To keep the device in place directly after the implantation and prevent device migration. The proposed solution, in this case, involves low-profile, inclined teeth present on the outer surfaces of both plates.
	Provide long-term fixation	For the device to work properly, a permanent connection must be established between the outer surfaces of both plates and the vertebrae. Therefore, the bone-contacting surfaces of the plates are designed to be either hydroxyapatite or plasma titanium-coated.
Patient	Not cause harm to the patient	To improve patient's well-being.
	Relieve pain (preserve decompression of the nerves)	To improve patient's well-being.

Fail safety	Have long-term durability (~25 years)	Made from durable materials and be characterized by a construct that will prevent early removal of the device. Intended as a single-use device.

During the process of formulating the design requirements, the emphasis has been on ensuring the viscoelastic properties of the disc. This can be achieved by introducing an elastomeric core enclosed inside the device. It may help to protect the adjacent spinal segments from degeneration and distinguish the device from those available on the market today.

3.4 Design Development

3.4.1 Design Solutions

Through the course of the design development process, the prototype of CDyn underwent multiple changes. The project development strategy assumed the continuous progress, in which modifications were made in an iterative manner. The introduced changes generated subsequent versions of the project shown in Figure 3.2.

| Version 1 | Version 2 | Version 3 |
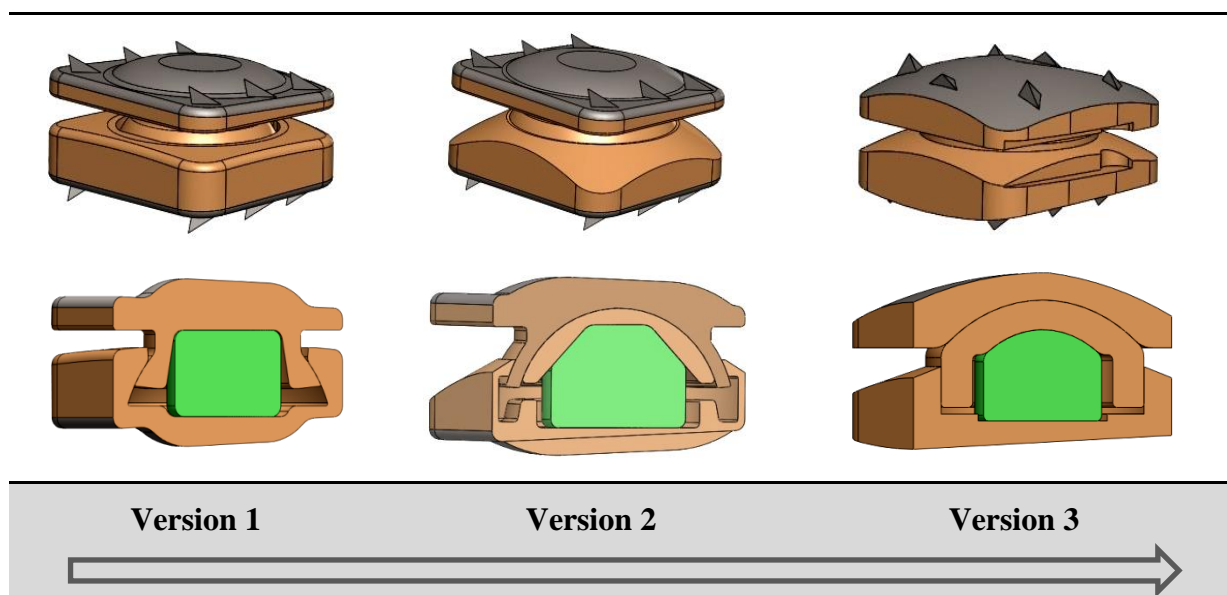
Figure 3.2 - Evolution of CDyn design.

The brief description of advantages and disadvantages of the three subsequent versions of the CDyn device are presented below.

Version 1

Version 1 consisted of three elements: upper and lower plate, made of PEEK 450G, and a cylindrical deformable core. Both plates were designed to be assembled together, securely enclosing the core. This version is closely based on the initial design concept provided by the company S14 Implants (Pessac, France). However, the company did not consider that their initial device fully exploited design strategies to maximise the effectiveness of the device for future clinical applications. Therefore, further attempts were made to modify the design in accordance with the design requirements, imposed by both the company and the surgeons. Both the advantages and disadvantages of this particular version are presented below.

Advantages:

1- The device consists of only three main parts (upper and lower plate and an elastomeric core).

2- Upper and lower plates are assembled together, eliminating the risk of their separation (Figure 3.3).

3- Axial compression is provided by the elastomeric core.

Disadvantages:

4- Mobility is entirely based on the deformable core, once the flexible core loses its properties due to fatigue, the whole device loses its mobility.

5- External geometry of the plates is designed as a flat surface, which can result in an insufficient contact area between the vertebrae and the device.

6- Flexible core is in direct contact with rigid parts of the device, exposing it to unwanted friction, which in the long run could irreversibly damage it.
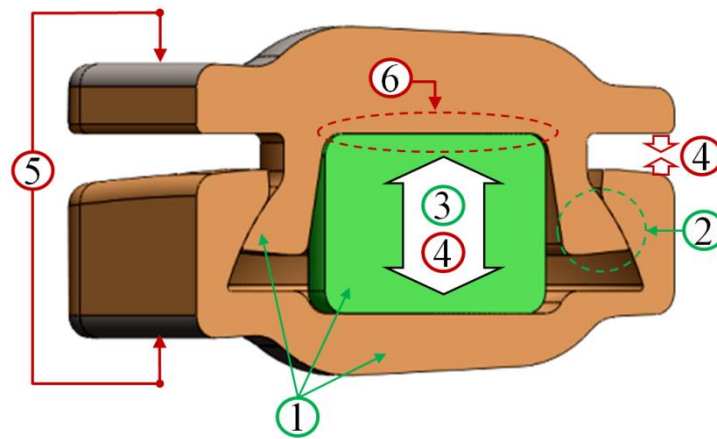
Figure 3.3 - Advantages (green) and disadvantages (red) of Version 1.

Version 2

In this version, the ball part (made of PEEK 450G) was added in order to increase the range of motion by introducing the ball-on-socket connection and additionally to protect the core from unwanted friction. The shape and size of the deformable core changed in order to enlarge the loading surfaces and to better accommodate the ball part.

Advantages:

1- Mobility is based on ball-on-socket connection. The device sustains the flexion-extension, lateral bending and axial rotation motion even when the flexible core loses its properties.

2- Axial compression is provided by the elastomeric core.

3- Elastomeric core is protected from unwanted friction by an additional part (the ball).

Disadvantages:

4- External geometry of the plates is designed as a flat surface, which can result in an insufficient contact area between the vertebrae and the device.

5- Upper and lower plates are not securely assembled together, creating the risk of their separation.

6- The possibility of an unstable connection between the lower plate and the ball part under non-axial compression forces.

7- Some parts of the assembly are prone to high-stress concentrations (Figure 3.5).
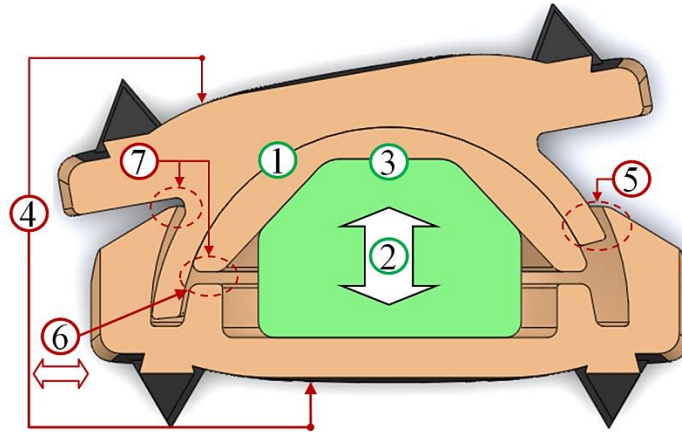
Figure 3.4 - Advantages (green) and disadvantages (red) of Version 2.

Figure 3.5 shows the example of the Version 2 geometry verification using finite element analysis. The design had been subjected to axial compression under the load of 1200 N and the whole setup along with the loading and boundary conditions corresponded to the scheme shown in section 3.6.2.
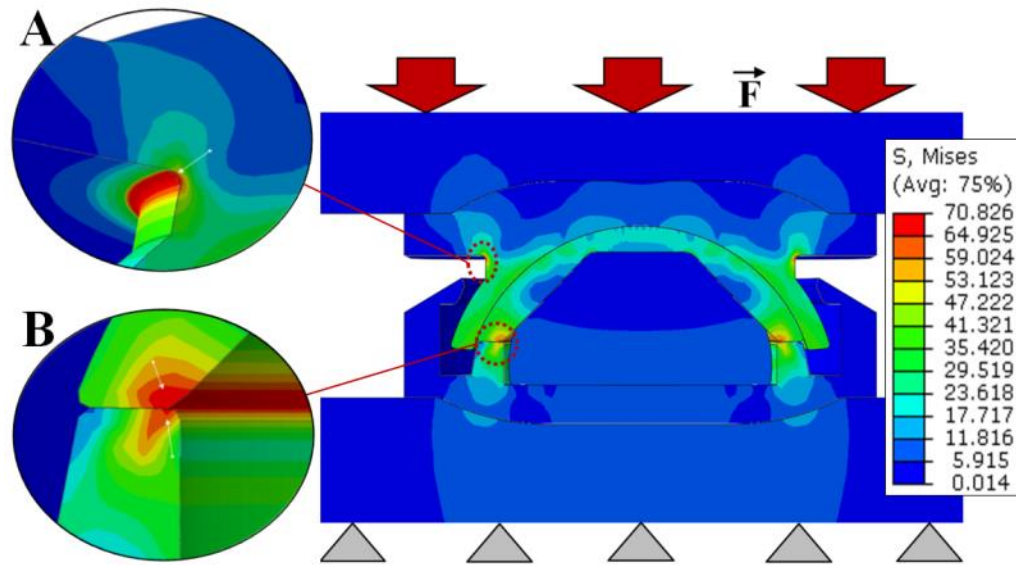
Figure 3.5 - The finite element analysis for the Version 2. A - Stress concentration in the neck region of the upper plate; B - Stress concentration at the connection between lower plate and the ball part.

Figure 3.5 shows that under high compressive load the neck region of the upper plate and the point of contact between the lower plate and the ball (highlighted in A & B in Figure 3.5) are prone to high-stress concentrations. Moreover, as it is illustrated by point "6" in Figure 3.4, the connection between the lower plate and the ball may be susceptible to a horizontal slippage, especially under high non-axial compression forces, which makes this idea not desirable. The overall evaluation established that this version was at high risk in terms of stress concentrations.

Version 3

The device has been subjected to further modifications. In this version, the shape and size of the ball part have undergone further development in order to better transfer and distribute the loading and form a more stable connection with a lower plate. The shape of the deformable core changed again to better accommodate the ball part. The external shape of the upper and lower plates, as well as their mutual interaction, has also been modified (Figure 3.6).

Advantages:

1- Mobility based on a ball-on-socket connection (device sustains the flexion-extension, lateral bending and axial rotation even when the flexible core loses its properties).

2- Axial compression is provided by the elastomeric core.

3- Elastomeric core is protected from unwanted friction by an additional part (the ball).

4- External geometry of the plates is designed to better fit the geometry of vertebral bodies.

Disadvantages:

5- Upper and lower plates are not assembled together, creating the risk of separation.
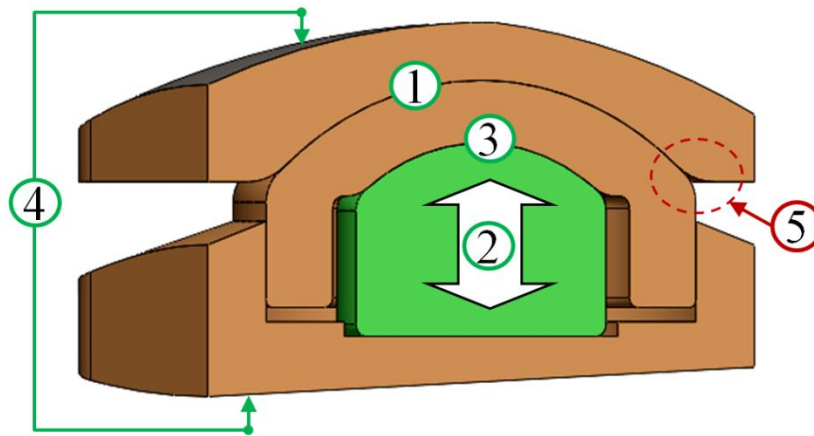
Figure 3.6 - Advantages (green) and disadvantages (red) of Version 3.

The modification process eventually stopped on the third version of the CDyn device, which was considered a good enough solution, based on the obtained FEA results.

The upcoming sections (3.4.2 - 3.4.5) present in detail the development process of each element of the device.

3.4.2   Upper and Lower Plates

Both upper and lower plates of the device have a rectangular footprint, to cover the largest possible area of the bony endplates (Figure 3.7). Both the shape and dimensions of the footprint are determined by anatomical characteristics of the cervical vertebrae.
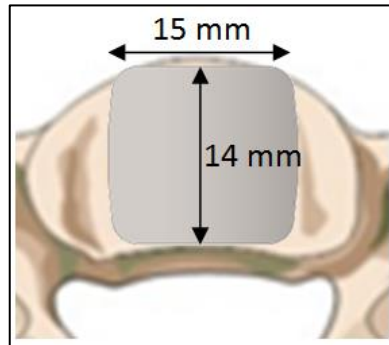
Figure 3.7 - Shape and dimensions of CDyn device footprint.

The chosen dimensions of 15 mm (width) and 14 mm (anterior-posterior diameter), for the smallest footprint, were based both on the dimensions used by cervical disc manufacturers and the results obtained by Thaler et al., (2013) and Lou et al., (2016). Thaler et al. showed in their study that footprint mismatch in a cervical arthroplasty is still a pressing issue and encouraged total disc manufacturers to enlarge their footprints to minimise the incompatibility. Therefore, the dimensions and an external shape of the plates were adjusted to match the average cavities and profiles of the vertebral body's endplates (Figure 3.8) (Lou et al., 2016). The modifications were intended to improve the load distribution and, as a result, lower the possibility of device breakage and subsidence into the immediate neighbouring vertebrae.

	Front view	Side view
Upper Plate	R = 20.44 mm	
Lower Plate	R = 40 mm	
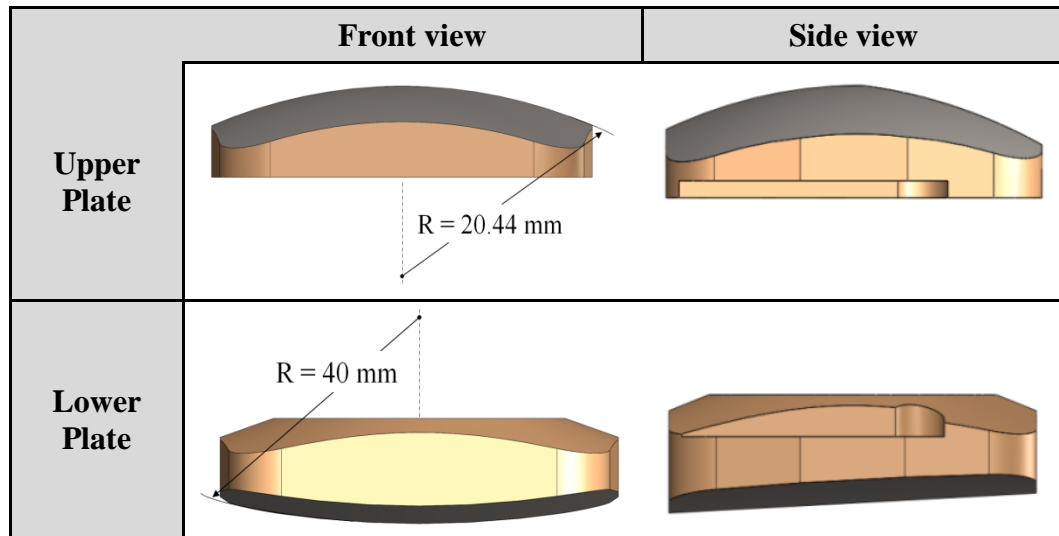
Figure 3.8 - Illustration of shapes and angles of both plates.

In order to increase the range of motion of the implant and minimize the risk of plate collision, the surface of the lower plate was modified. As shown in Figure 3.9, a radius of curvature was added across the surface of the lower plate in order to enlarge the clearance between both plates.

SURFACE MODIFICATION
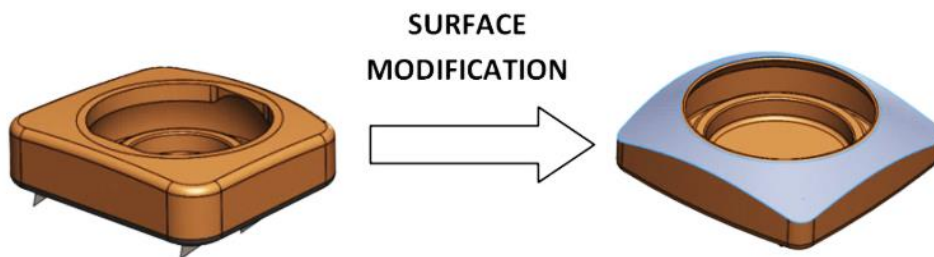
Figure 3.9 - Surface development of the lower plate.

Figure 3.10 illustrates the difference between initial and modified design of the lower plate and its influence on the interaction with the upper plate.

<div align="center">a)   b)</div>
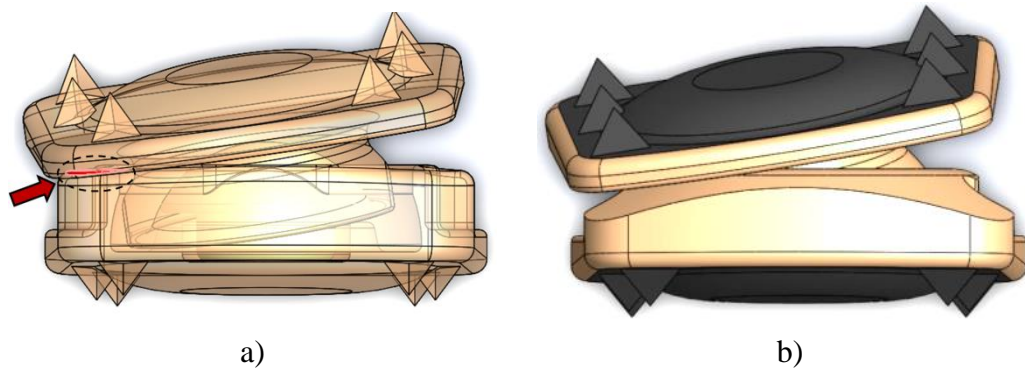
Figure 3.10 - a) Plates collision point (red arrow); b) Modified version of the lower plate.

To ensure primary anchorage of the device and, therefore, prevent migration, teeth were designed on the outer surfaces of both plates (Figure 3.11). The CDyn design eliminates features such as keels and screws found in other devices, thus enabling a bone-sparing surgical technique (Lin et al., 2009).
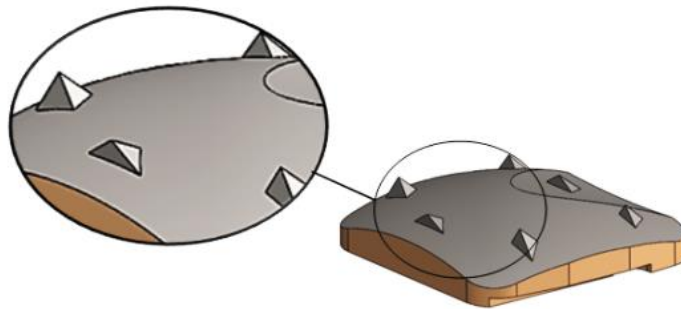
Figure 3.11 - Anchoring teeth.

3.4.3   Flexible Core

The flexible core is the main part of the new cervical disc replacement device. When designing the compliant core, it was important that the material had good fatigue properties and could be characterized by biostability and biocompatibility. Elastomers are the materials that can potentially meet these requirements. Elastomers have a long history of medical application and have the ability to deform under compressive stress and then recover to their original state when the stress is removed (Chen et al., 2013). These materials are also known

for their viscoelasticity, which is the ability to simultaneously store and dissipate energy via time-dependent, large strain behaviour. One of the factors that affects the way an elastomer deforms in compression is its shape. The shape factor (S) is calculated as a ratio of loaded area to force-free area (equation 3.1). The concept of shape factor is useful during the design process. If the elastomeric part deflects too much the shape factor can be increased by reducing the area free to bulge. For this reason, the elastomeric part of CDyn evolved during the design process from a simple cylinder to a dome shape (Figure 3.12).

$$S = \frac{(Loaded\ area)}{(Area\ free\ to\ bulge)} \qquad (3.1)$$
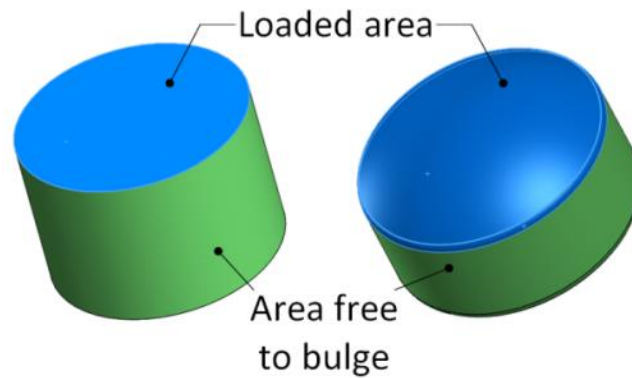
Figure 3.12 - Shape factor of an elastomeric part.

The shape factor for the cylindrical version of the elastomer was calculated from equation 3.2.

$$S_1 = \frac{\pi r^2}{2\pi r \times H} \qquad (3.2)$$

where, r is the radius of the base (3 mm) and H is the height of the cylinder (4 mm) (Figure 3.13a).

For the new proposed shape of the elastomeric part (dome shape), the shape factor was obtained using equation 3.3.

$$S_2 = \frac{2\pi R_2 \times h_2}{2\pi r_2 \times H_2} \tag{3.3}$$

where r_2 (3.34 mm) and R_2 (5 mm) are the radii of the base of the cap and the sphere, respectively. The h_2 (1.39 mm) and H_2 (2.61 mm) are the heights of a cap and the cylindrical part, respectively (Figure 3.13b).

a)   b)
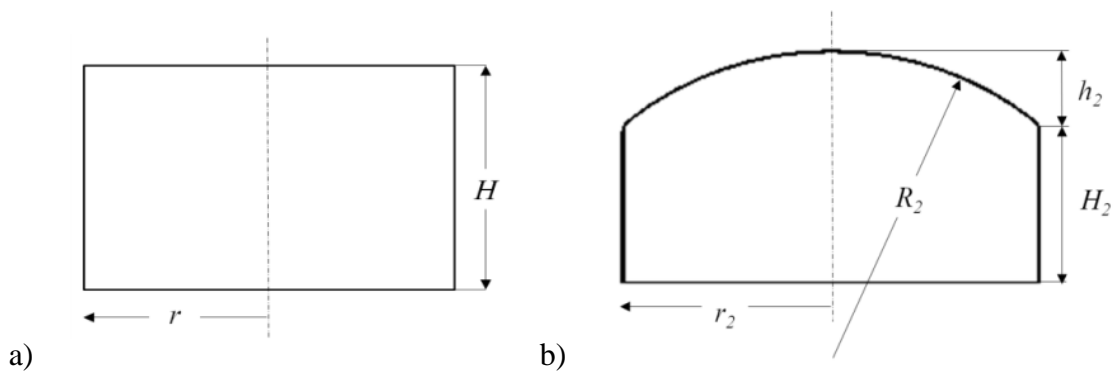
Figure 3.13 - Schemes of elastomeric parts: a) cylindrical version; b) dome-shaped version.

The calculations showed that $S_2 > S_1$, therefore, the new proposed shape of the elastomeric part should deflect less than a simple cylinder.

The other way to increase the shape factor and by default prevent excessive deformation of the elastomer is by increasing its hardness. Therefore, a few different elastomeric materials were proposed for the flexible part and will be described in the following section.

3.4.4   Flexible Core Material Selection

The previous section presented the change of the deformable core's shape factor, by changing its geometry. However, the core's susceptibility to deformation can also be altered by changing the material. In this section, the focus will be directed on the selection of the suitable type of the elastomer, as it turned out to be one of the most challenging tasks in the design process. The S14 Implants had previous experience with elastomers, as they used them in their earlier product, therefore based on their knowledge and experience, a few potential

materials characterized by different hardness and chemical structure were selected and compared via preliminary mechanical tests. Chosen materials represent silicone elastomers (MED 4770 and 4780), a family of polycarbonate-based silicone elastomers (ChronoSil) and a family of polyurethane-based silicone elastomers (Elast-Eon). Due to chemical structure, these materials combine the properties of silicones, such as increased elongation, flexibility and low coefficient of friction, with the advantages of urethanes and polycarbonate-based urethanes, such as high pressure strength and tensile strength. Moreover, they had been specifically engineered, to meet the demanding quality and biocompatibility requirement for the medical device market and are adaptable to most standard manufacturing processes.

3.4.4.1   Quasi-Static Compression Test

Five elastomeric materials, which were injection moulded by STATICE SANTÉ (Besançon, France) were used in this study (Table 3.4). The materials underwent preliminary quasi-static compression tests in order to verify their performance.

Table 3.4 - Elastomeric materials tested in quasi-static compression: MED 4770 - high consistency silicone elastomer, MED 4780 - high durometer silicone elastomer, ChronoSil - silicone-polycarbonate-urethane co-polymer, Elast-Eon - silicone polyurethane co-polymer.

Material	MED		ChronoSil		Elast-Eon
	4770	4780	5%	10%	
Durometer Hardness	70A	80A	80A		82A
Silicone ratio (%)	N/A		5%	10%	N/A
Density (g/cm^3)	1.21	1.16	1.13	1.12	1.08
Supplier	NuSil^{TM}		AdvanSource Biomaterials		Formulance
Ultimate Tensile Strength (MPa)	9.8	8.0	22.75 - 48.26		23
Tear Strength (kN/m)	52.9	39.7	N/A		60
Shape Factor	0.375				

Tests were performed using a BOSE ELF 3300 machine (Bose Corporation, ElectroForce Systems Group, Minnetonka, MN, USA) (Figure 3.14a) in accordance with ASTM D695 (2011). Investigated specimens had a cylindrical shape with a height and diameter of 4 mm and 6 mm, respectively (Figure 3.14b).

a)   b)
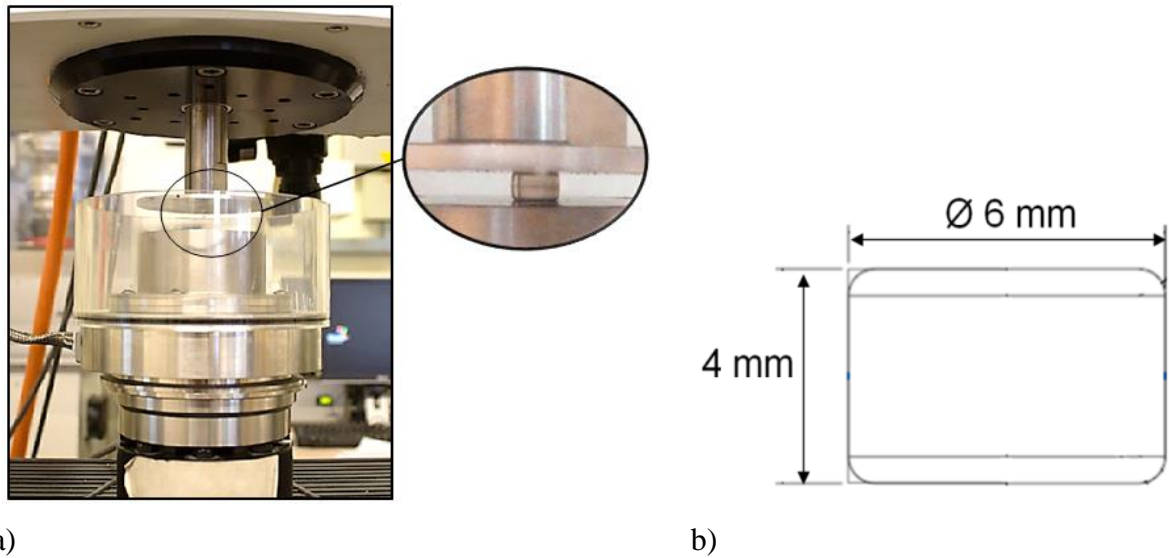
Figure 3.14 - a) BOSE ELF 3300 machine with a specimen during compression;

b) geometry of the specimen.

During tests, the displacement rate was set to 0.02 mm/s and the maximum displacement was equivalent to approximately 75% of the specimen's height (3 mm). The sample dimensions (diameter and height) were measured before and after each test, in order to gain information about the shape recovery.

3.4.4.2   Results

Throughout the experiment, all specimens deformed due to the high maximum displacement load. During the tests, previously cylindrical specimens adopted the shape of a barrel, with an example shown in Figure 3.15.

a) Before testing   b) After testing
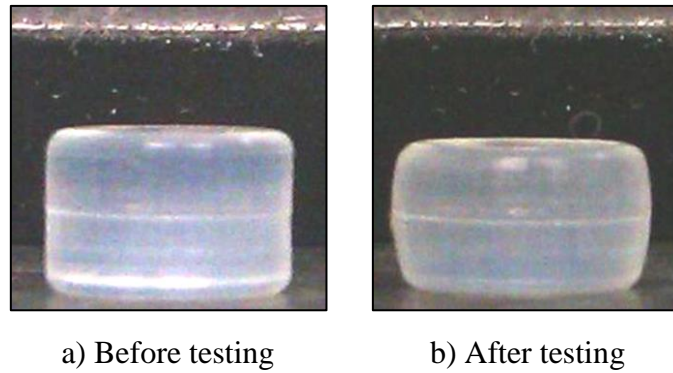
Figure 3.15 - Deformation of a MED 4780 specimen.

The force-displacement curves recorded for all tested materials are shown in Figure 3.16. In accordance with the requirements of specialists from S14 Implants (Pessac, France - company cooperating on the project), an appropriate elastomer for the cervical spine application has to withstand spinal compressive loads of at least 200 N, without exceeding more than 1 mm deformation. Members of the company have based their knowledge on the surgeons' experience, who claimed that the natural disc is deforming to this extent under a usual load (~200 N).
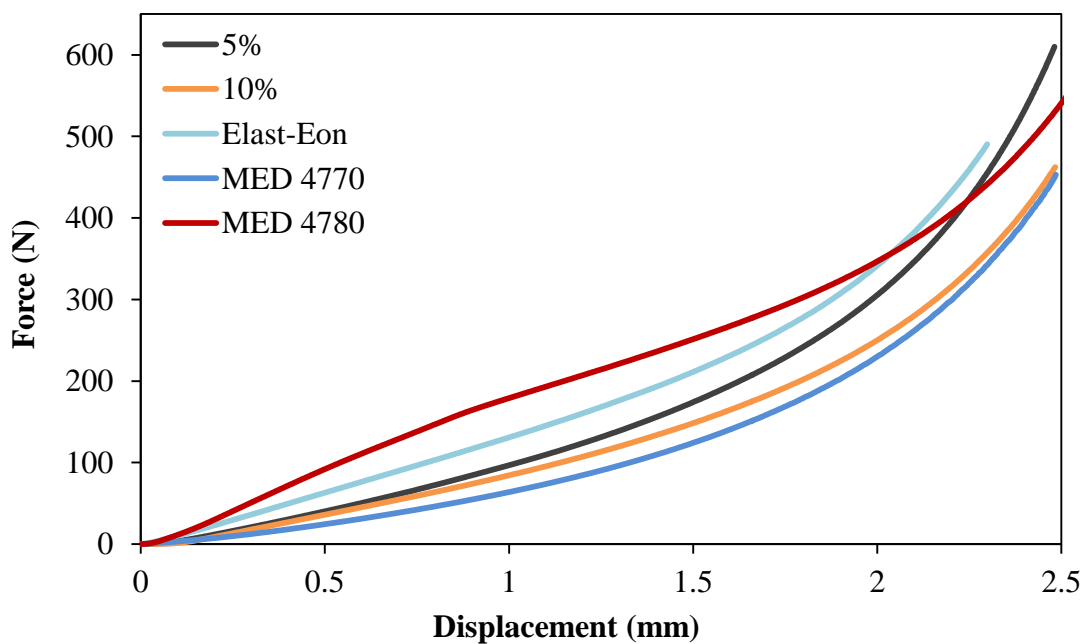
Figure 3.16 - Force vs. displacement trends for all tested materials.

Table 3.5 shows the mean results of displacement at 200 N, stiffness (defined as the slope of the initial linear part of the force/displacement curve) and Young's modulus (defined as stress/strain) calculated for all tested materials after compression testing.

Table 3.5 - Mean (± SD) displacement at 200 N, stiffness and Young's modulus (*E*) values of all tested elastomers.

| | **MED 4770** | **MED 4780** | **ChronoSil** | | **Elast-Eon** |
			5%	**10%**	
Displacement at 200 N (mm)	1.889 ± 0.001	1.148 ± 0.001	1.626 ± 0.001	1.789 ± 0.001	1.441 ± 0.251
Stiffness (N/mm)	70.2 ± 3.7	148.7 ± 4.0	109.2 ± 2.4	101.4 ± 1.8	134.5 ± 1.2
E (MPa)	11.3 ± 0.4	30.2 ± 0.8	16.5 ± 0.2	14.7 ± 0.2	19.0 ± 0.2

The results of the tests show that the highest values of both stiffness and Young's modulus were obtained for MED 4780. On the other hand, MED 4770 turned out to have the lowest stiffness. Out of all tested materials, MED 4780 was the closest to meeting the predefined design requirements and did not deform significantly under the load of 200 N. The material exceeded the value of 1 mm by only 14.8%. Table 3.6 shows the height and diameter values of the specimens measured before and after testing.

Table 3.6 - Mean (± SD) height and diameter of the specimens before and after the compression test.

	Initial deformation of specimens			
	Before		After	
	Height	Diameter	Height	Diameter
MED 4770	4.000 ± 0.001	5.996 ± 0.007	3.843 ± 0.037	6.090 ± 0.019
MED 4780	4.003 ± 0.009	6.003 ± 0.009	3.688 ± 0.035	6.272 ± 0.044
ChronoSil 5%	3.92 ± 0.01	5.98 ± 0.02	3.67 ± 0.05	6.13 ± 0.05
ChronoSil 10%	3.79 ± 0.02	6.09 ± 0.01	3.51 ± 0.11	6.32 ± 0.09
Elast-Eon	3.95 ± 0.01	5.98 ± 0.01	3.82 ± 0.01	6.09 ± 0.02

After initial compression, the heights of MED 4770 and 4780 specimens were approximately 96% and 92% of the original height, respectively. For ChronoSil 5% and 10% samples, the heights were 94% and 93%, respectively. Finally, for the Elast-Eon specimens, the height was approximately equal to 97% of the original height. The results show that all samples have not fully recovered in height after the initial deformation.

3.4.5   The Ball-on-Socket Connection

The biggest challenge, associated with the CDyn design, was to simultaneously ensure mobility and axial compression, at the same time minimising the friction between the elastomer and the plates (Figure 3.17a). It was also important to enclose the elastomeric core securely inside the housing, to protect it from tissue and exposure to body fluids.

a)   b)
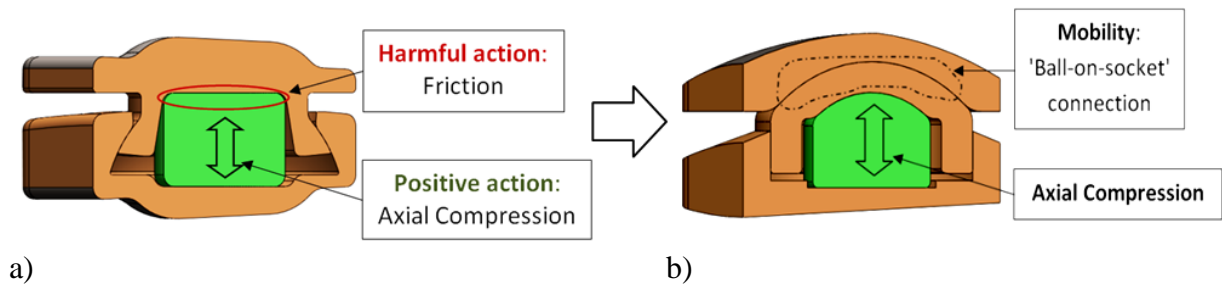
Figure 3.17 - a) Uncovered harmful and positive actions; b) Axial compression and mobility combined.

In this case, the tools offered by TRIZ proved to be particularly useful. While analysing the problem and its potential solutions, the following TRIZ Physical Contradiction was revealed: The elastomeric core needed to be present to allow axial compression, but absent for mobility to avoid friction. Such a Physical Contradiction leads to the question: 'Do we need these opposites at the same time and in the same place?' The answer is negative which means that we can try to separate the opposite parameters to have them both but either at a different time or in a different place. To solve this problem the TRIZ concept of *Separation in Space* was applied. Essentially it means that one solution is needed at one location and the opposite solution at another. The suggested Inventive Principles for Separation in Space include (1) Segmentation, (2) Taking Out, (4) Asymmetry, and (40) Composite Materials. In this particular case, *Segmentation* was chosen as a relevant solution for the physical contradiction. Applying Segmentation enabled the combination of axial compression provided by the elastomer with mobility provided by the 'ball-on-socket' connection (Figure 3.17b).

3.4.5.1   Theoretical Contact Stresses of the Ball-on-Socket Connection

The CDyn, which is a PEEK-on-PEEK articulating device, adopted the conventional ball-on-socket mating configuration with the radius of both the ball and the socket, defined as R_1 and R_2, respectively (Figure 3.18).
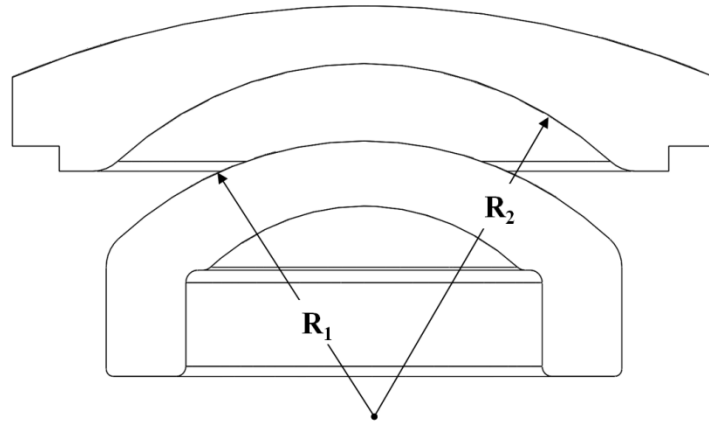
Figure 3.18 - Schematic view of the CDyn's 'ball-on-socket' connection.

R_1 - Radius of the ball (mm); R_2 - Radius of the socket (mm).

The next step involved investigating the possible operating conditions of such configuration as well as the effect of radial clearance between the ball and socket, defined as:

$$c = R_2 - R_1 \qquad \qquad (3.4)$$

where:

   c - radial clearance;

   R_1 - radius of the ball;

   R_2 - radius of the socket.

Therefore, a theoretical analysis of the maximum contact stresses occurring between the cooperating parts was carried out. For this purpose, a fully elastic Hertzian model was used, which allowed for investigation of the stress between the parts as a function of their shape, material properties and loading conditions (Goryacheva, 1998). Table 3.7 presents the parameters and their values that were employed during the analysis.

Table 3.7 - Parameters used in the contact stress analysis.

Parameter	Value		
Load, F (N)	150 - 1200		
Radius of the ball, R_1 (mm)	8		
Radial clearance, c (mm)	0.05	0.1	0.7
Young's modulus, E (GPa) (PEEK 450G)	3.7		
Poisson's ratio, v (PEEK 450G)	0.36		

The Hertzian contact model, applied in this study, neglected the surface adhesion forces within the contact area (Faghihnejad and Zeng, 2013) and was based on the following assumptions (Dintwa et al., 2008):

- The strains are small and within the elastic limit.

- The area of contact is much smaller than the characteristic radius of the body.

- The surfaces are continuous and non-conforming.

- The bodies are in frictionless contact.

Technically the Johnson-Kendall-Roberts model, which takes the adhesion force into account (Myshkin and Kovalev, 2009) could be used instead. However, Xin et al., (2012) showed in their study that there is no significant difference between these two models in case of PEEK because of its negligibly small surface energy (0.044 J/m^2).

According to the Hertz model the maximum contact stress P_{max} between the bearing surfaces was calculated from:

$$P_{max} = \left[\frac{(6FE'^2)}{(\pi^3 R^2)}\right]^{\frac{1}{3}}$$

(3.5)

where:

F - Applied force;

E' - Equivalent Young's modulus for the two bearing materials;

R - Equivalent radius for ball and socket.

The parameters E' and R, were calculated from:

$$E' = \frac{E}{2(1 - v^2)}$$

(3.6)

and

$$R = \frac{R_1(R_1 + c)}{c}$$

(3.7)

Figure 3.19 shows the variation of maximum contact stress (P_{max}) under different loads and radial clearance values for the CDyn device. Under the highest load of 1200 N, the P_{max} is in the range of 8.6 MPa (for $c = 0.05$ mm) to 47.3 MPa (for $c = 0.7$ mm). Under the lowest load of 150 N, the maximum contact stress, ranges between 4.3 MPa (for $c = 0.05$ mm) and 23.7 MPa (for $c = 0.7$ mm). The results indicate that the radial clearance of 0.05 mm provides the lowest contact stresses and, therefore, would be a good choice for the CDyn design.
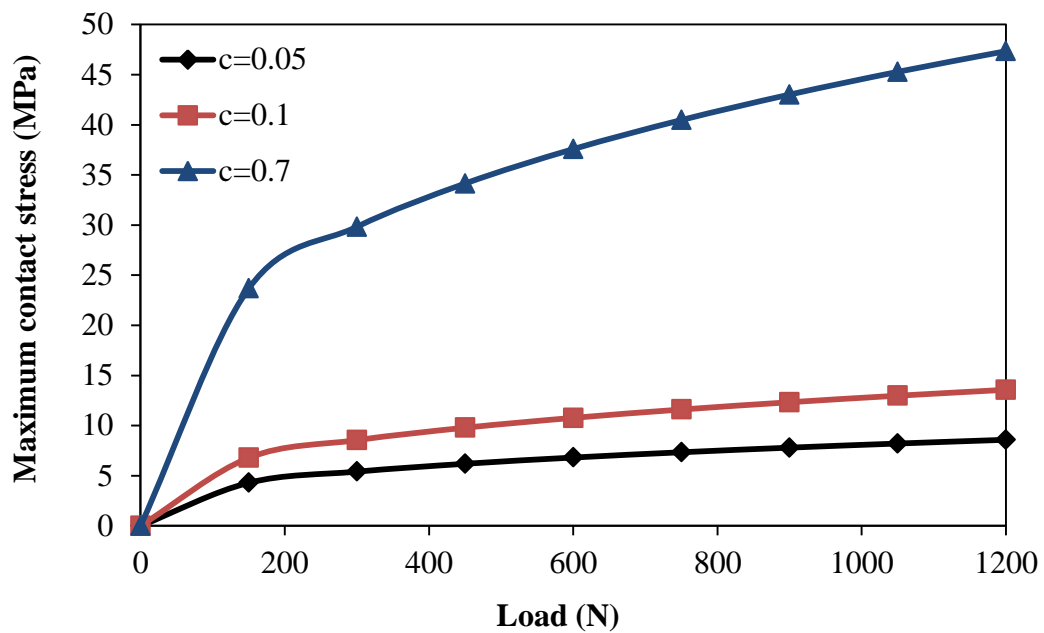
Figure 3.19 - Variation of the maximum theoretical contact stress with the load for different radial clearance values.

All maximum contact stress values obtained during analysis were far below the yield strength of PEEK 450G under compression, which is reported as 120 MPa (Victrex plc, 2009). Moreover, the fatigue strength of PEEK 450G with a crystallinity value of 22.5% was reported as 58.7 MPa, at 1 million cycles during the tension-tension fatigue (Bakar et al., 2003; Tang et al., 2004). Therefore, the obtained results show that the predicted stress experienced by the contact surface of the CDyn device will not result in material fatigue.

3.5   Final Design

3.5.1   Detailed Design

After taking into consideration all the design requirements and identifying the contradictions with the help of TRIZ, a concept CDyn device was proposed. The CDyn TDR is a PEEK-on-PEEK articulating device, which combines the conventional ball-on-socket configuration, as shown in Figure 3.20a, with a flexible core. With this solution, the device may better mimic the functionality of a natural disc. The final design is composed of four main parts: two plates and a bearing forming a curved surface (the ball), made of PEEK (Optima 450G), and a central elastomeric core (Figure 3.20b). The bone-contacting surfaces of the plates are designed to be either hydroxyapatite or plasma titanium-coated and feature low-profile, inclined teeth, designed to ensure plate fixation. Moreover, both plates incorporate a convex shape to match the natural cervical anatomy. According to the design requirements, the prosthesis is designed to provide a natural cervical lordosis of 5°.

a)   b)
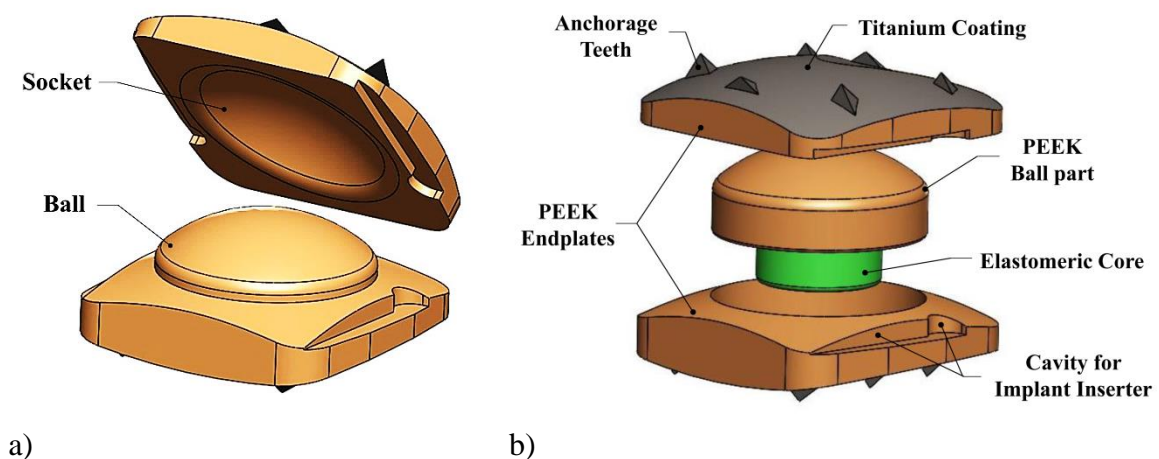
Figure 3.20 - a) 'Ball-and-socket' connection; b) Final design of the CDyn device.

The device allows four independent degrees of freedom flexion-extension, lateral bending, axial rotation and axial compression (Figure 3.21).

Presented in Table 3.8 is a summary of the range of movements offered by the CDyn device compared to individual segments of the cervical spine.

Table 3.8 - Range of motion for each cervical spine segment (Panjabi et al., 2001).

Disc segment	Flexion [°]	Extension [°]	Lateral bend [°]	Axial rotation [°]
C2-C3	3.5 ± 1.3	2.7 ± 1.0	9.6 ± 1.8	3.3 ± 0.8
C3-C4	4.3 ± 2.9	3.4 ± 2.1	9.0 ± 1.9	5.1 ± 1.2
C4-C5	5.3 ± 3.0	4.8 ± 1.9	9.3 ± 1.7	6.8 ± 1.3
C5-C6	5.5 ± 2.6	4.4 ± 2.8	6.5 ± 1.5	5.0 ± 1.0
C6-C7	3.7 ± 2.1	3.4 ± 1.9	5.4 ± 1.5	2.9 ± 0.8
CDyn	**10**	**10**	**8**	**Unrestricted**

a) Flexion-extension   b) Lateral bending

c) Axial rotation   d) Axial compression
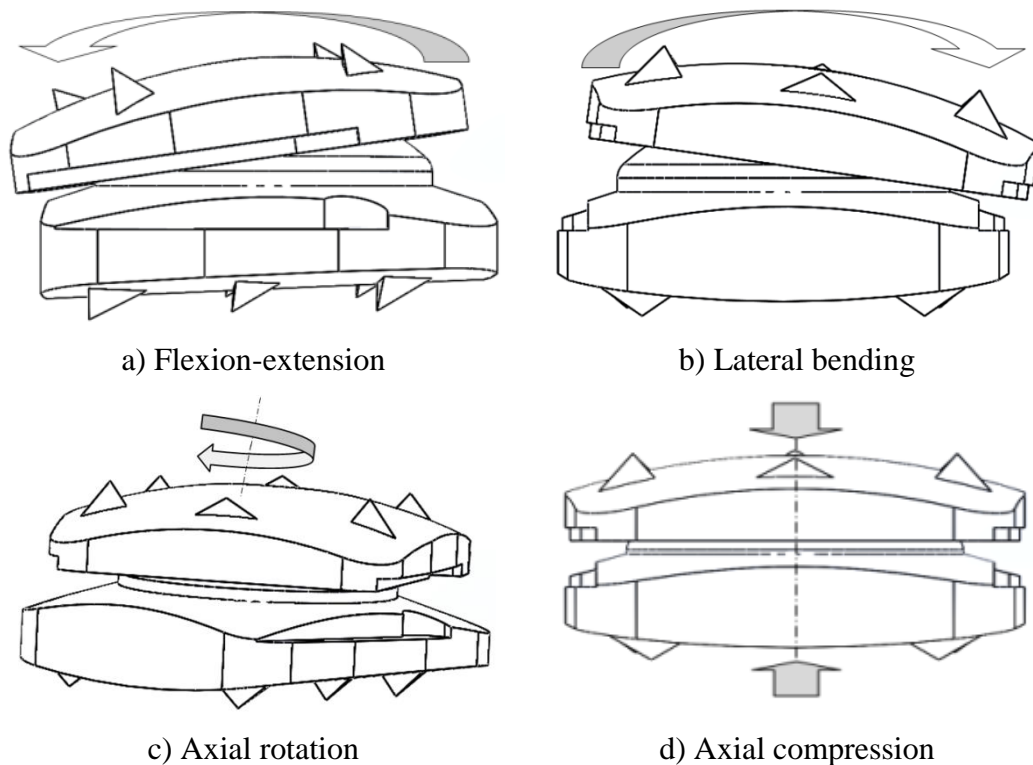
Figure 3.21 - CDyn device range of motion.

70

The CDyn device would be required to be available in a range of sizes to take into account the different cervical spinal levels and sizes of human vertebrae. In this study, the design was based on the smallest footprint size. The device had been adapted for insertion as one piece, through a small incision, using a standard anterior approach (Figure 3.22). Each part of the device was modelled using SolidWorks 2014 software (Dassault Systems SolidWorks Corp. MA, USA).
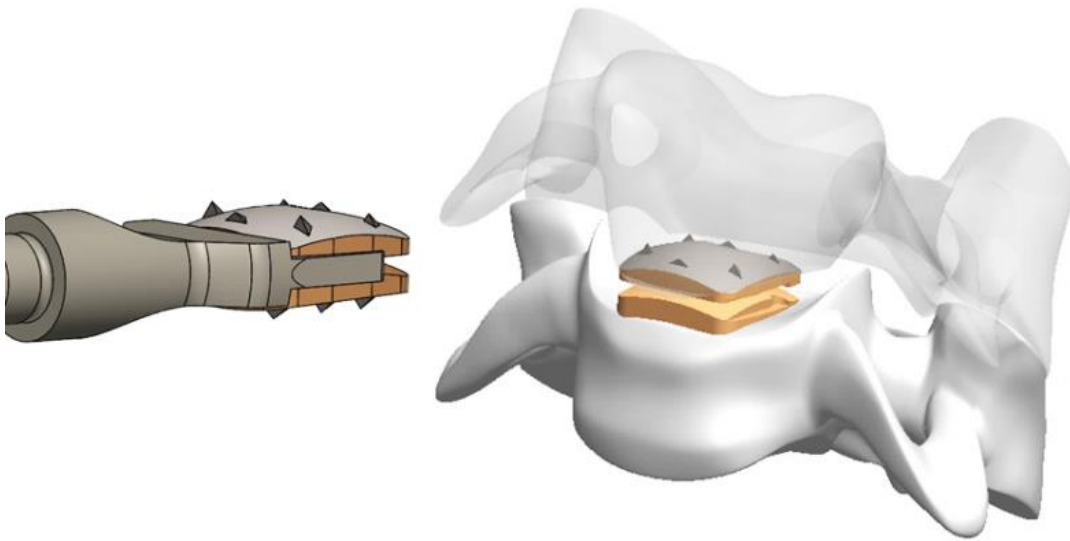
Figure 3.22 - Insertion of the CDyn device.

3.5.2   Failure Mode and Effect Analysis (FMEA)

In order to identify and minimise the hazards associated with the CDyn design, a Failure Mode and Effect Analysis (FMEA) was carried out in accordance with BS EN 60812 (2006). This allowed the identification of the high-level risks and provided a target for reducing them to an acceptable level as well as improving the design to enhance its safety. It is important to review the risk analysis regularly during the design development process.

According to the BS EN 60812 for each potential hazard associated with the device, there is the probability of damage occurring, represented by the occurrence (O), the consequences of this damage, represented by the severity (S) and the likelihood of detection of the damage (D). Each of these elements was rated on a scale from 1 to 5, for the hazards identified for the cervical device as shown in Table 3.9. The concept of assessed or resulting risk was based on risk priority number (RPN), which was calculated as:

$$RPN = Occurrence\ (O) \times Severity\ (S) \times Detection\ (D) \qquad (3.8)$$

Table 3.9 - Rating of occurrence, severity and detection levels.

Occurrence (O)		Severity (S)		Detection (D)	
Improbable	(1)	Negligible	(1)	Certain to be detected	(1)
Remote	(2)	Occasional discomfort	(2)	Almost certain to be detected	(2)
Occasional	(3)	Reversible effects	(3)	Easily spotted	(3)
Probable	(4)	Infection, irreversible injury	(4)	Unlikely to be spotted	(4)
Frequent	(5)	Death/ device will not function at all	(5)	Very unlikely to be detected	(5)

The results of the FMEA are presented in Table 3.10. It can be observed that the risk analysis identified subsidence of the device and the wear of the ball part as a potential source of unacceptable hazards with a risk priority number RPN equal to 40 and 30, respectively. The risk analysis was considered for the individual parts of the assembly and only the characteristics of design itself were concerned. Aspects such as sterilization, packaging and labelling, though important, were not considered during this study.

Table 3.10 - Results of the FMEA.

Item	Function	Failure mode	Failure causes	Failure effects	O (1-5)	S (1-5)	D (1-5)	RPN	Actions to reduce occurrence of failure
Upper and Lower Plates	Load bearing	Breakage	Fatigue failure	Device non functional	1	5	2	**10**	Device will be tested mechanically. If any part were to break during testing, the geometry of the part will be redesign or the material will be changed.
			Patient suffers unexpected high force		1	5	4	**20**	
			Unsuitable material		1	5	1	**5**	
		Subsidence	Footprint mismatch / Inflammatory response	Device non functional	4	5	2	**40**	Device will be provided in a range of dimensions. If the inflammation occurs the material will be changed.
Ball Part	Mobility	Wear	Sliding motion of the upper plate's socket to enable the required joint range of motion	Wear particles	5	2	3	**30**	The wear performance of the device will be tested. If needed the geometry will be altered.
Elastomeric Core	Viscoelastic properties (axial mobility)	Fatigue failure	• Wrong dimensions, • Unsuitable material	• Loss of axial mobility • Intervertebral height loss	4	2	2	**16**	Elastomer will be tested mechanically. If it were to fail during testing, the geometry will be redesign or the material will be changed.
		Tear	Friction force (Rubbing against endplates)	Wear particles	2	1	4	**8**	
Plates surface coating	Long-term fixation	Tear (delamination)	Wrong material & thickness of the coating	Implant loosening and migration	2	3	2	**12**	Mechanical tests will be performed. In case of failure occurrence the changes will be made.
		Insufficient bone ingrowth	Wrong size of the pores		2	3	2	**12**	

3.6   Final Design Verification

3.6.1   Rapid Prototype Models

Rapid prototyping is a very effective method for visually assessing the design at different stages of development. A multi-component assembly benefits from the use of rapid prototyping as it allows for:

- Verifying the geometry of each part.

- Checking the working mechanism of the device.

- Checking the compatibility of the assembled parts.

- Approving its shape, accessibility and functionality according to surgeon opinion.

During the development process of CDyn device, several rapid prototyped models were manufactured (Figure 3.23).

a) Prototype 1 ('Vero White', additive manufacturing stereolithography)

b) Prototype 2 (acrylic monomer based resin, PolyJet process)
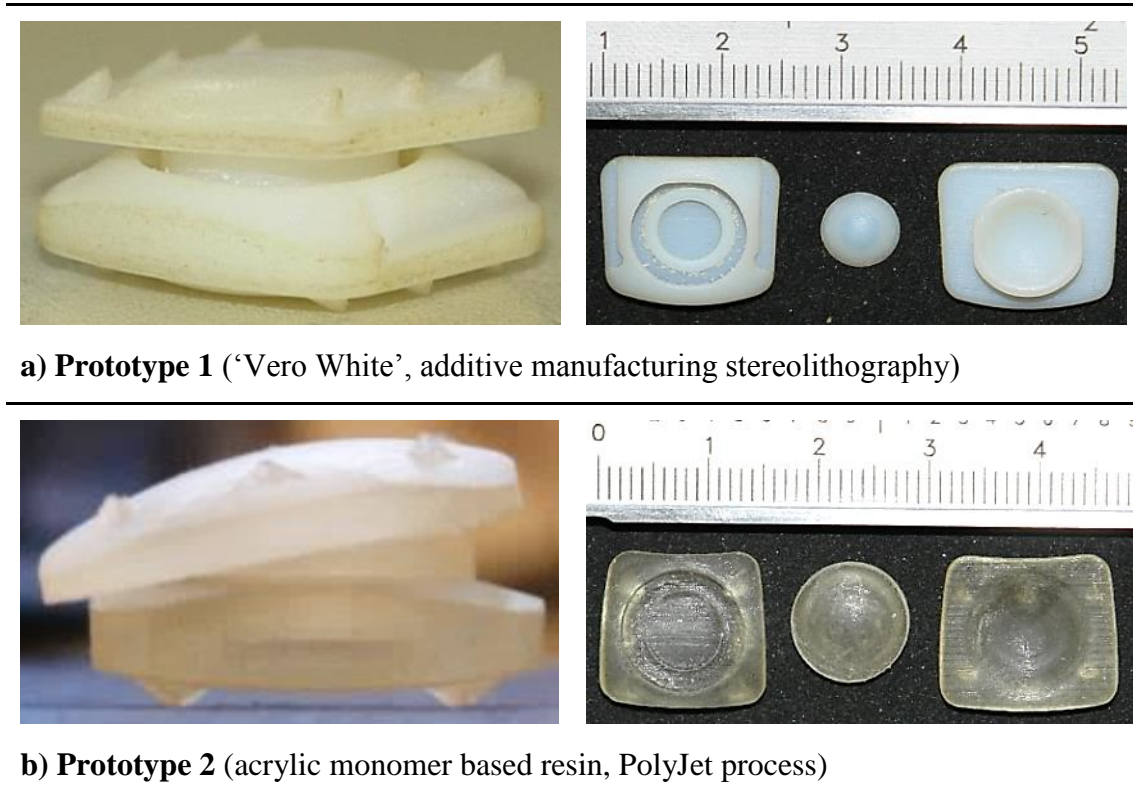
Figure 3.23 - Different prototypes of CDyn device.

Prototype 1 (RP1) was made to verify the accuracy of the dimensions and the compatibility of connection between plates. Prototype 2 (RP2) was manufactured in order to verify the functionality of the ball-on-socket mechanism. The first prototype helped to identify the problematic ball dimensions and, therefore, the ball-on-socket connection. CDyn RP1 was made of 'Vero White' (FullCure 830) a polyacrylate. It was created through the additive manufacturing stereolithography by AM PROTO (France). RP2 was manufactured using an Eden 250 3D Printer (Objet, Billerica, USA) using the PolyJet process from an acrylic monomer based resin (FullCure 720).

3.6.2   Finite Element Analysis

In order to further verify the mechanical performance of the final design, finite element analysis was carried out.

3.6.2.1   Geometry

In this study, the final design of the CDyn device was embedded between blocks mimicking vertebral bodies of C3 and C4 (Figure 3.24). The solid models of the device and blocks were modelled and assembled in SolidWorks 2014 (Dassault Systems SolidWorks Corp. MA, USA). The next step involved converting the SolidWorks assembly into Parasolid format and transferring it to ABAQUS (6.14-AP Dassault Systems) to carry out an FE analysis.
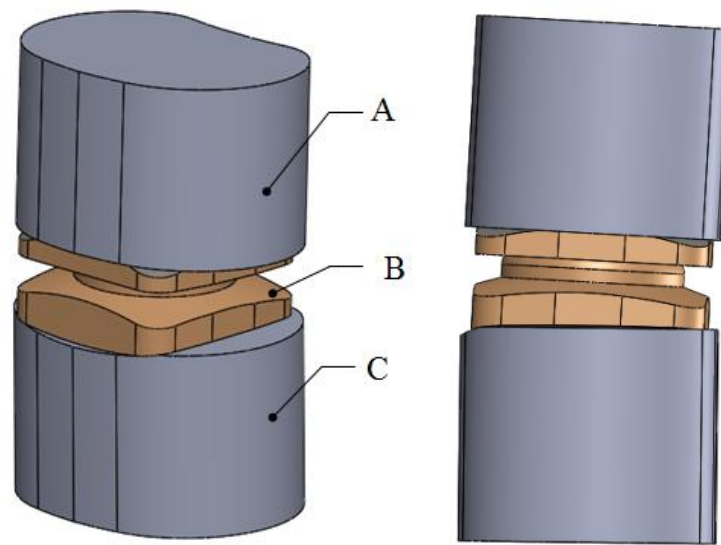
Figure 3.24 - SolidWorks models: A - vertebrae C3; B - CDyn prototype; C - vertebrae C4.

3.6.2.2   Material Properties

Table 3.11 presents material properties that were assigned to the upper and lower plates as well as the ball part (PEEK Optima 450G); vertebral bodies of C3 and C4 (cortical bone) and deformable core (MED 4780), respectively.

Table 3.11 - Material Properties.

Material	Young's modulus (MPa)	Poisson's ratio	Reference
Cortical Bone	12000	0.3	(Zhang et al., 2006)
PEEK Optima 450G	3700	0.36	(Xin et al., 2012)
MED 4780	30	0.49	(Rinde, 1970)

3.6.2.3   Mesh

All solid models of the individual parts of the assembly were meshed using quadratic tetrahedral (C3D10), linear hexahedral (C3D8R) and linear wedge (C3D6) elements. In order to reduce computational time, element numbers were increased only in parts and areas where the stress concentrations and significant displacements were predicted (Figure 3.25).

A mesh convergence study was carried out for each individual part of the CDyn device assembly, in order to find an acceptable balance between computational time and mesh size.
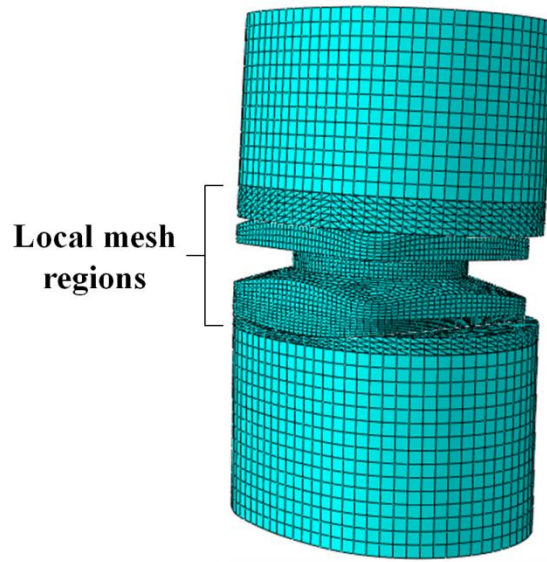
Figure 3.25 - Meshed models of the assembly.

Figure 3.26 shows an example of mesh optimization study performed for the deformable core.
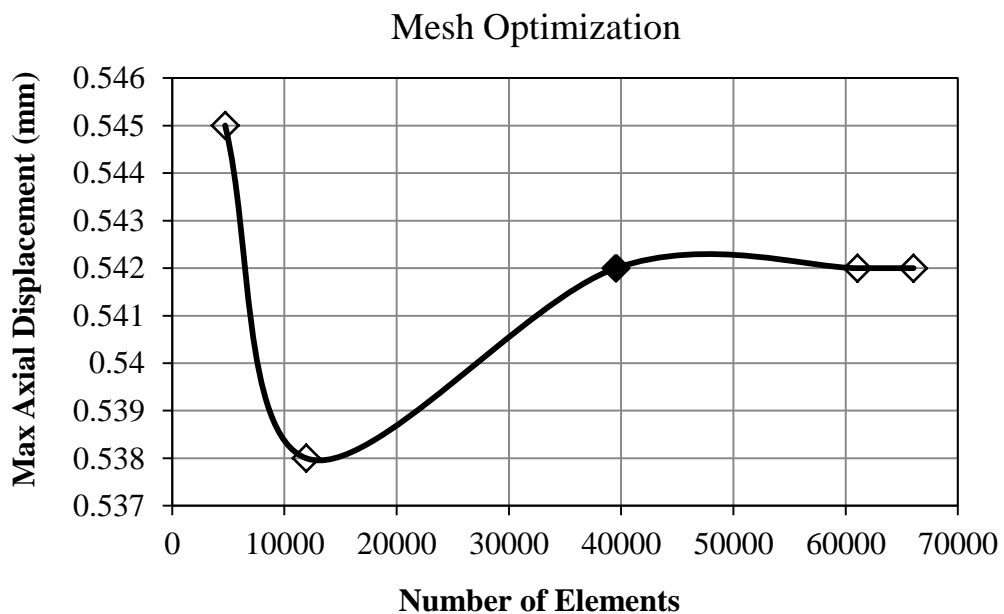
Figure 3.26 - Mesh optimization for the elastomeric core of the CDyn device. The filled point signifies the selected mesh.

For all parts of the assembly, the warning elements were defined as those that had an aspect ratio greater than 10 (brick elements) and shape factor less than 0.1 (tetrahedral elements). Manual definition of the mesh density helped to completely eliminate warning elements for the individual parts of the CDyn device and achieve quality warnings at the level of 0.07% and 0.08% for both C3 and C4 models, respectively. Overall the whole assembly consisted of 182467 elements. The mesh details for each individual component are shown in Table 3.12.

Table 3.12 - Mesh properties of different parts of the assembly used in the finite element model.

Component	Element type	Number of elements	Total number of elements	Ave. size (mm)
Upper plate	C3D8R	34384	34622	0.35
	C3D6	238		
Lower plate	C3D8R	20799	20799	0.45
Ball part	C3D8R	42228	57596	0.45
	C3D6	15368		
Elastomeric core	C3D8R	37052	39536	0.35
	C3D6	2484		
C3	C3D10	9190	16106	0.8
	C3D8R	6916		
C4	C3D10	4748	13808	0.8
	C3D8R	9060		

3.6.2.4   Boundary and Loading Conditions

The loads occurring in the cervical spine usually do not exceed 200 N, but can reach up to 1200 N during everyday activities, for example, during contact sports or heavy lifting (Vicars et al., 2011). Therefore, the compression analyses were carried out for two loading conditions: 150 N, with the value selected according to the ISO 18192-1 (2011) standard for testing cervical intervertebral disc prostheses, and 1200 N, which represented the worst case.

To calculate von Mises stress for the compression model, a uniformly distributed load $\vec{F}$ was applied to the superior face of C3 while the inferior face of C4 had an encastre constraint applied (Figure 3.27).
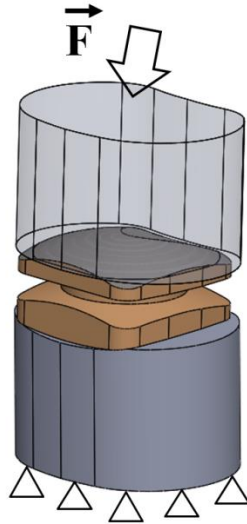
Figure 3.27 - Loading and boundary condition set up for compression model.

Special interactions (contacts) were defined between the cooperating parts of the assembly. A surface-to-surface contact with small sliding was assigned to the ball-on-socket configuration and between the elastomeric core and the rigid parts of the device. Tie constraints were assigned to the interface between the C3 and C4 blocks and the upper and lower plates of the CDyn device. This type of constraint bonds two separate surfaces together so that there is no relative motion between them. The anchoring teeth were omitted in this study as they did not significantly influence the results and could have only complicated the model geometry.

3.6.2.5   Results

Figure 3.28 shows the von Mises stress patterns for the whole CDyn device under loads of 150 N and 1200 N.
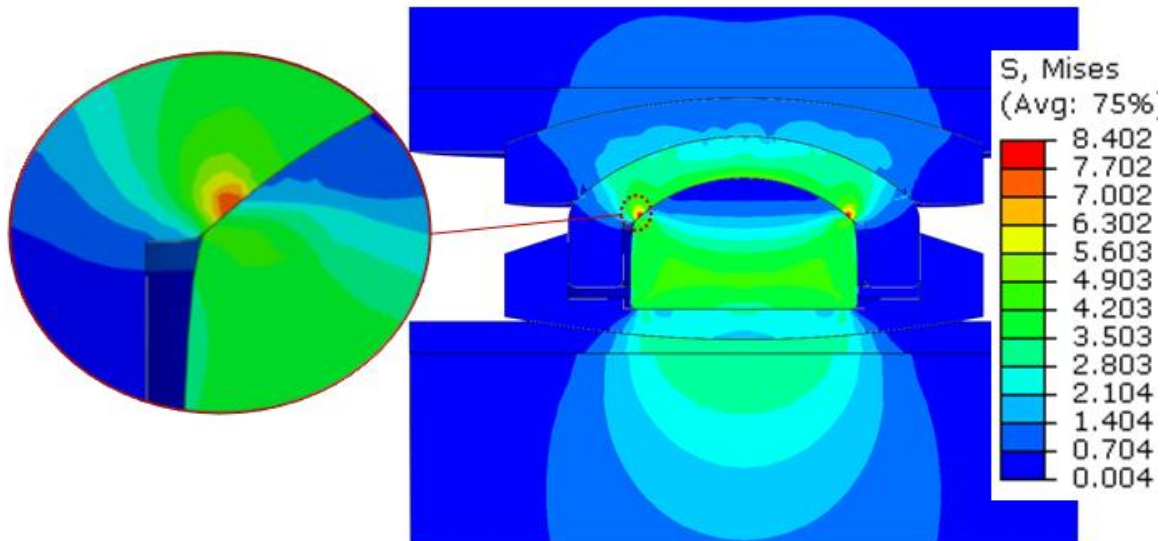
a) CDyn under the load of 150 N
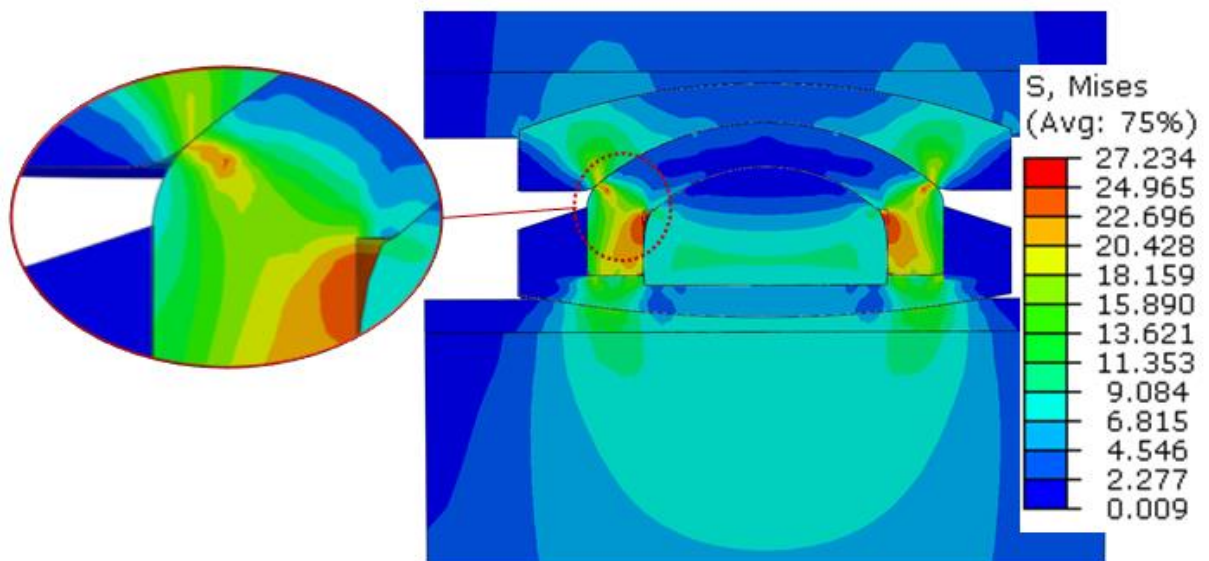
b) CDyn under the load of 1200 N

Figure 3.28 - The von Mises stress distribution (MPa) under the compression of a) 150 N; b) 1200 N.

It could be observed that for both cases, the maximum stress values were located within the ball part. The maximum von Mises stress obtained under 150 N loading (8.4 MPa) was over three times lower than the value obtained under the load of 1200 N (27.2 MPa). Overall, the maximum stresses for both loading conditions, did not exceed PEEK's compressive or fatigue strength, which are reported as 120 MPa (Victrex plc, 2009) and 58.7 MPa at 1 million cycles (at the crystallinity value of 22.5% during the tension-tension fatigue) (Bakar et al., 2003; Tang et al., 2004), respectively. Table 3.13 presents maximum von Mises stress values for each individual component, under both loading conditions.

Table 3.13- Maximum von Mises stress and displacement values for individual components of the model.

		Component					
		Ball	**Upper Plate**	**Lower Plate**	**Elastomer**	**C3**	**C4**
Max von Mises (MPa)	**150 N**	8.4	3.0	3.2	4.6	1.2	3.4
	1200 N	27.2	22.9	18.2	10.0	9.4	15.0
Displacement (mm)	**150 N**				0.42		
	1200 N				0.86		

In general, the stress patterns for both load cases are distinctively different. Under the compression of 150 N the load is carried mainly through the elastomeric core, therefore, the stress was focused in the centre of the vertebrae. The maximum displacement of the elastomer, in this case, was equal to 0.42 mm. Under the 1200 N load, there was complete compression that caused the closure of the gap between the bottom plate and the ball part. Therefore, the load was also transmitted through the rigid components of the device, which caused the stress to be concentrated more on the out edges of the device. In this case, the maximum displacement of the deformable core was equal to 0.86 mm.

3.7   Discussion

This chapter has proposed a new design concept for a cervical disc replacement device (CDyn). The device was composed of biocompatible PEEK (Optima 450G), which has been widely used in medical applications (Scholes and Unsworth, 2010; Xin et al., 2013; Kurtz and Devine, 2007; Brown et al., 2012). It is radiolucent on X-rays and CT scans and MRI compatible, which is important during the implantation procedure and later follow-up. PEEK is also characterized by bone-like stiffness, which may reduce the occurrence of stress shielding (Kurtz, 2011). Moreover, PEEK-on-PEEK is a promising bearing material that was chosen according to the requirements of specialists from S14 Implants (Pessac, France), cooperating on the project.

The new design concept provides both the standard 'ball-on-socket' mobility and axial compression due to the elastomeric core. By combining these two systems, the CDyn device has the advantages of both, while eliminating most of their shortcomings. Most of the current designs are either based on the 'ball-on-socket' mechanism or the elastomer itself (Darden, 2012; Freedom Cervical Disc, 2012; Lauryssen et al., 2012). The devices with a 'ball-on-socket' connection ensure spinal segment mobility but fail to provide the axial compression. Therefore, these devices do not reflect the full biomechanics of the cervical segment, which may be the cause of adjacent segment disease. On the other hand, implants based on elastomers provide axial compression, but may not provide sufficient mobility, which can result in spontaneous fusion. Moreover, with the elastomeric core being exposed and in direct contact with the rigid material of both endplates, it is more prone to fracture due to unwanted friction (Popov et al., 2014; Shepherd and Johnstone, 2005). By encapsulating CDyn's core within the device, there is a better chance that the elastomer's integrity will be preserved.

Existing designs of cervical TDR can be prone to dislocation, loosening and subsidence (Sekhon and Ball, 2005). This is usually caused by the profile of the disc prostheses, which is either limited to a flat endplate, or at best, a minor convexity. This oversimplification of the design could result in an insufficient contact area between the vertebrae and the device, eventually causing its subsidence (Lou et al., 2016). Hence, both plates of the proposed design have a convex shape, to better match the morphological complexity of cervical vertebral bodies. Moreover, the bone-contacting, convex surfaces of the plates feature low-profile teeth, designed to ensure immediate fixation, preventing dislocation. To some degree, subsidence and loosening also depend on the stiffness of the implant-bone construct. This makes PEEK a favourable choice for CDyn's bearing material because as mentioned before, it is characterized by bone-like stiffness, which may prevent implant loosening and subsidence.

The physical prototypes of the device obtained through rapid prototyping were assessed for functionality and dimensional tolerance. The prototypes did not include the elastomer core, as the focus was directed at the rigid parts of the device.

The elastomeric core was optimised using shape factor calculations, in order to decrease the potential for deflection under compressive loads. Quasi-static tests of the elastomers were also conducted to find a suitable material for the cervical application. All tested materials, except MED 4780, did not meet the design requirements and deformed far more than the required 1 mm under 200 N. However, the materials were tested without any constraints, which is not the case when it comes to the device. The elastomeric core is designed to be encapsulated inside the device, in order to prevent it from excessive deformation that may damage it.

The Hertzian contact model was used in order to investigate the likely working conditions of the ball-on-socket configuration. It was established that the clearance of 0.05 mm was

optimal for this design solution, as it was a source of low contact stresses and as a result may keep wear at the low level.

Also, choosing the right radius of the ball and socket connection was an important aspect of the design. From the clinical point of view, if the radius is too big, the connection between surfaces is too flat and as a result, the device may migrate. At the same time studies suggested that the large radius may reduce the risk of subsidence and wear rate in the long term as it better distributes the load (Li et al., 2017). Therefore, the radius of 8 mm was chosen as an optimal size for this application.

Finite element (FE) analyses along with a range of TRIZ tools, presented in this study, were used to verify and guide the development of the design. TRIZ methods helped in finding a design solution that solved the physical and technical contradictions and met formulated design requirements. FE analyses helped in verifying prototypes at the early stages of the development by identifying regions of high-stress concentrations. This resulted in modifications made to the geometry, which improved stress patterns and reduced the potential for fracture by compression and fatigue load. FE analysis of the final design has proven that the device is unlikely to fail due to a material failure, as obtained stress levels were far below the compressive and fatigue strength of PEEK (Optima 450G). The FEA results obtained for the final design under the 150 N loading, which is a value selected according to the ISO 18192-1 standard for testing cervical intervertebral disc prostheses, showed relatively low stresses. Furthermore, the compression force of 150 N did not cause the absolute closure of the gap between the ball part and the lower plate, maintaining the mobility. The accuracy related to presented load model was limited, as vertebral models were assigned properties of cortical bone only, whereas the actual geometry of the vertebral bodies represents combined structure of cortical and cancellous bone. Though this structure simplification could have

slightly altered the stress distribution patterns within the vertebral models, it should have minimum effect on the device itself. It has to be mentioned that the FEA study has not taken into account other spinal structures like muscles and ligaments as well as the influence of facet joints, which assist load bearing and motion in a spinal segment. It is assumed that had these factors were taken into consideration, the stress pattern of the device would have been more favourable as it would have better reflected the biological model.

The next stage in the development of the device would include further mechanical tests of the elastomeric material in order to verify its performance. There would also be a need to evaluate the performance of a whole assembly in a simulated operating environment, where it could be incorporated into a fully defined cervical spinal segment and subjected to anatomical loads. Finally, after the manufacture of a last-stage working prototype, a series of mechanical tests using a spine simulator would be conducted. This would help to validate the FE analysis and provide information about the tribological properties of the device.

3.8   Chapter Summary

This chapter has described the process of developing a new cervical disc replacement device (CDyn), designed with a view to decrease or eliminate the occurrence of ASD and become an alternative to fusion. The CDyn TDR is a PEEK-on-PEEK (Optima 450G) articulating device, which combines the characteristics of the traditional 'ball-on-socket' connection with viscoelastic properties of an elastomeric core. Combining these two solutions is a completely new design concept, which may enable the device to better mimic the functionality of a natural disc. In summary, the CDyn device concept may in the near future provide better quality in the cervical disc replacement procedure. The next chapter presents a comparative analysis of two types of pedicle screws being part of the lumbar stabilisation system.

4   Comparison of Mechanical Performance of the Polyaxial Pedicle Screws

Chapter Overview

The aim of the study presented in this chapter was to evaluate and compare the mechanical performance of pedicle screws with different geometries. An introduction to the study is presented in section 4.1; materials and methods specific to this chapter are described in sections 4.2 and 4.3, respectively. The results obtained during the investigation are presented in section 4.4, while section 4.5 presents finite element analysis studies of both screw designs. A discussion and chapter summary are presented in sections 4.6 and 4.7, respectively.

4.1   Introduction

Pedicle screws are often the weakest part of a lumbar posterior stabilisation system, which consists of rods and screws (Jutte and Castelein, 2002). Pedicle screw breakage is still a common clinical failure causing a hazard to the patients and the need for further surgery. Moreover, broken screw fragments are difficult to remove, which complicates the revision surgery. Thus, improving the biomechanical performance of pedicle screws is crucial for good clinical outcomes (Chao et al., 2010).

There have been a few cases of breakage *in vivo* involving the screws investigated in this study, characterized by cylindrical geometry (BFus 2). In order to eliminate this problem, the company S14 Implants (Pessac, France) has proposed a new design solution in the form of a dual-core screw (BFus 2+).

The study presented in this chapter describes a series of mechanical tests and finite element analysis, which were conducted in order to evaluate and compare the mechanical performance of both screw types. Moreover, the fracture surfaces of the specimens that failed during the mechanical tests and screws retrieved from the patients, were investigated, in order to gain a

better understanding of the origin of the failure. In addition, a critical visual assessment of the screws that failed *in vivo* was conducted, based on the radiological images provided by S14 Implants.

4.2   Materials

4.2.1   Pedicle Screws BFus 2 and BFus 2+

Two designs of pedicle screws were investigated in this study: cylindrical (BFus 2) and dual-core (BFus 2+), both with a major diameter of 5.5 mm and different lengths of 45 mm and 45.7 mm, respectively (Figure 4.1).
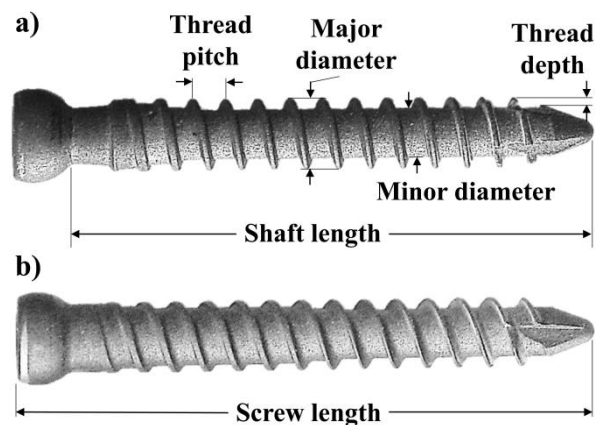
Figure 4.1 - Pedicle screws: a) 5.5 mm cylindrical screw (BFus 2);

b) 5.5 mm dual-core screw (BFus 2+).

Both screws, obtained from S14 Implants (Pessac, France), were manufactured from a medical grade titanium alloy, Ti-6Al-4V (TA6V ELI), in accordance with ASTM F136 (2013). The surface of the screws has been corundum blasted in order to obtain an appropriate roughness to help induce integration with bone.

87

Design Modifications

The geometry of the screws differs mainly in the size of the core diameter, the geometry of the neck and thread profile (Figure 4.2).
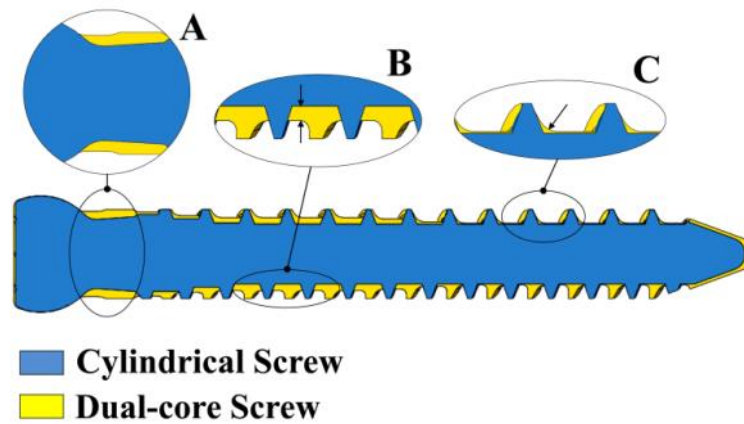
Figure 4.2 - Illustration of the geometric differences between both screw designs. The letters in the photo indicate A - The geometry of the neck; B - Core diameter; C - Thread profile.

The first screw type had a single V-shaped thread and a cylindrical core up to 3/4 of its thread length and a minor diameter of 3.7 mm. The second screw type was characterized by a double lead (Figure 4.3a), a buttress thread and dual-core connected by a conical transition. The thread of the dual-core screw varied down the shank, at the proximal end it was characterized by a larger core diameter (4.5 mm) with low and broad threads, designed in order to grip in dense, cortical bone (Figure 4.3). From the midpoint of the shank to the tip, the thread had a smaller cylindrical core (3.8 mm) with tall and thin threads, designed for anchoring into spongy cancellous bone.
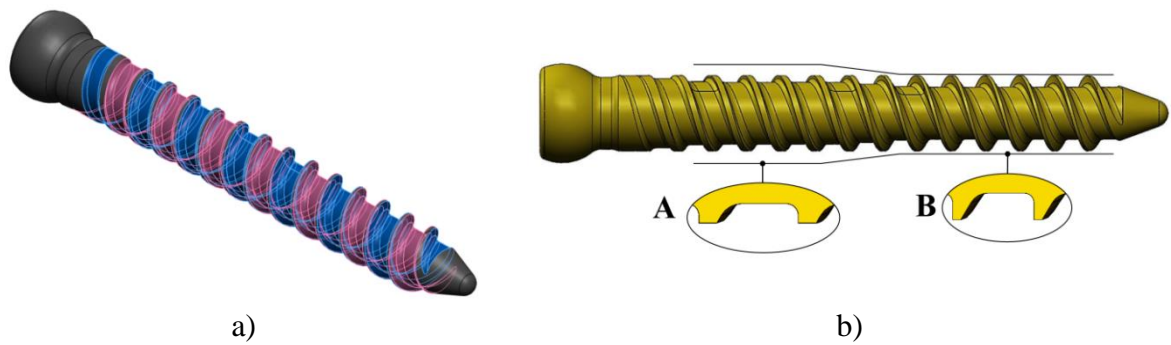
Figure 4.3 - Detailed view of the dual-core screw (BFus 2+) geometry: a) Dual thread;

b) A - Cortical core profile; B - Cancellous core profile.

In addition, the thread of the dual-core screw had a smoother transition between the base of the thread and inner (minor) diameter due to a fillet, which may help to reduce stresses in the screw (Figure 4.4) (Griza et al., 2012).
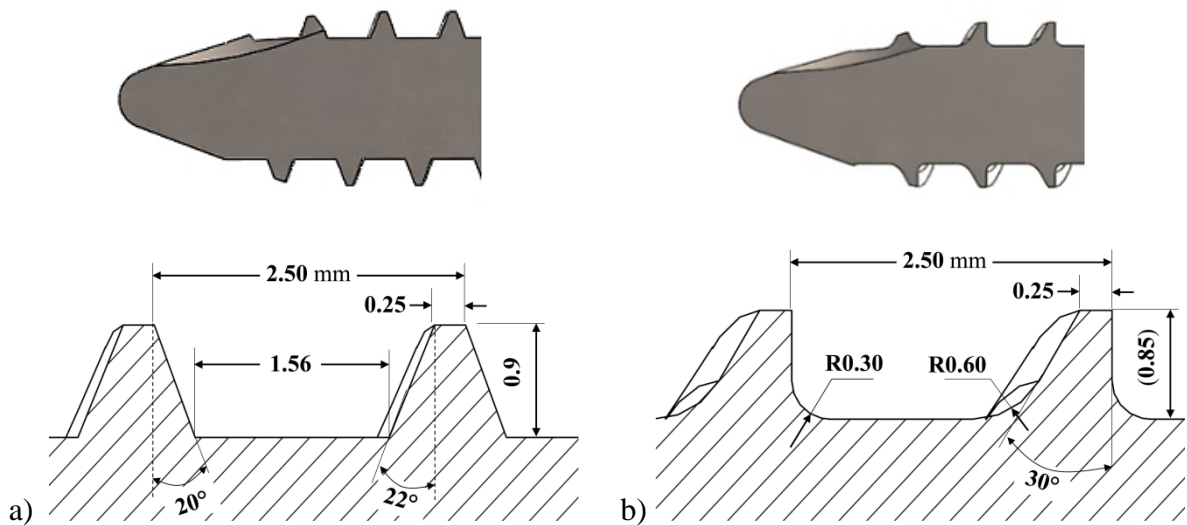
Figure 4.4 - Thread profile: a) Cylindrical screw (BFus 2); b) Dual-core screw (BFus 2+).

The detailed dimensions along with the defined total flank overlap area (FOA) of each screw type are listed in Table 4.1.

Table 4.1 - Specification of the pedicle screws employed in this study.

Screw type	Major diameter (mm)	Minor diameter (mm)	Screw length (mm)	Shaft length (mm)	Thread pitch (mm)	Thread depth (mm)	FOA (mm^2)
Cylindrical	5.5	3.7	45	40	2.5	0.9	187.5
Dual-core	5.5	*4.5 †3.8	45.7	41.3	2.5	*0.5 †0.85	*48.4 †99

*Dimension corresponding to the cortical portion of the screw

†Dimension corresponding to the cancellous portion of the screw

4.2.2   Explanted BFus 2 Pedicle Screws

Five broken, explanted BFus 2 screws, provided by S14 Implants (Pessac, France) were investigated (Figure 4.5). Available parts are the fragments of the screws with a major diameter of 7 mm and 5.5 mm and the screw length of 35 mm and 40 mm. The purpose of the investigation was to identify the location and mode of failure and compare it with the results obtained for the mechanically tested screw samples.
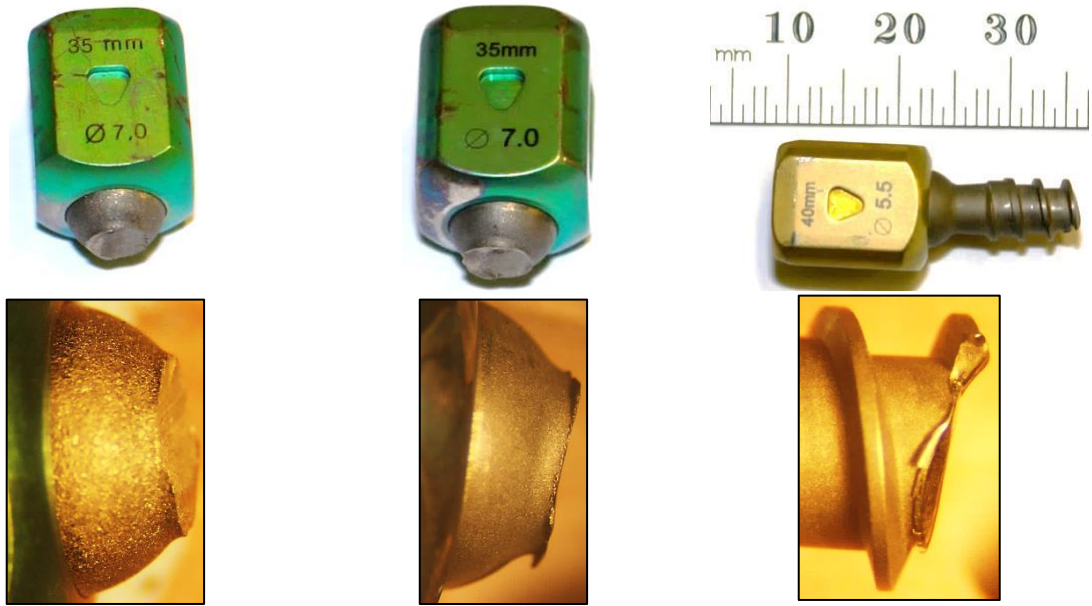
a) Screw 1:

Ø = 7 mm, S_L = 35 mm

b) Screw 2:

Ø = 7 mm, S_L = 35 mm

c) Screw 3:

Ø = 5.5 mm, S_L = 40 mm
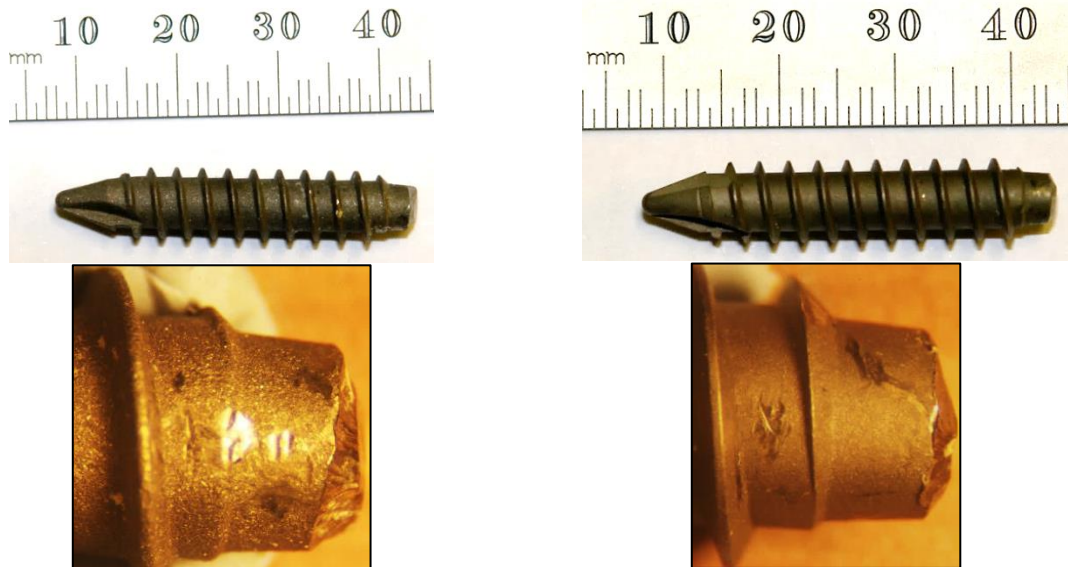
d) Shank 1: Ø = 7 mm, S_L = 35 mm

e) Shank 2: Ø = 7 mm, S_L = 35 mm

Figure 4.5 - Explanted cylindrical pedicle screws BFus 2. Ø - Major diameter; S_L - Screw length.

4.2.3   Reported Incidences of BFus 2 System Fractures *in vivo*
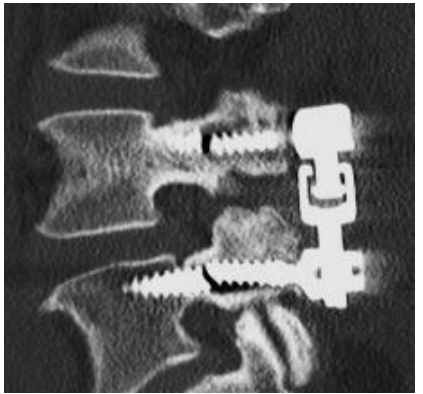
There have been a few incidences of BFus 2 screw breakage *in vivo*. Five cases of screw failure that were reported by the company and surgeons collaborating with them are presented in Table 4.2. In the presented examples, the investigated pedicle screws were coupled with the BDyn − the lumbar dynamic posterior stabilisation device (S14 Implants, France) (Lawless et al., 2016) (Figure 4.6).
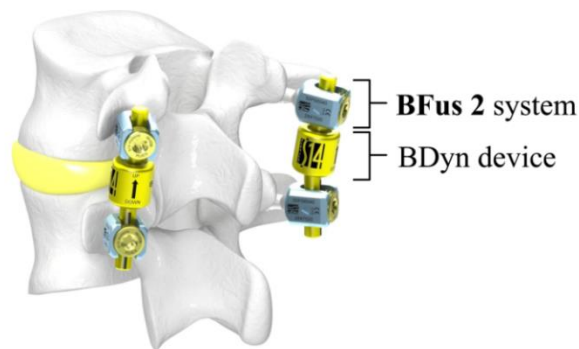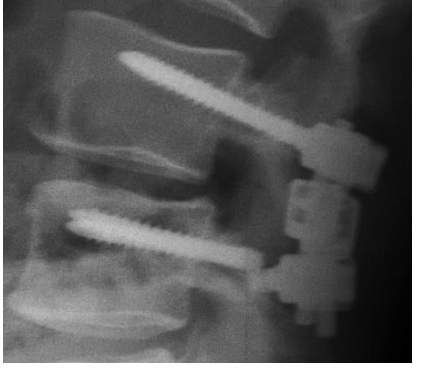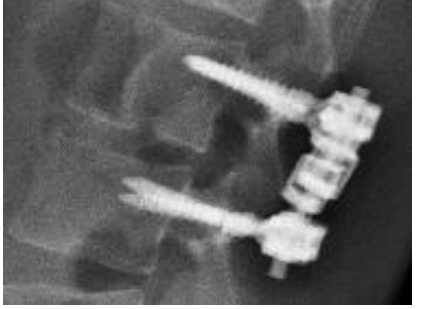
Figure 4.6 - BDyn device secured by the BFus 2 systems (S14 Implants).

An attempt to identify the likely causes of screw failure was made based on the visual assessment of the radiological images and the limited information obtained from the surgeons.

Table 4.2 - Reported incidences of BFus 2 system fractures *in vivo*.

Case 1	Date of the incident: 3rd of February 2014 - Two BDyn devices, - Four pedicle screws: BFus **Description:** A patient was operated on in 2011. During the consultation, the surgeon who operated on the lumbar part discovered failure of 3 out of 4 screws in vertebrae L4 and L5.
Case 2	Date of the incident: 9th of February 2014 - Two BDyn devices, - Four pedicle screws: BFus **Condition:** Bilateral sciatica of L4-L5 with instability on either side, a positive sacral radiculopathy compression during standing. **Description:** The patient was operated on the 4th of October 2011. During the consultation, the surgeon discovered the failure of the 2 out of 4 screws.
Case 3	Date of incident: 31st of October 2014 - Two BDyn devices, - Four pedicle screws: BFus **Condition:** The narrow channel slight Retrolisthesis. **Description:** The patient was operated on in 2012. During the review, the radiographs of L3-L4 showed that a one pedicle screw broke flush with the pedicle.

Case 4	Date of incident: 5th of November 2014 - Two BDyn devices, - Four pedicle screws: BFus **Description:** The patient was operated on in 2013. During the consultation, the surgeon discovered the failure of 2 screws placed in the L4 vertebra in conjunction with the dynamic posterior stabilisation device BDyn, mounted in the L3-L4 segment.
Case 5	Date of incident: 6th of November 2014 - Two BDyn devices, - Four pedicle screws: BFus **Description:** During the consultation, the surgeon discovers the breakage of 2 screws placed in the vertebrae L2 and L3 in combination with the posterior dynamic stabilisation device BDyn.

4.3   Methods

4.3.1   Stiffness and Bending Resistance of the Pedicle Screws

Since screws are frequently subjected to bending moments in posterior instrumentation, the bending strength of the screws has significant clinical importance. As described in section 4.2.1, the changes introduced to the screw design included enlarging both the neck of the screw and its core diameter. These changes were intended to increase the flexural strength of the bolt and, as a result, reduce its susceptibility to fracture. Figure 4.7 shows two selected sections C and D, representing areas most prone to failure, in which the screw geometry has changed.
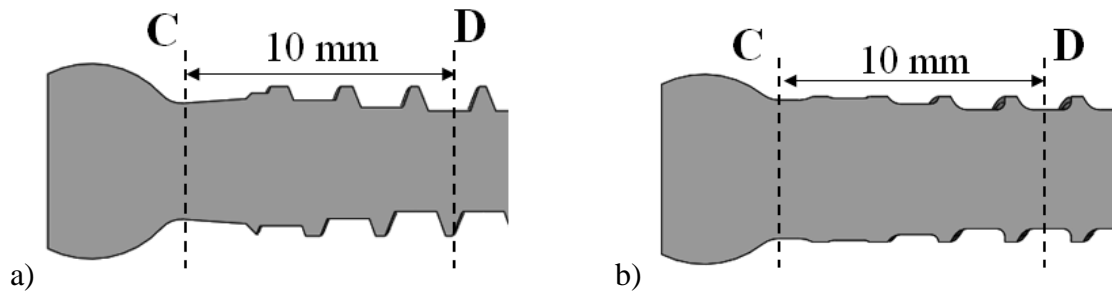
Figure 4.7 - Chosen cross-sectional areas for screws: a) Cylindrical - BFus 2; b) Dual-core - BFus 2+.

To calculate the change in bending resistance in these selected sections, the area moment of inertia was used. It is a geometrical property of the cross-sectional area of the structure, which reflects its ability to resist bending. The area moment of inertia is related to the bending resistance of the screw, mainly through the minor (core) diameter. In case of a screw of circular cross-section, resistance to bending is proportional to the fourth power of the minor diameter (Haher and Valdevit, 2009).

Calculation method

The calculations are based on a comparison of the moments of inertia for both screws corresponding to specific cross-sections (C and D) according to equation 4.1:

$$I = \frac{\pi \times d^4}{64} \tag{4.1}$$

where:

I - area moment of inertia (mm^4),

d - inner diameter of both screws in one of the selected cross-sections C or D (mm).

95

The increase of resistance is equivalent to the relative rates of the area moments of inertia calculated by the following equations:

- Cross-section at the collar of the screw (point C):

$$\frac{\Delta I_C}{I_C} = 100 \times \frac{(I_{C(BFus\,2+)} - I_{C(BFus\,2)})}{I_{C(BFus\,2)}} \tag{4.2}$$

- Cross-section 10 mm from the collar of the screw (point D):

$$\frac{\Delta I_D}{I_D} = 100 \times \frac{(I_{D(BFus\,2+)} - I_{D(BFus\,2)})}{I_{D(BFus\,2)}} \tag{4.3}$$

4.3.2 Testing Technique

The pedicle screws undergo a series of standard tests in order to verify or compare their mechanical performance before they are used in clinical practice. As mentioned before the most common clinical failures of the pedicle screws include breakage and loosening/pullout. Standards published by American Society for Testing of Materials (ASTM) that evaluate screw pullout strength and resistance to both static and fatigue bending include ASTM F543 (2013) and ASTM F2193 (2014), respectively.

- The ASTM F543 standard requires force-displacement curves and based on them allows for interpreting the following biomechanical properties: pullout strength, pullout yield, pullout stiffness and pullout energy to failure.

- For the static bending test, the ASTM F2193 standard allows interpreting the following properties: bending stiffness, bending structural stiffness, bending yield moment and bending ultimate moment. For the fatigue bending test, the standard allows interpreting the bending fatigue run-out moment and identification of the failure mode and location for each specimen that failed.

4.3.3 Axial Pull-out Test

Three rigid polyurethane (PU) foams were used for the pullout tests: grade 10 (density: 0.16 g/cm^3), 20 (density: 0.32 g/cm^3) and 40 (density: 0.64 g/cm^3), as specified by ASTM F1839 (2012). All foams were supplied by Sawbones® Europe AB (Malmö, Sweden) as blocks (130 mm x 180 mm x 40 mm). A smaller block (43 mm x 60 mm x 40 mm) was cut from the main blocks for each test. The mechanical properties of the foams enable them to be used as osteoporotic, normal and higher than normal bone models (Patel et al., 2008; Patel et al., 2010). This eliminates variability that would occur with human samples, in order to provide more reliable results (ASTM F136:2013; ASTM F1839:2012; Patel et al., 2008). In this study, the conditions of the pullout test for pedicle screws followed ASTM F543 (2013). Pilot holes of 3.5 mm diameter, as specified by the manufacturer, were drilled into a PU test block before the insertion of each screw. Each screw was inserted at the centre of a foam block to a depth of 20 mm, through a pullout fixture previously used by Patel et al. (2013) (Figure 4.8). In this case, FOA calculated for embedded parts of both screws, were comparable and had values of 104 mm^2 and 99 mm^2 for cylindrical and dual-core screws, respectively. The screws were hand-tightened, using a bespoke tool provided by the manufacturer. The pullout fixture was then attached to a Bose ELF 3300 materials testing machine (Bose Corporation, ElectroForce Systems Group, Minnetonka, MN, USA) (Figure 4.9a). The lower fixture of the test assembly, used to secure the foam block, was clamped to the base of the testing machine. Due to the load limit of the ELF 3300, being 2000 N, a Universal Testing Machine (INSTRON TT-CM A0093, UK) was used during the pullout test involving the PU foam grade 40 (Figure 4.9b).
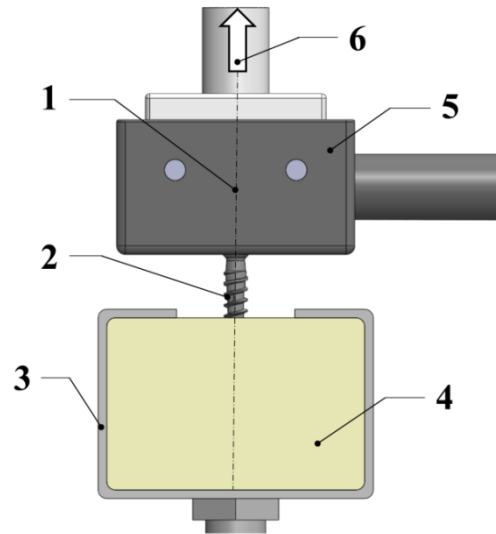
Figure 4.8 - Pullout test setup: 1 - Pullout axis; 2 - Pedicle screw; 3 - Test block grip;

4 - PU foam test block; 5 - Pullout rig; 6 - Pullout force.

a)   b)
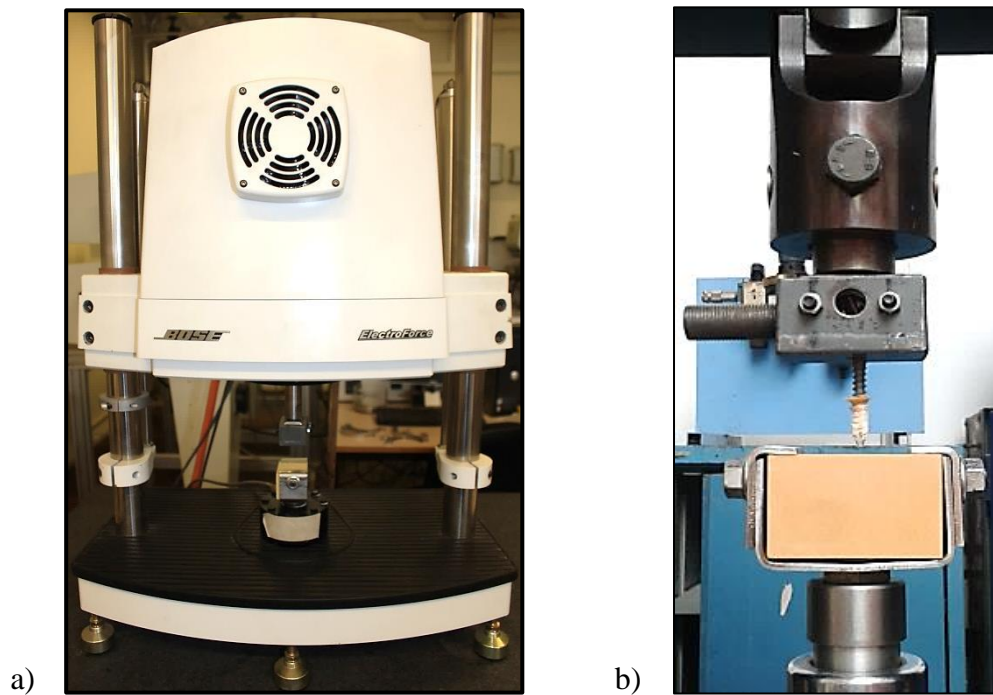
Figure 4.9 - a) BOSE ELF 3300 machine; b) Universal Testing Machine INSTRON.

Each screw was pulled by its head and along the axis perpendicular to the top surface of the test block. Nine axial pullout tests were performed for each screw type. All tests were performed in displacement control at a rate of 5 mm/min. The load-displacement curves were recorded and the screw pullout strength was defined as the maximum force sustained before the pullout. The same screws were used for all tests. This has been justified, as the Young's modulus of the PU foam, according to the specification ASTM F1839 (2012), ranged from 0.3 MPa to 934 MPa (Patel et al., 2008), whilst Young's modulus of titanium alloys ranged between 100 GPa and 120 GPa (Gere, 2008). The tensile strength for the highest density PU foam grade 40 was 19 MPa (Sawbones® Europe AB, Malmö), whilst the ultimate tensile strength for titanium alloys was reported as 1 GPa (Hibbeler, 2004). It should be noted that the screws showed no sign of observable damage or deformation as a result of the tests.

4.3.4   Quasi-Static Bend Test

Five tests for each screw type were conducted for the quasi-static cantilever bending tests according to ASTM F2193 (2014). All tests were performed to obtain the ultimate static strength of each screw, defined as the maximum force before either plastic deformation or breakage. In order to rigidly constrain the head of the screw, the original polyaxial head was removed and replaced with a custom-made stainless steel head. Next, a test specimen was mounted in the Bose ELF 3300 testing machine in a specially designed mini-vice (Figure 4.10, Figure 4.11). The threaded region of each screw where the load (F) was applied was embedded into a test block made from rigid polyurethane foam (grade 40). All tests were performed in displacement control at a rate of 0.2 mm/s. The exposed length of the screws and the bending moment arm (L) were recorded and kept constant for all tests. The load-displacement curves were recorded. The loading continued until plastic deformation of the screws occurred.
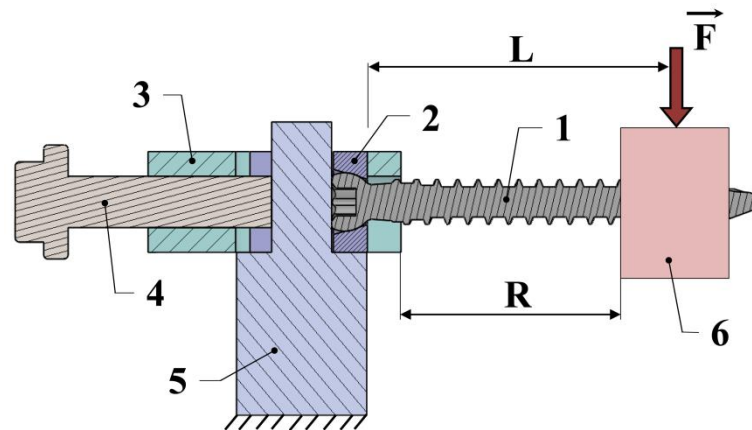
Figure 4.10 - Schematic view of the mounting for the quasi-static test: 1 - Pedicle screw;

2 - Custom made head; 3 - Mini-vice jig; 4 - Securing screw; 5 - Pin; 6 - Test block;

R - Exposed length; L - Bending moment arm; F - Load.
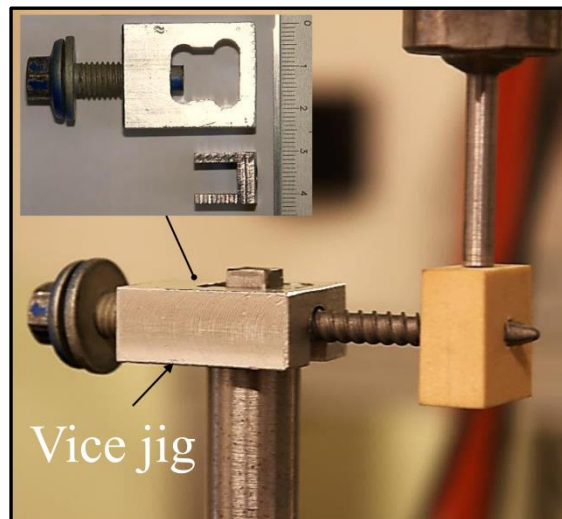
Figure 4.11 - Photograph of the jig for the quasi-static test.

4.3.5   Dynamic Bend Test

With the same setup as quasi-static tests, dynamic tests were performed for six specimens of each screw with peak forces corresponding to 10%, 30%, 40%, 50%, 65% and 75% of the ultimate static strength of each screw type, defined in quasi-static tests. Each specimen was subjected to a sinusoidal load at a frequency of 5 Hz and a constant load ratio, R (F_{max}/F_{min}),

of 10 according to ASTM F2193 (2014). All tests were performed until the sample fractured or the tests exceeded 2.5 million cycles and in doing so were determined as having an infinite fatigue life.

4.3.6   Microscopic Evaluation of the Pedicle Screws Fracture Surfaces

In order to identify the characteristics of a failure during both quasi-static and dynamic tests, microscopic evaluation of the fracture surfaces was performed. The broken screws were investigated using a low magnification stereomicroscope (Wild M3Z Heerbrugg Stereo Microscope, Switzerland) (Figure 4.12).

The analysis allowed qualitative examination of the screw surface to identify the fracture morphology. The same procedure was applied to the parts of the screws explanted from the patients, presented in section 4.2.2.
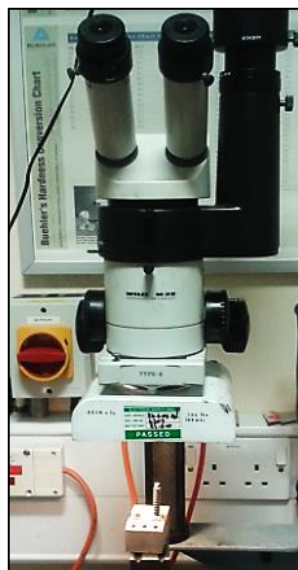
Figure 4.12 - Wild M3Z Heerbrugg Stereo Microscope.

4.4   Results

4.4.1   Stiffness and Bending Resistance of the Pedicle Screws

The results of the moments of inertia for specified cross-sectional areas C and D for both screw types are presented in Table 4.3.

Table 4.3 - Moments of inertia of the screws at the collar - C and section - D.

	Collar area (C)			10 mm from the collar (D)	
	Cylindrical	Dual-core		Cylindrical	Dual-core
d_C (mm)	4.27	5.24	d_D (mm)	3.7	4.5
$d_C{}^4$ (mm^4)	332.44	753.92	$d_D{}^4$ (mm^4)	187.42	410.06
I_C (mm^4)	**16.32**	**37.01**	I_D (mm^4)	**9.2**	**20.13**

The results show a substantial increase of the bending resistance of the dual-core screw (BFus 2+) in both defined cross-sections. At the collar area of the screw (C) the resistance to bending has increased by a $\frac{\Delta I_C}{I_C} =$ 127% and 10 mm further down the shaft (D) by a value of around $\frac{\Delta I_D}{I_D} =$ 119%. In both cases, a small change in the diameter had a significant effect on the resistance to bending.

4.4.2   Axial Pull-out Test

The pullout strength for each investigated screw design was recorded. Figure 4.13a shows how during screw extraction, the load initially increased and then decreased when the screw pulled out from the polyurethane foam. In all tests, the failure mode was shear of the PU foam surrounding the screws and the threads showed no observable damage or deformation.

102
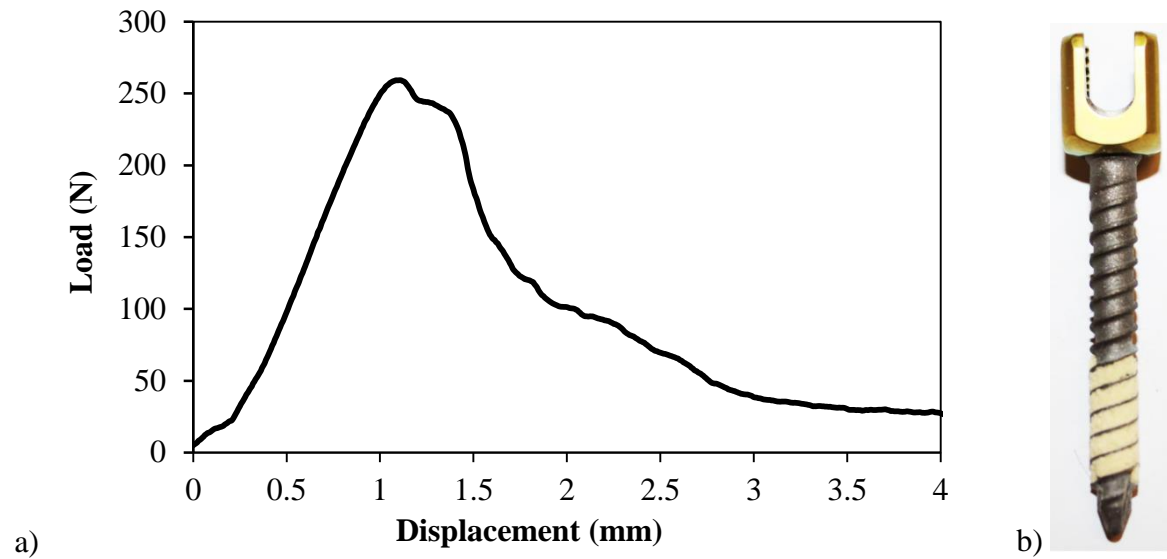
Figure 4.13 - a) An example of a load-deformation curve in pullout tests;

b) Typical pullout failure: dual-core screw extracted from PU foam.

The PU foam filled the gaps between the screw threads as they were pulled out of the synthetic bone block (Figure 4.13b). Table 4.4 shows the mean values of screw pullout force and stiffness for the cylindrical and dual-core pedicle screws.

Table 4.4 - Mean (± SD) pullout force and stiffness of screws in PU foam models.

PU Foam Grade	Pullout Force (N)		Stiffness (N/mm)	
	Cylindrical	Dual-core	Cylindrical	Dual-core
10	235 ± 16	243 ± 10	321 ± 24	356 ± 25
20	914 ± 44	919 ± 46	817 ± 127	917 ± 54
40	3340 ± 181	3349 ± 271	1446 ± 117	1525 ± 146

Pullout force was defined as a maximum load at failure of the PU foam and pullout stiffness as the slope of the linear elastic region of the curve before the yield point. Though not significantly different ($p > 0.05$), the mean value of pullout force of dual-core screws was higher than that of cylindrical screws in all three polyurethane foam grades.

The average stiffness of dual-core screw during pullout from the grade 10 and 20 PU foams was significantly higher compared to the cylindrical screw ($p < 0.05$). Though not significantly different ($p > 0.05$), the mean value of stiffness in PU foam grade 40 was higher for dual-core screws (1525.3 N/mm and 1445.7 N/mm for dual-core and cylindrical, respectively). The screw displacement at the point of peak load was less than 2 mm for the screws embedded in foams grade 10 and 20, and less than 3 mm for the foam grade 40. The results of the ANOVA showed that there was a significant ($p < 0.05$) effect of foam density on the average value of pullout force and stiffness. Both values were consistently higher in the foams with higher density (Figure 4.14, Figure 4.15).
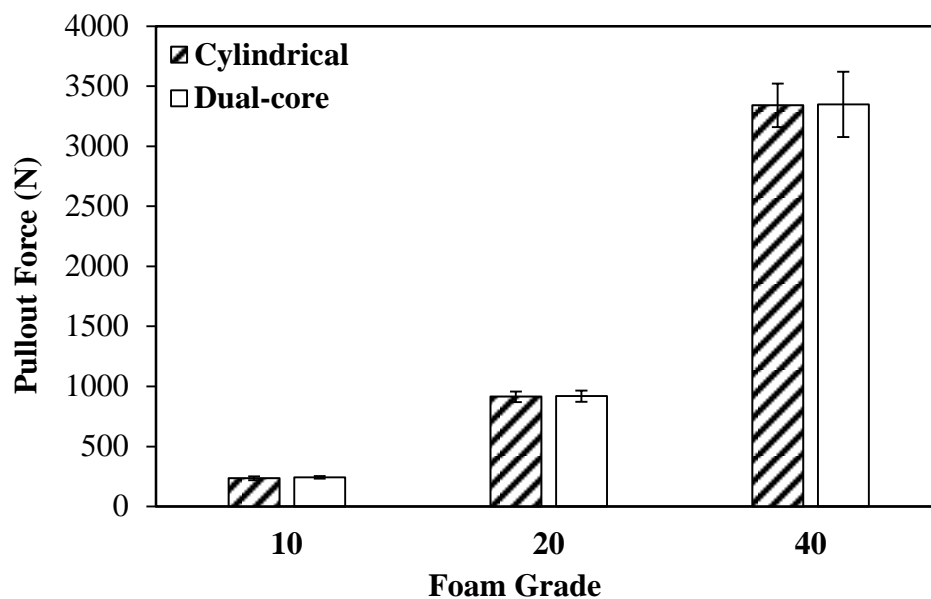
Figure 4.14 - Mean (± SD) values of pullout force for each screw in different PU foam models.
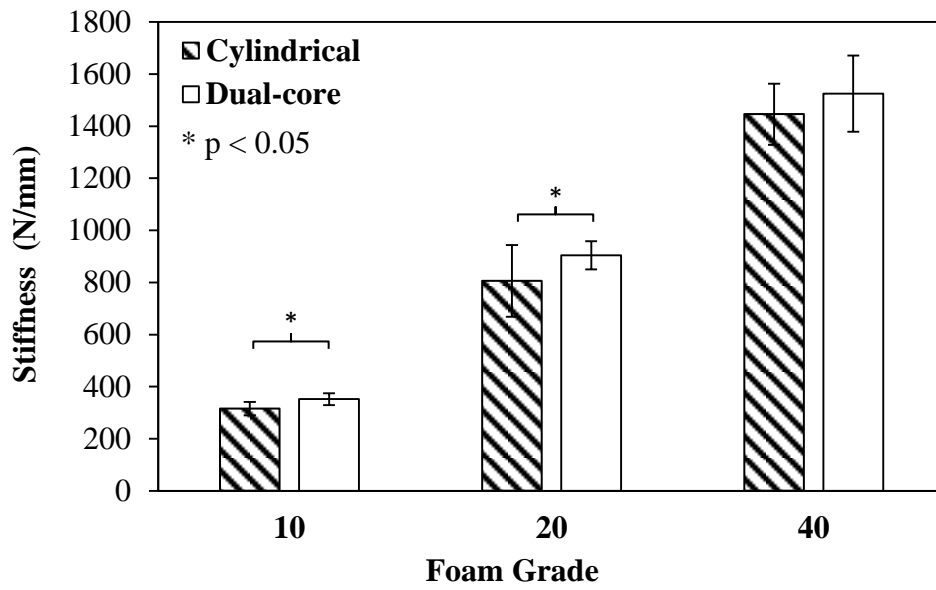
Figure 4.15 - Mean (± SD) values of stiffness for each screw in different PU foam models,

(*Significant at p < 0.05).

4.4.3 Quasi-Static Bend Test

During tests, three cylindrical screws (BFus 2) failed due to a crack formation, while the rest of the samples, including all dual-core (BFus 2+) screws, showed signs of plastic deformation (yielding) (Figure 4.16). The failure modes were consistent with the mean load-displacement characteristics for both screws, shown in Figure 4.17.
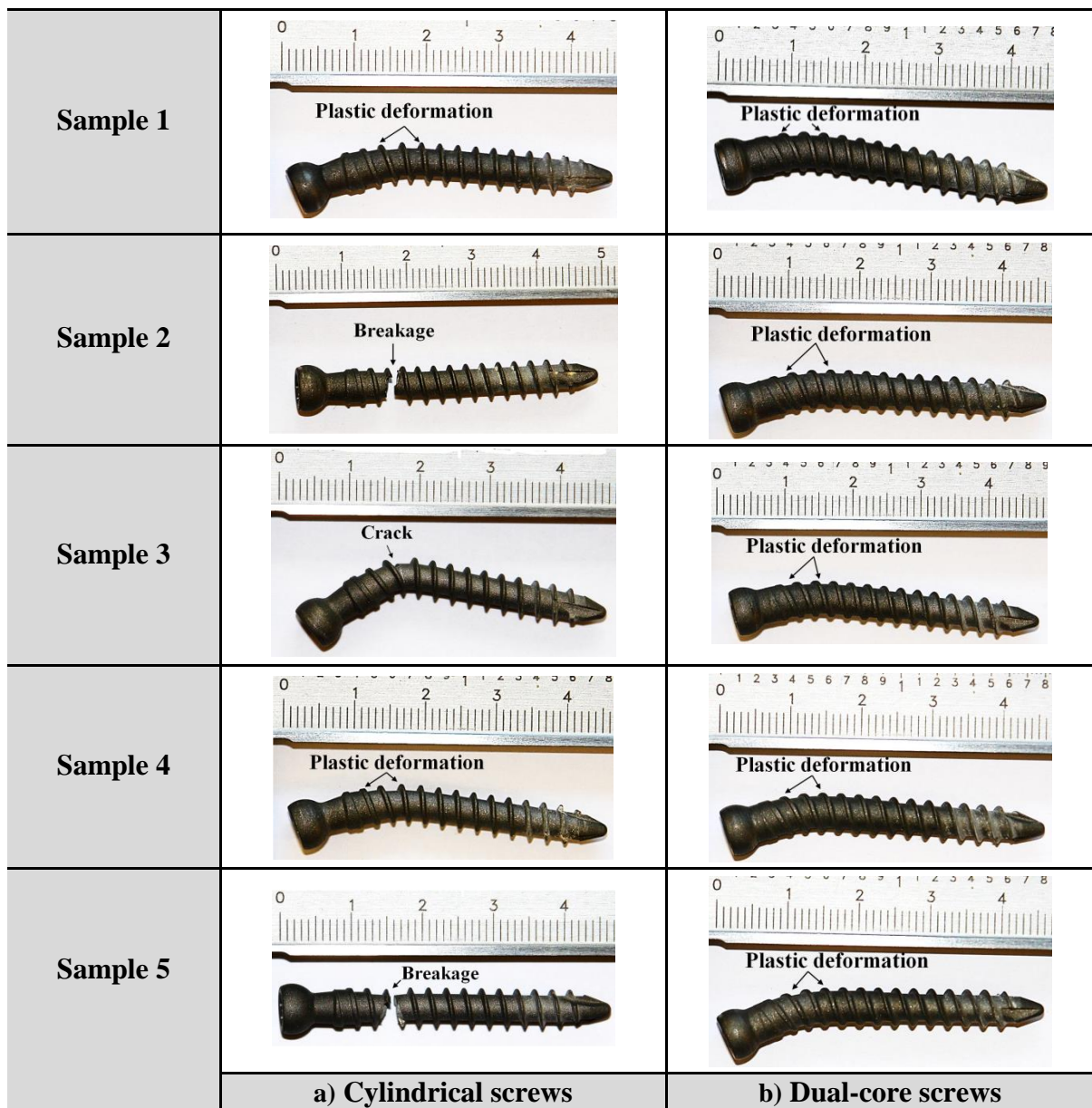
Figure 4.16 - Quasi-static failure and plastic deformation: a) cylindrical screw;

b) Dual-core screw.
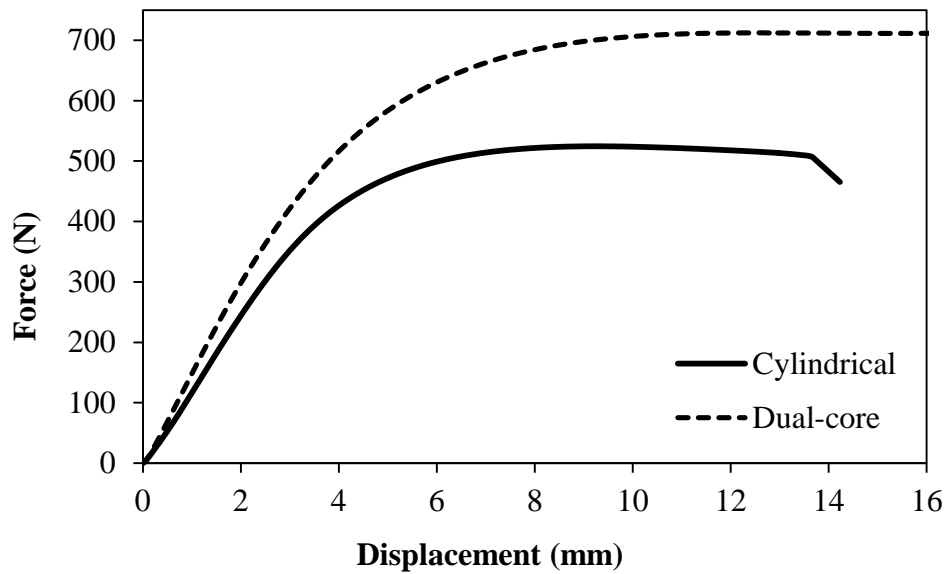
Figure 4.17 - Mean quasi-static bending force-displacement trends for each screw.

Both breakage and deformation of the samples occurred at roughly the same location for both screw types, between the third and fourth thread. For the dual-core screw (BFus 2+) there was a rapid rise in force for a small displacement followed by a large displacement with a little increase in force. The trend was observed for the cylindrical screw (BFus 2), with the addition of a reduction of a force that proceeded failure. The bending stiffness was defined as the slope of the initial linear region of the curve; 0.2% offset yielding strength and structural stiffness (El_e) were defined according to ASTM F2193 (2014). The results showed that the dual-core screws had significantly higher mean values of bending ultimate load, bending stiffness and structural stiffness ($p < 0.05$) (Table 4.5). While there were no significant differences between values of bending yield load ($p > 0.05$). The failure load data obtained from the quasi-static bending tests was used as an absolute upper limit when choosing subsequent bending fatigue load values.

Table 4.5 - Mean (± SD) quasi-static structural properties of the screws.

Screw design	Ultimate Static Load (N)	Bending Yield Load (N)	Bending Stiffness (N/mm)	EI_e (N·m^2)
Cylindrical	525 ± 15	272 ± 29	126 ± 4	1.25 ± 0.04
Dual-core	721 ± 8	284 ± 65	156 ± 24	1.55 ± 0.24

4.4.4   Dynamic Bend Test

In the dynamic bend tests, the screws deformed steadily during loading. The tests were ended at the point at which the deformation abruptly increased and the screws failed. Both cylindrical and dual-core screws were able to complete 2.5 million cycles under 10% and 30% of the ultimate bending loads but failed for the remaining load levels of 40%, 50%, 65% and 75% (Figure 4.18). During testing, it was observed that the dual-core screws had longer fatigue lives for all loading levels. Moreover, the magnitude of load levels for the dual-core screws was significantly higher than for cylindrical screws ($p < 0.05$), with an average increase of 38%. The biggest differences between fatigue lives of both screw types occurred at 40% and 75% load levels with a 204% and 192% increase, respectively. It was observed that the failures for the cylindrical screws at higher load levels (65%, 75%) occurred at the head-shank junction, whereas for the lower load levels (40%, 50%) it occurred between the third and fourth thread (Figure 4.18a). The situation was reversed in the case of the dual-core screws (Figure 4.18b). No plastic deformation of the screws was observed. The deformation of the PU foam blocks where the load was applied was insignificant in both the yielding and cyclic tests.
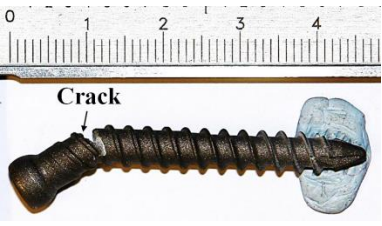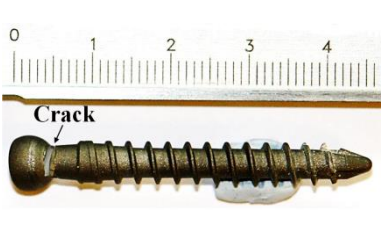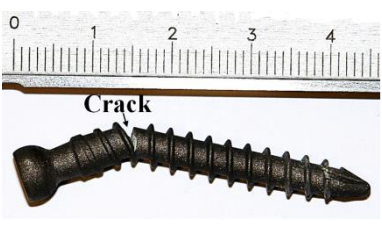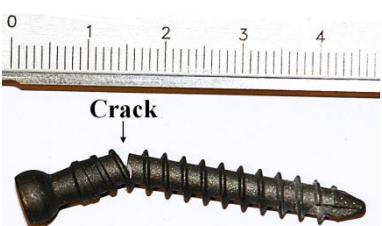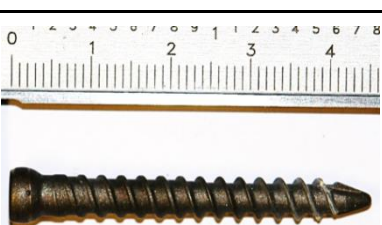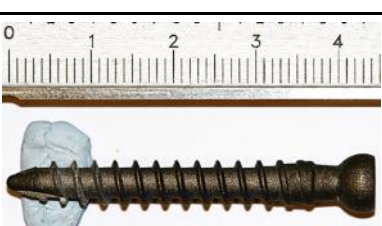
75% load level		
65% load level		
50% load level		
40% load level		
30% load level		
10% load level		
	a) Cylindrical screws	**b) Dual-core screws**

Figure 4.18 - Fatigue failure: a) Cylindrical screws; b) Dual-core screws.

Table 4.6 and Table 4.7 present the results of the cyclic tests for both types of pedicle screws. Figure 4.19 shows fatigue (F-N) curves for both cylindrical and dual-core screws, where it can be seen that each point showed a regular trend.

Table 4.6 - Results of the cyclic tests for the cylindrical screw (BFus 2).

Cylindrical Sample Nº	Ultimate static strength (%)	Peak force (N)	Cycles to failure	Position of failure
1	75	390	2,290	Head-shank junction
2	65	340	7,489	Head-shank junction
3	50	260	32,772	Third or fourth thread
4	40	210	129,640	Third or fourth thread
5	30	160	2,500,000	No visible cracks/reached run-out
6	10	50	2,500,000	No visible cracks/reached run-out

Table 4.7 - Results of the cyclic tests for the dual-core screw (BFus 2+).

Dual-core Sample Nº	Ultimate static strength (%)	Peak force (N)	Cycles to failure	Position of failure
1	75	540	6,693	Third or fourth thread
2	65	470	13,818	Third or fourth thread
3	50	360	47,454	Head-shank junction
4	40	290	393,663	Head-shank junction
5	30	220	2,500,000	No visible cracks/reached run-out
6	10	70	2,500,000	No visible cracks/reached run-out
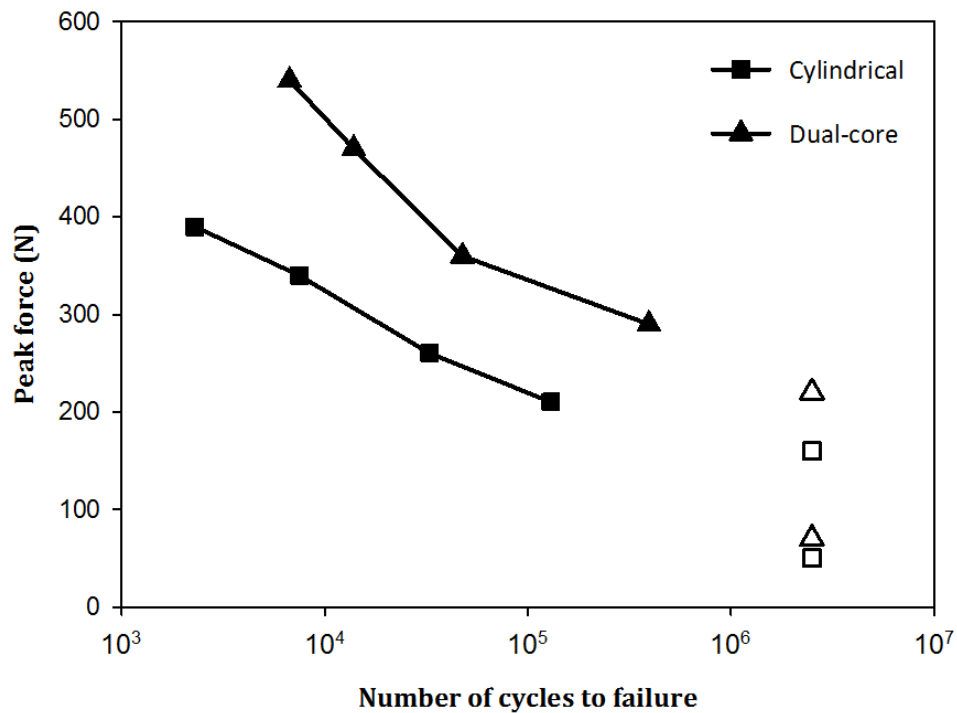
Figure 4.19 - Fatigue curves obtained by plotting the sinusoidal force peak value in relation to the number of cycles to failure, N. All results are taken from Table 4.6 and Table 4.7. The results of the test that did not fail are presented as the unfilled squares and triangles.

4.4.5   Microscopic Evaluation of the Pedicle Screws Fracture Surfaces

4.4.5.1   Quasi-static Bend Test

Figure 4.20 shows optical microscope (OM) images of the fracture surfaces of three cylindrical screws. The fractures consisted of three regions: area of the origin of the crack, the crack propagation region and region of the failure, which are clearly seen and marked, wherever it was possible. The images indicate the occurrence of brittle fracture due to a single bending force.

a) Sample 2 — Proximal — Distal

b) Sample 3

c) Sample 5 — Proximal — Distal
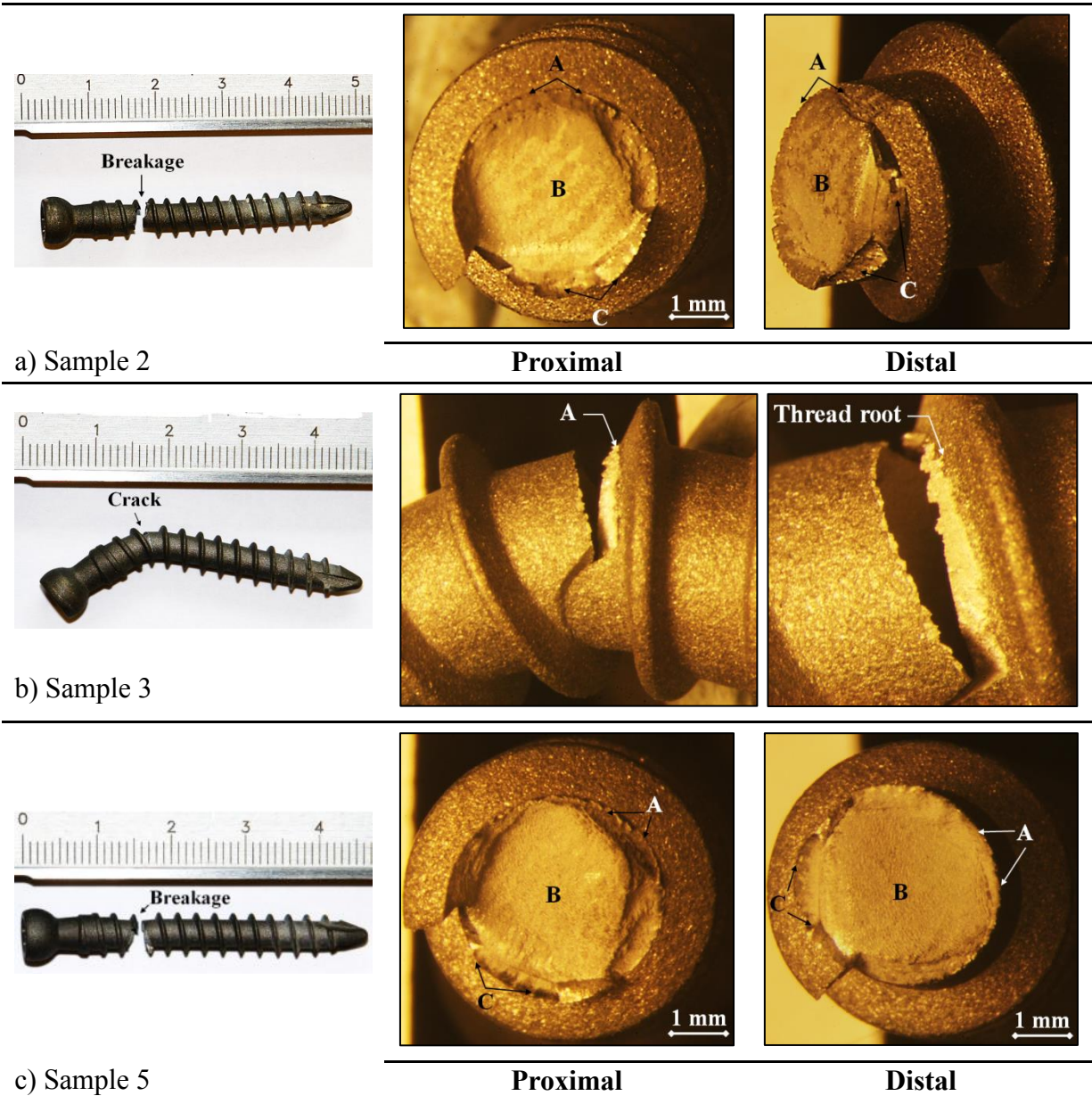
Figure 4.20 - Stereo microscope images of BFus 2 screws fracture surface. The letters in the photography indicate A - Initiation of the crack; B - crack propagation; C - Brittle failure.

All cracks occurred in between the third and fourth thread and seemed to initiate at the root of the thread. As mentioned before in section 4.2.1, the profile of the cylindrical screw thread has a sharp transition between the inner diameter and the base of the thread. Therefore, this may be a location of stress concentration, which leads to crack formation and eventually to complete failure. For sample 3 (Figure 4.20b), the crack did not lead to an absolute failure of

112

the screw, therefore, it was impossible to view and evaluate the fracture surface. Though, it is clearly seen that the crack originated in the same way as in the case of the other two samples.

4.4.5.2 Dynamic Bend Test

Microscopic evaluation of the fracture surfaces of the screws after dynamic bending tests was performed. Figure 4.21 shows both proximal and distal parts of the fractured BFus 2 screws. It can be observed that for the higher loading levels (Figure 4.21a, b) the failure occurred at the head-shaft junction. The fracture was brittle and was characterized by a smooth surface. The fracture at the lower loading levels (Figure 4.21c, d) occurred at the same locations as it did during quasi-static tests (between the third and fourth thread). The photos of the surfaces clearly indicate that the cracks were initiated at the thread root and that the breakage was brittle with no significant plastic deformation.

BFus 2 (Cylindrical)	Proximal	Distal
a) 75% load level		
b) 65% load level		
c) 50% load level		
d) 40% load level		
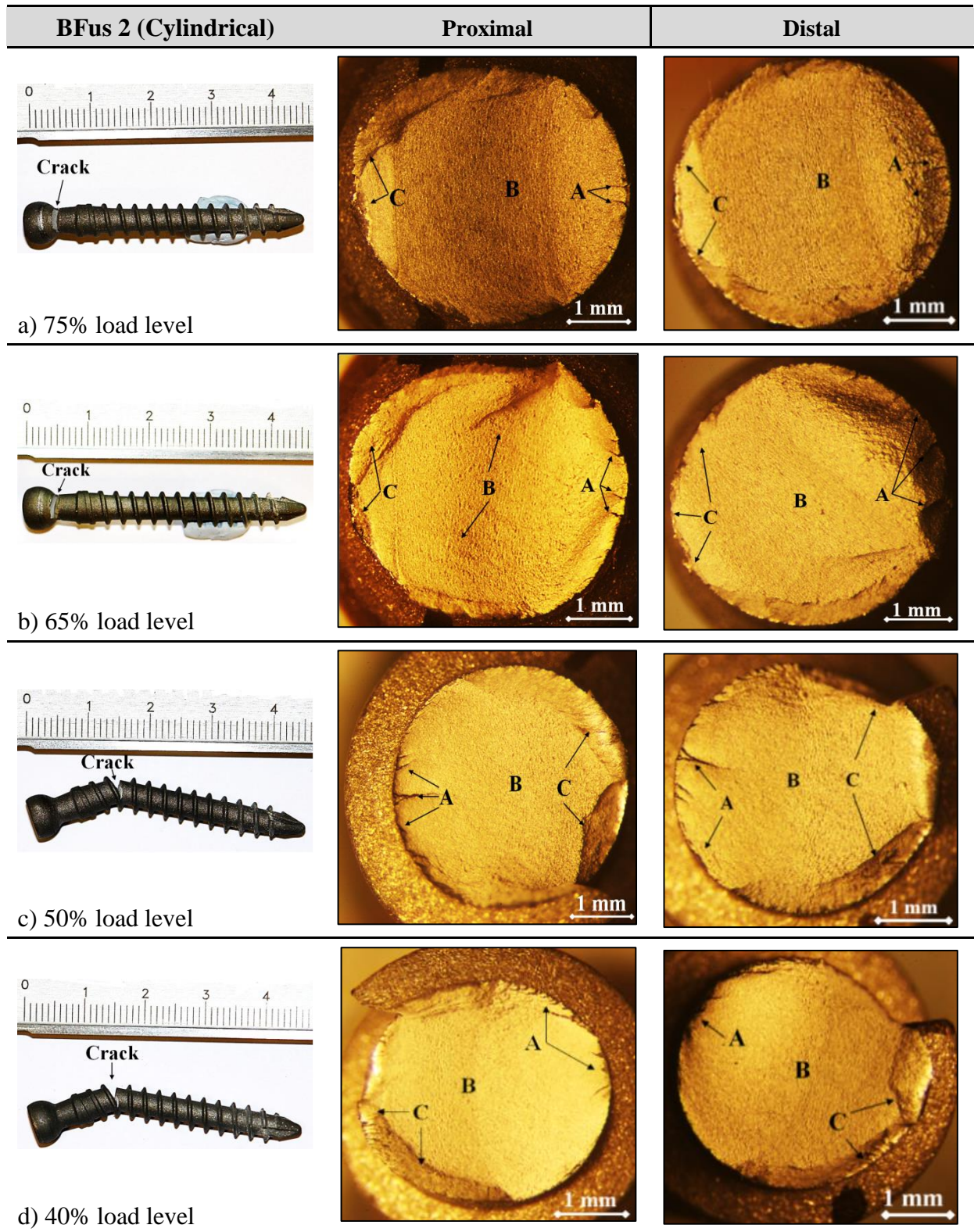
Figure 4.21 - Stereo microscope images of BFus 2 screws fracture surface. The letters in the photography indicate A - Initiation of the crack; B - Fatigue crack propagation; C - Brittle failure.

The situation was reversed in the case of BFus 2+ screw failures (Figure 4.22). Fractures occurred at the head-shank junction at the lower loading levels (50%, 40%), and between the third and fourth thread for higher loads (75%, 65%). In this last case, the crack does not seem to initiate at the base of the thread, but slightly further down the shank. Additionally, in Figure 4.22c and d, besides the fracture surfaces, the fragments of the star-shaped cavity in a screw head with a rough machining finish can be seen. It seems that when the crack propagation reached that region, it has stripped a large part of it. The images indicate that all breakage was brittle without significant plastic deformation.
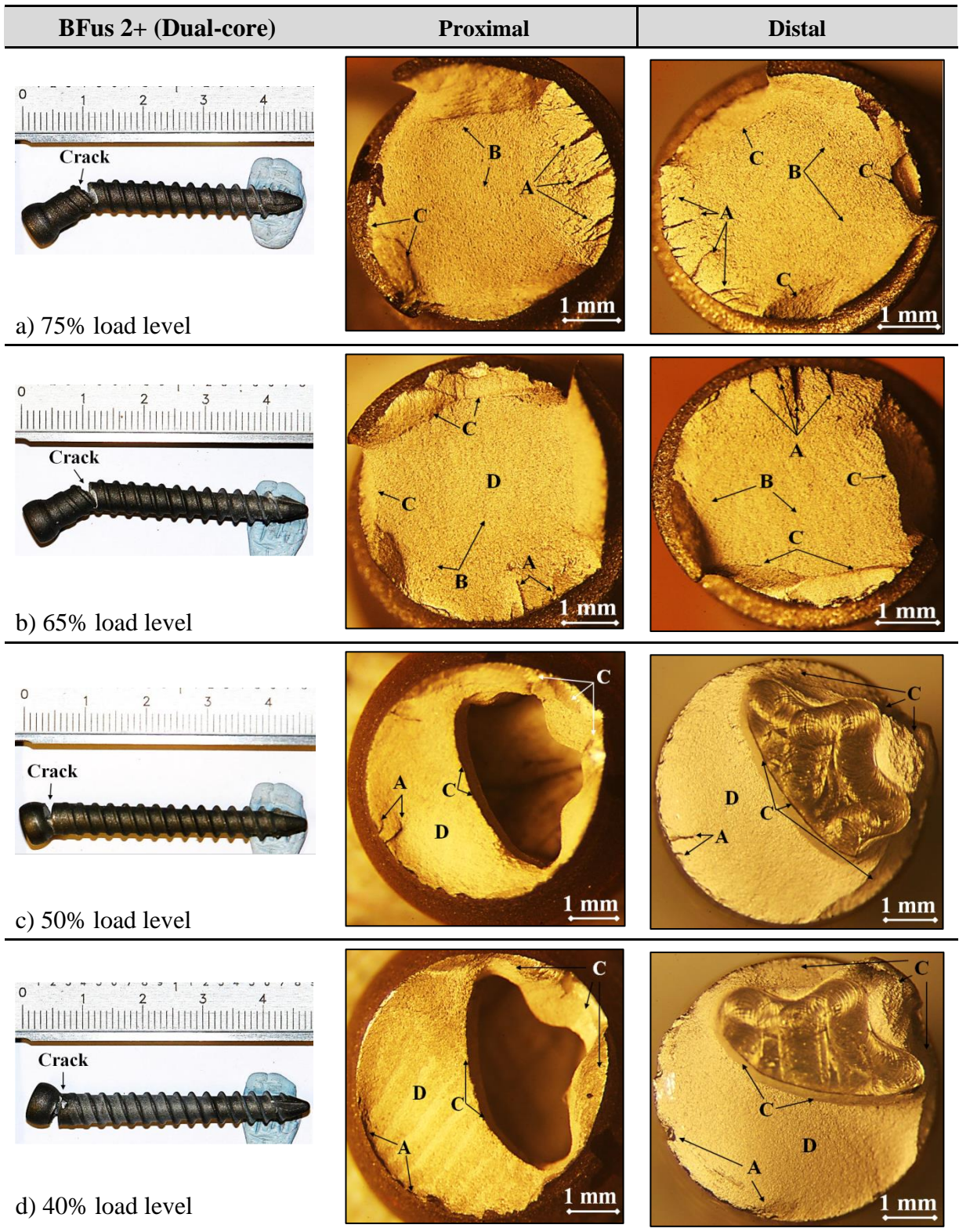
Figure 4.22 - Stereo microscope images of BFus 2+ screws fracture surface. The letters in the photography indicate A - Initiation of the crack; B - Beach marks; C - Brittle failure; D - Fatigue crack propagation.

4.4.5.3   Explanted Pedicle Screws

Figure 4.23 shows the fracture surfaces of the explanted BFus 2 screws. After analysing the images, bending fatigue was identified as the main cause of failure. Surfaces show typical characteristics of fatigue bending failure, beach marks, ratchet marks, a crack initiation site and brittle failure. For Screw 1 and 2 (Figure 4.23a, b) the breakage occurred at the head-shank junction of the screw. The fracture surfaces of the proximal parts show clearly visible beach marks that take up more than half of the fracture area, which may indicate that screws were working under low levels of nominal stress. Additionally, the surface of Screw 1 reveals several potential points of crack origin. In the case of Screw 2, the area of the final fracture region showed signs of plastic deformation. The failure of Screw 3 (Figure 4.23c) occurred on the shank, between the third and fourth thread. The image of the fracture surface shows that the cracks were initiated at the root of the thread, the lack of pronounced beach marks suggest that they progressed quickly leading to a complete failure.

a) Screw 1   b) Screw 2   c) Screw 3

d) Shank 1   e) Shank 2
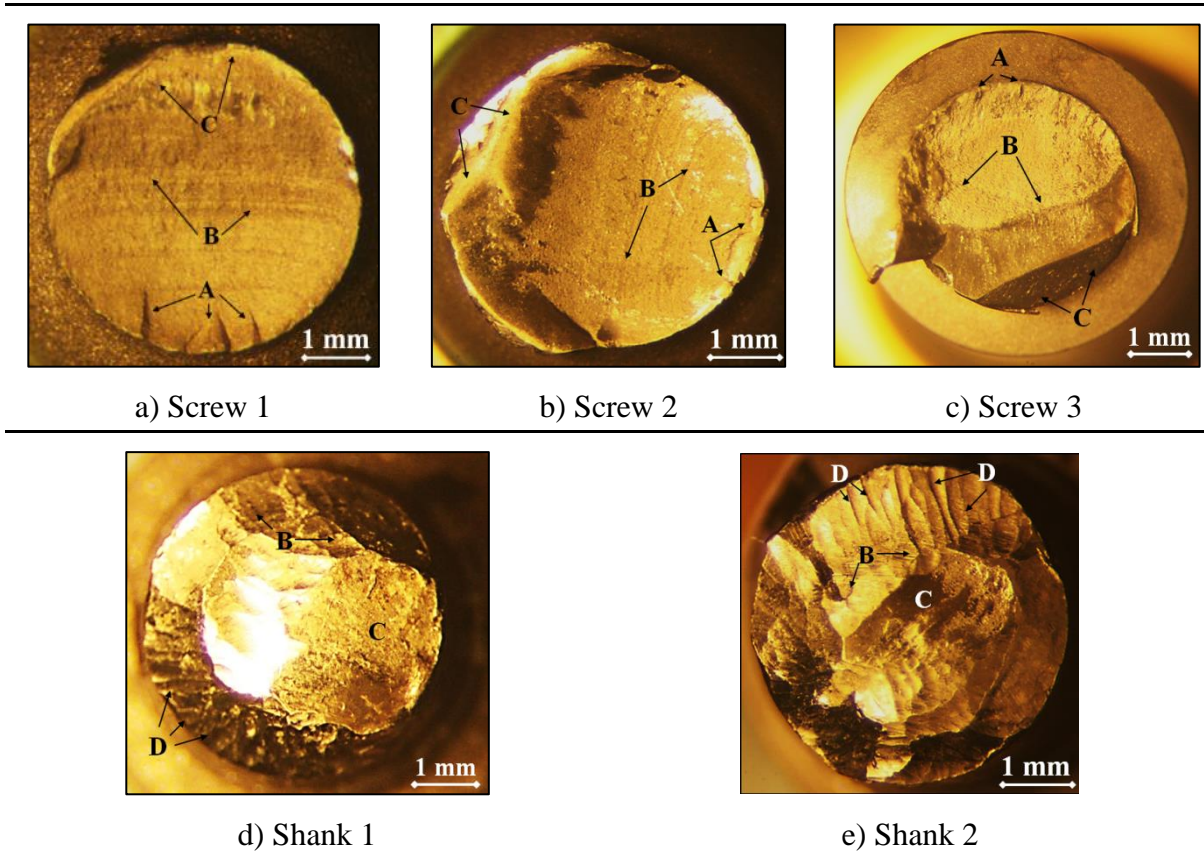
Figure 4.23 - Stereo microscope images of explanted broken pedicle screws fracture surface characterized by cylindrical geometry. The letters in the photography indicate A - Initiation of the crack; B - Beach marks; C - Final fracture region; D - Ratchet marks.

Fracture surfaces of the distal part of the screw in Figure 4.23d and e show examples of the damage caused by the combination of bending and torsion. Ratchet marks that can be clearly seen suggest multiple crack origins. The ratchet marks are the planes between adjacent crack origins and grow perpendicular to the crack propagation. This can be an indication of a high-stress concentration, such as a shaft step with a very small radius.

4.4.6 A Critical Review of the Failed Cylindrical Screws

This section presents a critical review of failed cylindrical screws BFus 2 (Figure 4.24). This investigation has been conducted in order to identify the likely causes of breakages and to refer them to the results obtained during the mechanical testing.

a) Case 1	b) Case 2	c) Case 3

d) Case 4	e) Case 5
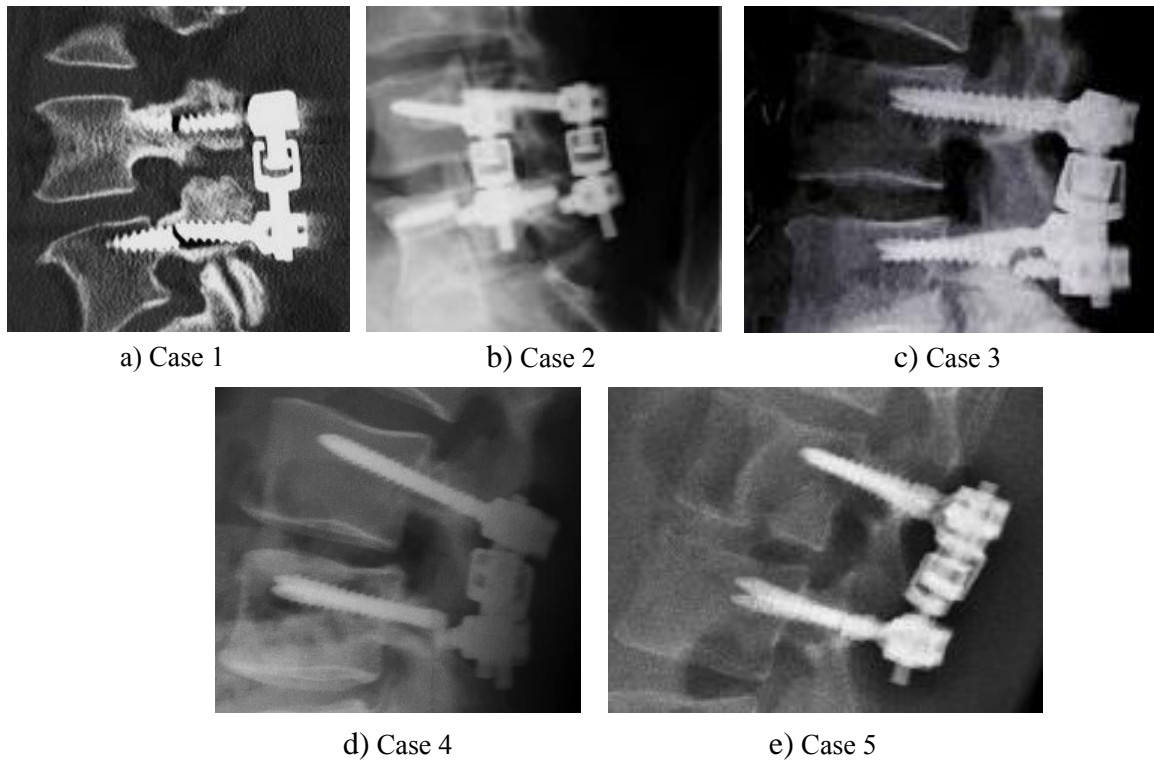
Figure 4.24 - Radiographs of the lumbar spine showing failed cylindrical screws provided by S14 Implants.

Case 1 presents breakage of a pedicle screw in both cranial and caudal side in the L4-L5 spinal segment. It is clearly visible that screws suffered fracture around halfway through the threaded shaft length. The radiological observation revealed the emergence of a mobility chamber (a free space between the screw and the bone tissue) around the proximal parts of the broken screws, which indicates that they might have been insufficiently embedded into the pedicles. Only the distal half of the screw shaft seems to be properly embedded in the bone.

Case 2 shows the fracture of the pedicle screws at the caudal side in the spinal segment L4-L5. The breakage occurred at the junction with the bone and no mobility chamber was observed.

In Case 3 it was observed that the screw broke at the caudal side in the L3-L4 spinal segment. It seems that the fracture occurred at the junction with the bone or just slightly further down the shank, around the initial threads. Again, no mobility chamber was observed and the three remaining screws were intact.

Case 4 is characterized by the caudal breakage of the screws in the segment L3-L4. Similarly to case 2, the fracture occurred at the junction with the bone and there was no visible mobility chamber. Additionally, the operative report revealed isthmic lysis (spondylolysis) on the L4 vertebra detected intraoperatively, which was causing destabilisation.

Case 5 presents fractured pedicle screws in both cranial and caudal side in the L2-L3 spinal segment. The breakage occurred around the initial threads at the junction with the bone without any signs of the mobility chamber.

4.5　FEA of the Pedicle Screws

A linear static finite element analysis of both screw models was conducted, in order to understand how the changes in geometry have influenced the stress distribution under the same loading and boundary conditions.

4.5.1　Finite Element Models

The solid models of the screws were created and assembled in SolidWorks 2014 (Dassault Systems SolidWorks Corp. MA, USA). The geometry and dimensions of the screws were provided by the S14 Implants and coincided with the tested screws.

In order to mimic the performed quasi-static tests, the assemblies consisted of screws and cubic testing blocks (Figure 4.25). The SolidWorks assemblies were converted into Parasolid format and transferred to the ABAQUS (6.14-AP Dassault Systems) to carry out a linear FE analysis.
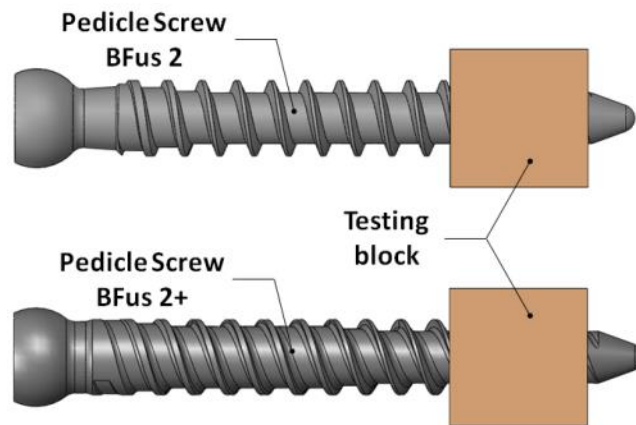
Figure 4.25 - SolidWorks models of pedicle screws.

4.5.2   Material Properties

The material properties of the screws and testing blocks were set to match the test specimens used in this study. The pedicle screw specimens and testing blocks were made from Titanium Alloy (TA6V ELI) and PU foam grade 40, respectively. Therefore, to carry out the finite element analyses and calculate von Mises stress distribution, the same material properties were assigned to each part of the assembly (Table 4.8).

Table 4.8 - Material properties of different parts used in the finite element model.

Component	Material	Young's modulus (MPa)	Poisson's ratio
BFus 2	Titanium Alloy (TA6V ELI)	114000	0.34
BFus 2+			
Testing block	PU Foam grade 40	1000	0.3

4.5.3   Mesh Control

All solid models of screws and testing blocks were meshed using quadratic tetrahedral (C3D10) and linear hexahedral (C3D8R) elements. The mesh convergence study was carried out for each of the screw models in order to find an acceptable balance between computational time and mesh size. In order to reduce computational time, element numbers were increased only toward the areas where the stress concentrations were predicted, namely the head-shank junction and the proximal screw shaft (Figure 4.26).
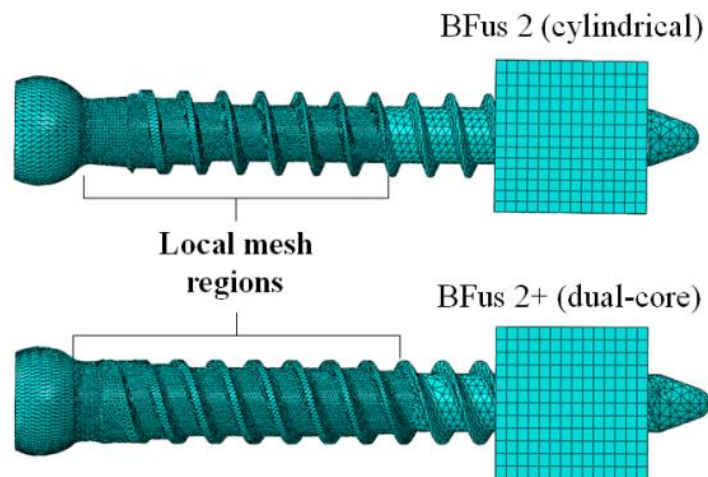
Figure 4.26 - Meshed models of both screw designs.

Figure 4.27 shows an example of mesh optimization study for BFus 2+ screw. Additionally, the warning elements were defined as those that had a shape factor less than 0.1. Manually adjusting the mesh seeds helped to achieve quality warnings at the level of 0.06% and 0.03% for both BFus 2 and BFus 2+ screw models, respectively. The details of the mesh for each individual component are shown in Table 4.9.
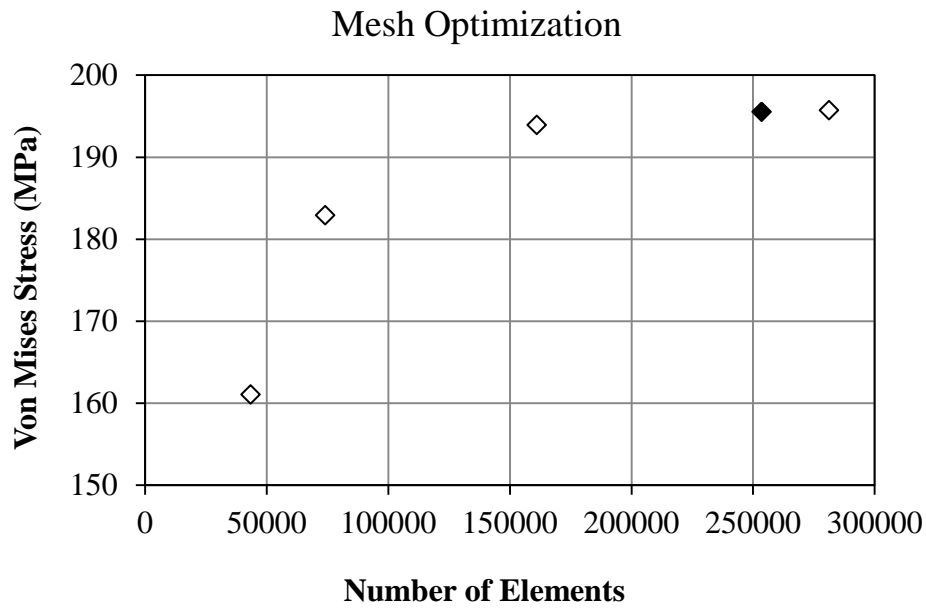
Mesh Optimization

Figure 4.27 - Mesh optimization for BFus 2+ screw model. The filled point signifies the selected

mesh.

Table 4.9 - Mesh properties of different parts used in the finite element model.

Component	Element type	Number of elements	Total number of elements	Ave. size (mm)
BFus 2	C3D10	219433	**219433**	0.7
Testing block 1	C3D10	5286	**7798**	0.7
	C3D8R	2512		
BFus 2+	C3D10	253476	**253476**	0.7
Testing block 2	C3D10	9515	**11317**	0.7
	C3D8R	1802		

4.5.4   Boundary and Loading Conditions

In order to conduct the comparison study between the screws, the same boundary and loading

conditions were applied to both models. Similarly to the earlier mechanical tests, both screws

were loaded as a cantilever beam. In both cases, the head of the screw had been completely

constrained and the uniformly distributed load F had been perpendicularly applied to the part

of the surface of the testing block (Figure 4.28). To avoid plastic effects, the load magnitude of 50 N was chosen so that the material's elastic limit was not exceeded. To simplify the simulation, a "tie" constraint was assigned to the interface between the testing block and the thread embedded in it. This type of bonding ties two separate surfaces together in a way that there is no relative motion between them.
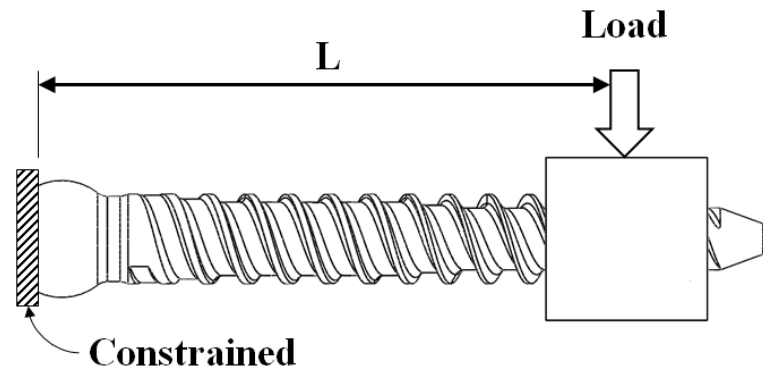
Figure 4.28 - Loading and boundary conditions of investigated screws tested in cantilever bending.

4.5.5   FEA Results

Table 4.10 presents the analysis results of the stresses and the displacement in the models in units of MPa and mm, respectively under the load of 50 N.

Table 4.10 - Maximal displacement and stress values of the models after FE analyses.

| Component | Bending Force of 50 N | | | | |
| | Max von Mises (MPa) | Max Principal (MPa) | Max displacement (mm) | Collar area | |
				von Mises (MPa)	Principal (MPa)
BFus 2	349.0	444.6	0.542	275.2	305.6
BFus 2+	195.5	211.8	0.323	155.6	171.9

The maximum von Mises and tensile stress values obtained for the dual-core screw (BFus 2+) accounted for 56% and 48% of the values obtained for the cylindrical screw, respectively. The maximum displacement in the downward direction of the dual-core design was significantly lower than that of the cylindrical screw, and the percentage decrease was approximately 40%. Figure 4.29 presents the distribution of stress for the entire deformed screw models, along with the maximum value locations. The results show that the maximum stress concentrations were located in the proximal part of the screw shank, between the third and fourth thread, for both designs.
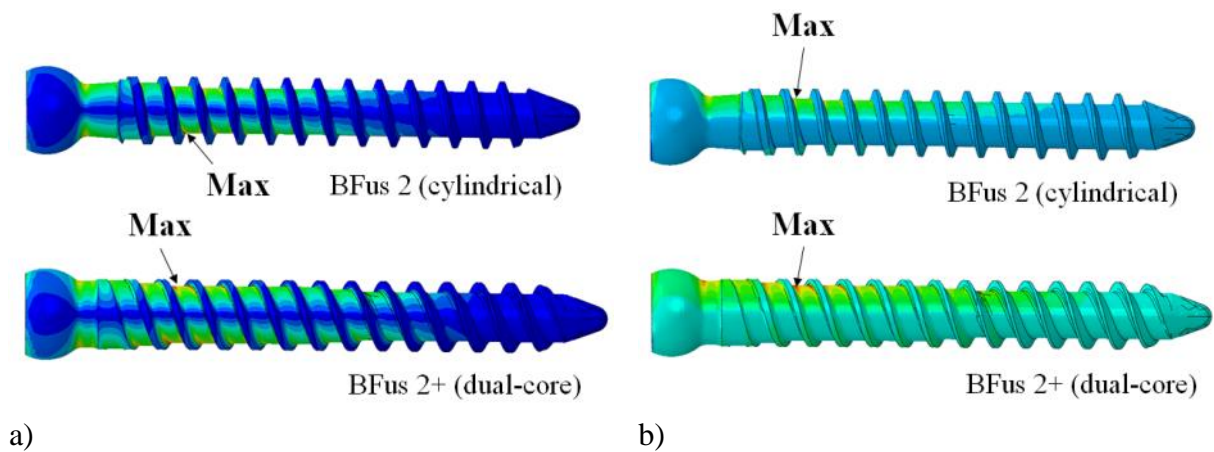
Figure 4.29 - The stress distribution of the pedicle screws: a) von Mises stress; b) tensile stress.

Figure 4.30 shows detailed views of the locations of stress concentration and thread geometry. The highest stress concentrations occurred at the root of the thread, but their distribution was different for each screw and highly depended on the geometry of the thread. In Figure 4.30a it can be clearly seen that the geometry of the cylindrical screw thread was the cause of high local stress concentrations. On the other hand, Figure 4.30b shows how introducing a thread root radius helped to better distribute and decrease the magnitude of the stress.

a) BFus 2 screw

b) BFus 2+ screw

c) BFus 2 screw

d) BFus 2+ screw
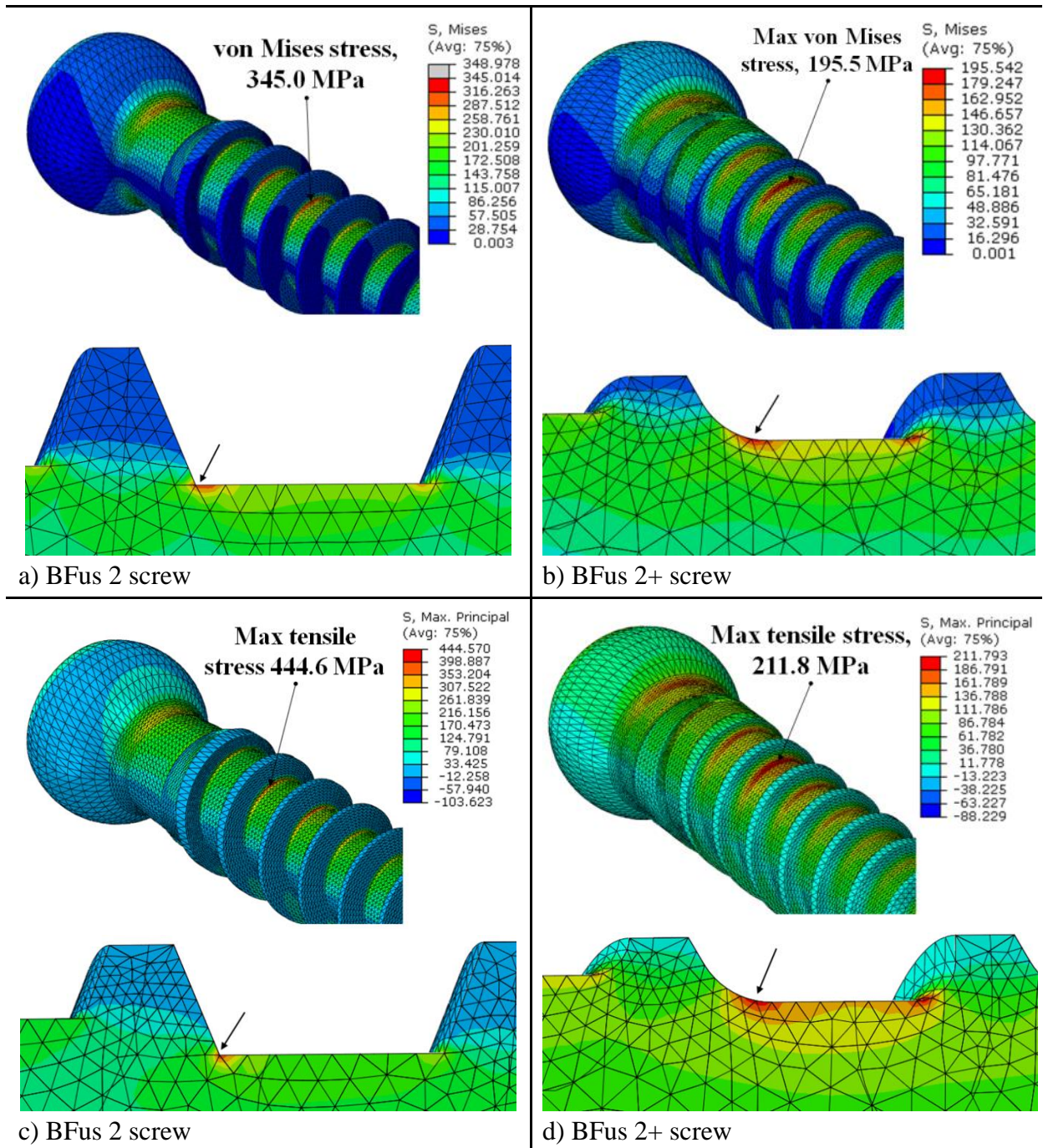
Figure 4.30 - Detailed view of the locations of stress concentration at the proximal part of the screw shank for both designs.
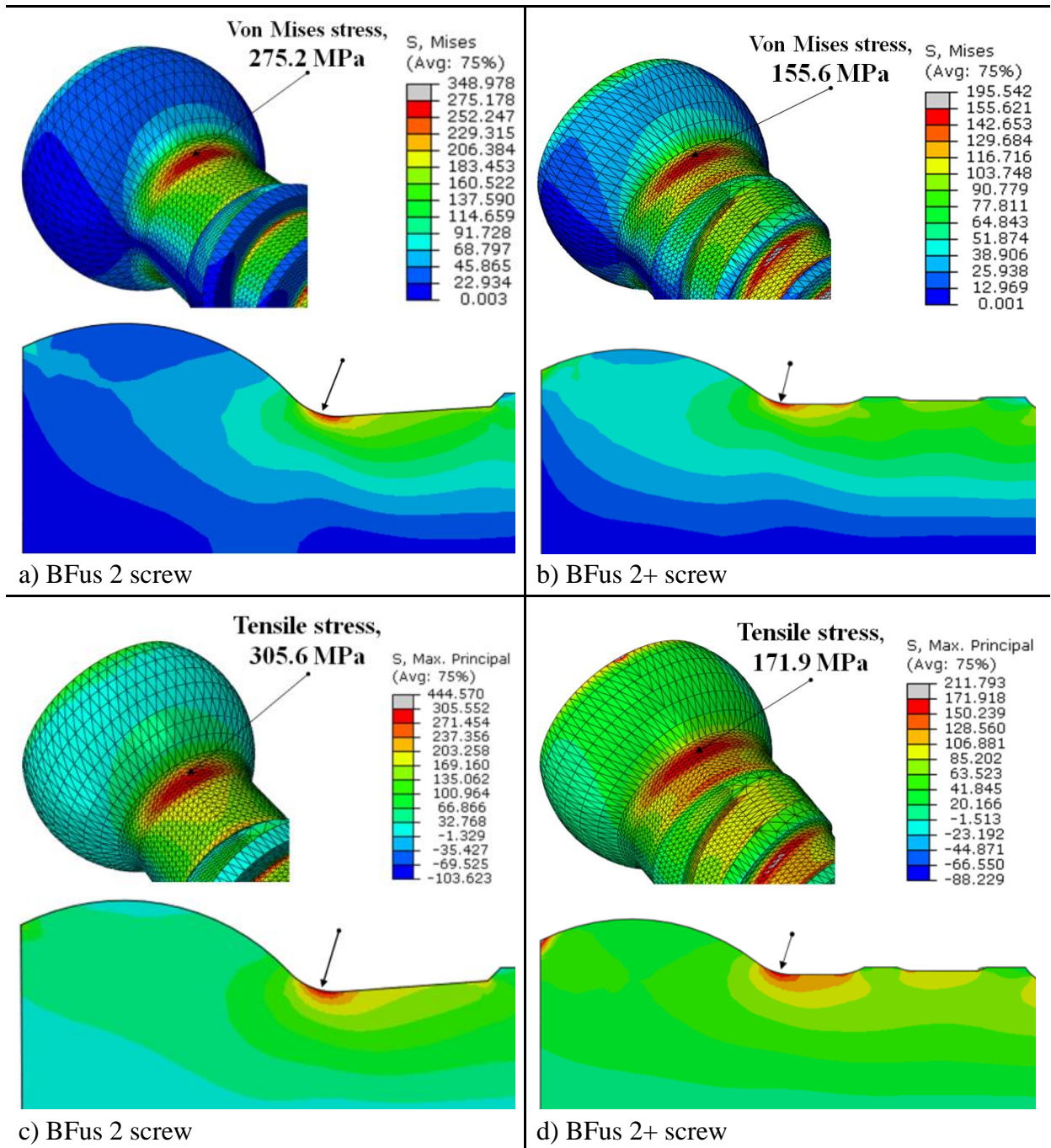
Figure 4.31 - Detailed view of the stress concentration at the collar of the screw designs.

Another region that required a closer look was the junction between screw's head and shank. Figure 4.31 shows a detailed view of stress distribution at the collar region of both screws under the load of 50 N. It can be seen that the value of both the von Mises and tensile stresses is significantly lower for the BFus 2+ screw design and the percentage decrease was approximately 43% and 44%, respectively.

The results of the FE analysis were in good agreement with the results obtained during mechanical testing. Table 4.11 presents the results of the displacement under the load of 50 N, obtained during finite element analysis and the quasi-static bending tests. The differences between the values were reasonably small, given the idealized conditions of the simulation which did not take into account e.g. the surface finishing of the screws. The displacement obtained during the simulation for both BFus 2 and BFus 2+ screws was 12% higher and 15% lower compared to the real situation (test), respectively.

Table 4.11 - Comparison of the maximal displacement between the FEA models and experimental results.

Component	Maximum displacement under 50 N (mm)	
	FEA	**Mechanical Test**
BFus 2	0.542	0.483 ± 0.002
BFus 2+	0.323	0.382 ± 0.002

The regions of the maximum stress concentration corresponded with the failure sites of breakage and plastic deformation (Figure 4.32). If the load would have been higher and plastic effects were taken into the account, plastic deformation would have occurred, just like they did during the mechanical testing.
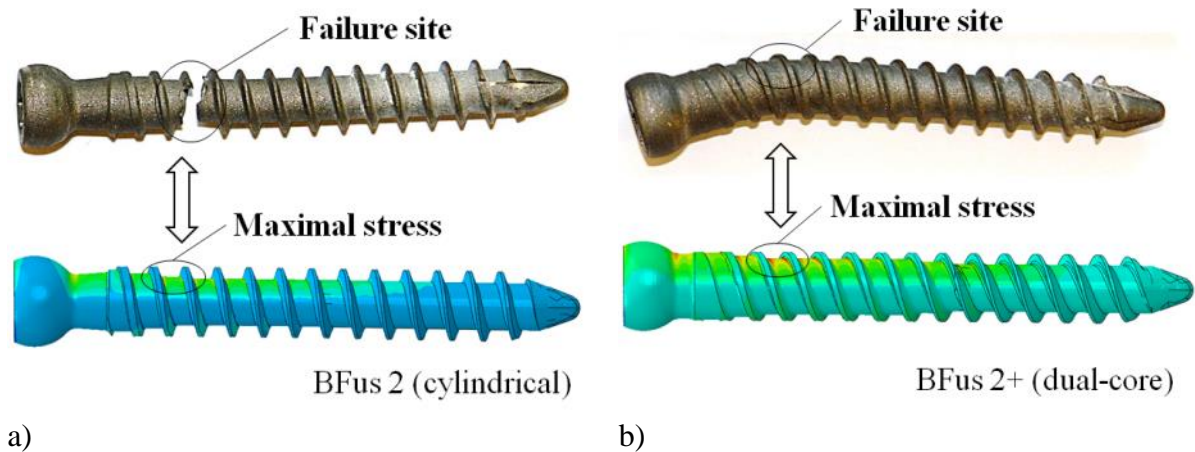
Figure 4.32 - Maximum tensile stress concentrations in finite element analysis corresponding to, failure sites of the screws during mechanical testing.

4.6   Discussion

The study presented in this chapter has sought to determine whether the dual-core screw design with a double start thread (BFus 2+) would provide improved pullout resistance as well as increased bending and fatigue strength compared with the single-threaded, cylindrical pedicle screw (BFus 2).

Stiffness and bending resistance of the pedicle screws

The comparison of the area moments of inertia for both screws have revealed that even a slight alteration in the inner diameter size, can considerably increase the resistance to bending. The calculations have been made for two specific cross-sections: the collar of the screws – C and 10 mm further down the shank – D. According to the results, changing the diameters by just 0.97 mm and 0.8 mm increased the moments of inertia and thus the resistance to bending in both cross-sections, by over two times. It has thus been proven that the changes introduced to the BFus 2+ screw design can potentially increase its bending strength.

Mechanical tests

Pullout strength is strongly associated with the screw design, especially its internal and external diameter, and thread profile (Demir and Basgül, 2015; Yaman et al., 2015; Krenn et al., 2008). According to previous studies (Wittenberg et al., 1993), increasing the core diameter at a constant outer diameter, reduces the flat overlap area and as a result, decreases the pullout strength. As mentioned before, the thread design is another feature that affects the pullout strength (Kim et al., 2012; Krenn et al., 2008; Hsu et al., 2005). In the present study, the thread pitch was equal for both screws however, the thread profile was different. The cylindrical screw had a single, V-shaped thread while a dual-core screw had a double start buttress thread. Both investigated screws were inserted into foam blocks to a depth of 20 mm according to ASTM F543. Therefore, only the distal parts of the threads of both screws were taken into account during the pullout tests and their FOA were comparable and had values of 104 mm^2 and 99 mm^2 for cylindrical and dual-core screws, respectively. In this study, standardized polyurethane foams were used rather than vertebrae to minimize bias from anatomic characteristics and bone density. The results of the pullout tests in three different foams have shown that the characteristics of the dual-core pedicle screw have not significantly increased resistance to pullout force compared with the cylindrical screw. Therefore, neither the double start nor the buttress thread profile significantly influenced the pullout resistance of the screw. However, whether the double lead has any effect on pullout strength is debatable. Brasiliense et al., (2013) compared dual threaded pedicle screw with the standard screw. The results of their study showed that the dual threaded screws exhibited higher pullout strength on high-density foams and lower on low-density foams compared to standard screws. This suggests that a dual lead is a more suitable solution for healthy bone cases. Mummaneni et al., (2002) conducted similar studies and compared the pullout strength

of dual lead and single lead pedicle screws in human vertebrae. However, in this case, the obtained results were similar to the present study and suggested that the pullout strengths of those two screws were not significantly different from each other. Yaman et al., (2015) compared pullout performance of three different screw designs: conical, dual threaded and dual-core with a double thread. In their studies, they used PU foams and ovine vertebra as a testing medium. In all cases, the highest pullout strength values were noted for dual-core and dual threaded pedicle screw. Yaman et al., (2015) have also observed that double threaded screws provided them with doubled insertion depth with same screwing round. Also in the present study, it was observed that the dual-core screw with its double lead provided faster insertion time into test blocks than a cylindrical screw, which is an important consideration for surgeons.

The results of the quasi-static and dynamic bending tests showed that the pedicle screw with dual-core geometry had significantly higher bending strength and fatigue life compared to the cylindrical design. During quasi-static bending tests all dual-core screws underwent plastic deformation, but no cracks were observed, whereas more than 50% of the cylindrical screws fractured between the third and fourth thread. During dynamic tests all investigated screws failed, except the ones under 10% and 30% loading levels, both lasting 2.5 million cycles. Failures in all cylindrical screws were located at the head-to-shaft junction for the higher load levels (65%, 75%) and between the third and fourth thread for the lower load levels (40%, 50%). The situation was reversed in the case of the dual-core screws. These observations agree with the results obtained by Griza et al., (2012) where the most common site of screw failure is at the junction of screw's hub and threaded part or in the middle section of the threaded part.

Previous studies have shown that the core diameter of the pedicle screw greatly influences its bending performance and fatigue life (Cho et al., 2010). The bending strength of a screw is proportional to the section modulus (Z), which is in turn proportional to the cube of the inner/core diameter ($Z{\sim}CD^3$). Therefore, even a slight change of the ID has a significant impact on the bending strength of the screw. Moreover, as the most frequent sites of pedicle screw breakage are usually located at the proximal part of the screw, the geometry of the neck also plays an important part in a bending strength. For this reason, tapering of the ID may also reduce the risk of screw breakage at the thread end. By comparing different designs, Chao et al., (2008) proved that the conical screws achieved higher bending strength than cylindrical designs.

In general, the dual-core screw was more difficult to deform or break and more durable during fatigue, compared with the cylindrical design because of the thicker core diameter at the proximal area of the screw and the reinforced geometry of the neck. The results from the quasi-static bending tests of the cylindrical screws suggest that the highest stress concentrations causing failure occurred in the region between the third and fourth thread. For both screws, this particular area was affected by the change in the size of the inner diameter (ID). In case of the cylindrical screw (BFus 2) the change was more abrupt as well as the overall size of the ID was smaller. Moreover, Griza et al., (2012), have suggested that pedicle screws with a small thread root radius should be avoided, as it may be a source of undesired stress concentrations that can lead to breakage. Contrary to a cylindrical screw, the thread of the dual-core screw had a thread root radius, which probably helped in reducing stress and avoiding fracture. After analysing the fracture surfaces of the cylindrical screws, it could be concluded that the lack of thread root radius may be the starting point of the crack propagation, leading to complete failure. These features may be a contributing factor to the

failures in the static tests and a mode of failure in the cyclic tests. Based on previous studies, it could be stated that the features improving bending and pullout strength are contradicted (Amaritsakul et al., 2014; Chao et al., 2008; Chao et al., 2010). Hence, screws that perform well under bending may not effectively resist loosening.

Microscopic surface evaluation

The microscopic analyses of the fracture surfaces of the tested screws have revealed that the applied bending forces have caused brittle fractures. During mechanical tests, two observed failure sites involved the head-shaft junction and the proximal part of the threaded shank. During mechanical tests, most of the cylindrical screws have failed at the thread root. While analysing the fracture surfaces, the sharp transition between the thread root and core diameter was observed. It was concluded that it may be the starting point of the crack propagation and, therefore, be a contributing factor to the failure in both static and cyclic tests. On the other hand, the dual-core screw was characterized by a small thread radius. In this case, the failure did not originate at the thread root but slightly more in the middle of the threads and the screw withstood higher load. These observations agree with the findings made by Griza et al. (2012), where the lack of thread root radius decreased fatigue performance.

The second failure site of the screws, which occurred during the dynamic tests, involved the junction between the head and shank. In case of the cylindrical screw, this region was recognized as one of the weakest parts of the geometry, due to shaft step with a small radius. This feature has weakened the cross-section causing stress concentrations which eventually caused failure. On the other hand, the dual-core screw was characterized by a wider collar with a smoother transition and bigger radius, which helped to withstand higher loads. In general, the fractures in both cases were characterized by smooth surfaces. However, in case of the dual-core screws, besides the fracture surfaces, the fragments of the star-shaped screw's

head could be observed. There is a possibility that the star-shaped cavity went too deep into the screw head and found itself too close to the collar and as a result has weakened it. Therefore, decreasing the depth of this cavity may help to increase the strength of this region.

While investigating the fracture surfaces of explanted screws, it was concluded that the fatigue bending and fatigue bending coupled with torsion, were the causes of failure. The assumption was made based on five broken screws, which were understood to be a limited number of samples. No additional information about the patients and an actual fixation of explanted screws were available. In general, the fracture sites of the explanted screws corresponded with the screws tested mechanically. In clinical use, screws are embedded into the vertebrae and if the fixation into the cortical bone is stiff enough the highest strains occur at the collar area of the screw. This seems to be the case in four explanted samples, which failed at the head-shank junction. In case of the fifth investigated screw, which was the only sample characterized by the same geometry as the tested BFus 2 design, the fracture was observed in the proximal part of the shank. The breakage occurred between the third and fourth thread and corresponded with the failure of BFus 2 screws under the quasi-static bending and the low loading levels during the dynamic tests. This could be due to the insufficient support provided by the cortical bone, which caused the bending stress to be transferred further along the screw shaft.

After analysing the fracture surfaces of both mechanically tested and explanted screws, in some cases, multiple crack initiation sites were observed. Fatigue crack initiation usually occurs at or near the surface, where the cyclic loading stresses are at a maximum. Therefore, the surface finish of the screws is significant and plays a part during crack initiation. The applied corundum blasting treatment was meant to give a certain amount of roughness to the surface, to induce cell proliferation, but it could have also been a source of micro-cracks,

which can be particularly dangerous during the fatigue loading. As it is commonly known, a rough surface finish has an adverse effect on the fatigue performance of high strength materials (Giacaglia and Queiroz, 2015). Therefore, some studies suggest (Griza et al., 2012) that pedicle screws should be machined with a smooth surface finish in order to reduce a failure rate. On the other hand, corundum blasting, as a type of shot-peening, could have induced surface residual compressive stresses. The presence of these stresses would have prevented cracks from opening and enhance fatigue resistance.

A critical review of the failed screws

In clinical use, pedicle screws function as a load-bearing cantilever beam. The load is applied to the head of the screw and the vertebral body acts as the support (Chen et al., 2003). During the insertion, the screw penetrates a finite thickness of cortical bone and enters the central cancellous bone of the vertebrae. Both a shear stress and a rotational moment are resisted at the bone-screw interface, involving both cortical and cancellous bone. The cortical bone has a higher yield strength compared to the cancellous portion, especially in the region of the pedicle, thus it can be regarded as a fulcrum (the support point). The failure at the bone-screw connection occurs in response to the bending moment if the yield strength of either the cortical or the cancellous bone behind the support point is exceeded.

The fracture location in case 1 indicated that the posterior part of the pedicle screw was unsupported. The emergence of the mobility chamber around proximal parts of the screws was observed, which indicates that the contact area at the cortical bone-screw interface was insufficient. Only the half distal length was properly embedded in the bone, thus the optimal support for the screw was not achieved. This lack of support resulted in high bending loads being transferred further down the shaft and thus was the root cause of the failure. It could be explained by a poor choice of screw size: screws too short with too small diameter. In order to

increase the contact area and thus increase the yield strength for both cortical and cancellous regions, the screw diameter and length must be increased. The larger screw diameter increases not only the bone-screw contact area behind the support point but also the area moment of inertia (Suk and Kim, 2016). It should be noted that a longer screw increases contact area only in the cancellous region, whereas contact area for an established screw diameter and thickness of cortical bone is fixed. The use of longer screws increases not only the contact area between cancellous bone and screw but also the length of the lever arm in the portion of the bone that lies behind the cortical support. However, it causes the increase of the bending moment at the screw entry point, simultaneously.

In four remaining cases, the screw breakage occurred at the junction with the bone. It is the most common site of pedicle screw failure, especially in a single-level fusion. In general, if the fixation into the cortical bone, which acts as a fulcrum, is stiff enough the highest strains occur in the collar area of the screw. Additionally, in case number 4 the operative report revealed isthmic lysis on the L4 vertebra detected intraoperatively, which was causing destabilisation. Thus it can be concluded that the screws in case 4 have undergone additional excessive stress due to the wrong surgical indication, which also contributed to its breakage. In most cases though, the failure involved low resistance to bending in the neck region and possibly a choice of screws with too small diameter. It is important to note that the size of the screws diameter is restricted by the size of the pedicle. As the results of the mechanical tests performed in this chapter suggest, the screw with a larger core diameter and reinforced neck offered more effective resistance to cantilever bending moments.

FEA

The FEA study was conducted to compare the performance of both pedicle screws under the same loading conditions and thus to verify whether the changes made to the geometry, significantly improved the bending resistance.

Based on the results obtained during the mechanical tests, the focus was on two main areas: the neck and the proximal part of the screw shaft. As expected the simulated cantilever bending put a high strain in these particular regions. The locations of the maximum stress concentration corresponded with the failure sites of the breakage and plastic deformations observed during the mechanical testing. It can be concluded that if the load would have been higher and plastic effects were taken into the account, plastic deformations would have occurred just like they did during testing.

Moreover, compared with the cylindrical screw, the magnitudes of stresses for the new dual-core design have been reduced significantly. The maximum tensile stresses for the threaded proximal part and the collar area of the screw have decreased 2 and 1.8 times, respectively. The detail views of both screws confirmed that the geometry of the thread had a significant influence on the stress distribution. The FE analysis explained that the fractures of cylindrical screws usually occurred at the thread root, because of the sharp transition between the core diameter and the base of the thread. The FE analysis confirmed that this feature was the source of high local stress concentrations, which contributed to the screw failure. After analysing the results for the dual-core screw it was confirmed that the change made to the thread geometry had stress-reducing qualities. The fillets introduced to the thread helped to decrease and distribute the stresses more evenly and as a result, reduce the possibility of breakage. The results of the FE analyses have confirmed that the new design of the screw has higher bending resistance compared to the previous design.

4.7   Chapter Summary

A completely new design of the dual-core screw BFus 2+ (S14 Implants, France) has been for the first time, mechanically tested and evaluated using FEA, and compared to commercially available cylindrical screw BFus 2 (S14 Implants, France).

The general conclusions of this chapter were:

- Dual-core screw (BFus 2+) showed improved mechanical performance than the previous cylindrical version (BFus 2), with the exception of pullout resistance.

- In all investigated examples the fracture occurred either at the head-shaft junction or in the proximal part of the threaded shank.

- The results of the FE analysis have confirmed that the new dual-core screw (BFus 2+) had higher bending resistance compared to the cylindrical (BFus 2) design.

- Mechanical tests along with the FE analysis showed that the design modifications have significantly decreased the magnitude of stresses and as a result lowered the possibility of screw breakage.

- The visual assessment of the broken screws based on the X-ray images, introduced a new variable, in the form of the importance of the screw size, which can have a crucial influence on the screw's mechanical performance in vivo. It was revealed that the likely causes of screw failure may not always be directly related to the hardware itself but to surgeon's wrong choice of the screw size.

5   Overall Discussion

Chapter Overview

The purpose of this chapter is to summarise the thesis, provide its main goals and conclusions as well as outlining some potential areas for future investigation. Section 5.1 provides a reminder of the main objectives of the study undertaken. The summary of the main results of this thesis is presented in section 5.2. Future work is detailed in section 5.3. Finally, the main conclusions drawn from the results are listed at the end of the chapter, in section 5.4.

5.1   Main Objectives

The aim of this thesis was to design and evaluate implants used in the treatment of intervertebral disc disorders. For this purpose, a new dynamic solution for the device to replace the degenerated intervertebral disc in the cervical spine was proposed. The specific objectives of this thesis concerning dynamic cervical disc prosthesis included:

- Developing a new dynamic design of cervical disc replacement device.

- Subjecting selected compliant materials to quasi-static compression tests.

- Manufacturing a prototype of the new disc device.

- Analysing the new disc design using the finite element method.

The research in this thesis has also described an assessment and comparison of the mechanical properties of two pedicle screw designs: a single-threaded cylindrical and a dual-core with a double start, which are part of a proprietary posterior lumbar stabilisation system. The specific objectives concerning the pedicle screw study included:

- Performing mechanical tests in order to assess and compare mechanical properties of both screw designs.

- Analysing both screw designs using the finite element method.

- Critical analysis of failed, explanted cylindrical screws, in order to identify the likely

  causes of failure and to refer them to the results obtained during mechanical testing.

5.2   Summary

Chapter 3 described the process of developing the design, prototyping and FE analysis of a

new dynamic cervical disc implant (CDyn), aiming to become an alternative to spinal fusion

and delay or eliminate the occurrence of adjacent spinal disease (ASD). The implant is

defined as dynamic, as it was designed as a combination of the traditional ball-on-socket

connection with the addition of an elastomeric core with viscoelastic properties. This is a

completely new design concept, as most of the current devices available on the market are

either based on the ball-on-socket mechanism or a compliant elastomer cushion. Combining

these two solutions enables the device to provide such movements as flexion-extension,

lateral bending, axial rotation as well as axial compression, and therefore may better mimic

the functionality of a natural disc. CDyn consisted of 4 elements: the upper plate

(incorporating the socket), the lower plate, and the ball (bearing surface), all to be

manufactured from PEEK (Invibio Ltd. Optima 450G), and an elastomeric deformable core.

The ball and the upper plate create the ball-on-socket connection, whereas the deformable

elastomeric core is enclosed within the device, between the ball and the lower plate. The

CDyn device was designed in such a way, that during high compression the movement of the

ball part closed the gap between it and the lower plate, thus preventing complete compression

of the elastomeric core, and potentially protecting the core from damage. Furthermore, the

CDyn device was designed to maintain the mobility provided by the ball-on-socket

connection, even when the elastomeric core loses its properties. Unlike other available

devices whose profile is limited to flat endplates, or at best, a minor convexity, the external surfaces of CDyn device are characterized by a convex geometry. This is to ensure a better fit of the device and thus increase the contact surface between the device and the vertebrae. Moreover, the device uses a bone-sparing technique as the endplates feature low-profile teeth, designed to ensure immediate fixation, eliminating the need for a special bone adaptation. The proposed concept was modelled with a use of SolidWorks 2014 (Dassault Systèmes SolidWorks Corporation, Waltham, USA) and represents the smallest footprint size (anterior-posterior: 14 mm and lateral: 15 mm).

A Hertzian contact model was used in order to investigate the likely contact stresses of the ball-on-socket as well as the effect of radial clearance between the mating parts. A theoretical analysis of the maximum contact stresses occurring between the mating surfaces of the ball and socket was carried out for three different values of the radial clearance: 0.05, 0.1 and 0.7 mm. The results showed that all maximum contact stress values obtained during analysis were far below the yield strength of PEEK 450G under compression, which is reported as 120 MPa. Moreover, it was found that the predicted stress experienced by the contact surface of the CDyn device would not result in material fatigue.

In order to find a suitable material for the deformable core, a number of elastomeric materials including ChronoSil, MED 4770, MED 4780 and Elast-Eon were tested in quasi-static compression. According to predefined requirements, an appropriate material had to withstand compressive loads of at least 200 N, without exceeding more than 1 mm deformation. It was found that only MED 4780 met this requirement and was therefore selected for further testing. It should be noted that the materials were tested without any constraints, which is not the case when it comes to the device as a whole.

In order to further verify the mechanical performance of the device, a finite element analysis was carried out in which, using ABAQUS (6.14-AP Dassault Systems), the whole assembly was subjected to axial compression. The results showed that maximum von Mises stresses obtained under 150 N (selected according to the ISO 18192-1) and 1200 N (representing the worst loading case), did not exceed PEEK's compressive and fatigue strength.

Additionally, in this study, several rapid prototype models made of Vero White polyacrylate (Fullcure 830) and a resin based on the acrylic monomer (Fullcure 720) were produced. The prototypes were used to visually assess both the functionality of the ball-on-socket connection as well as the device dimensions. The last rapid prototype of the device was evaluated and was found to work as intended. The prototype made from final materials (PEEK for the upper, lower plates and the ball part) however has not been made so far, due to costs beyond the scope of the project.

Considering the current state of work that had been made on this project, as well as the fact that there is a similar device made of PEEK, already in use, the NuNec device (Pioneer Surgical Technology Inc., Driebergen, Netherlands), it could be assumed that this concept may successfully pass through future mechanical tests, and in the near future provide better quality treatment for cervical disc replacement.

Chapter 4 presented the mechanical tests, finite element analysis and visual assessment of two pedicle screw designs with different geometries. The first screw type was characterized by a cylindrical shaft and a single V-shaped thread, while the other screw had a dual-core shaft with a double start buttress thread, as well as a wider neck. The studies were carried out, in order to compare both designs and better understand the impact of design features on their mechanical behaviour. Mechanical tests included axial pullout, quasi-static and dynamic bending tests, and have sought to determine whether the dual-core, double start pedicle screws

would provide better pullout strength as well as increased bending and fatigue strength compared to a single-threaded cylindrical screw. In order to avoid variability associated with the use of the human samples and provide more reliable results, the axial pullout tests were carried out using three polyurethane foams (PU) grade 10 (density: 0.16 g/cm^3), 20 (density: 0.32 g/cm^3) and 40 (density: 0.64 g/cm^3). The pullout test conditions were determined according to ASTM F543, whereas the quasi-static and dynamic bending tests followed ASTM F2193. Quasi-static cantilever bending tests were performed to obtain the ultimate static strength of each screw, defined as the maximum force before either plastic deformation or breakage. The dynamic tests were performed for six loading levels with peak forces corresponding to 10%, 30%, 40%, 50%, 65% and 75% of the ultimate static strength of each screw type, defined in quasi-static tests.

It was found that the dual-core screws had higher pullout strength in each PU foam, however, the differences were not statistically significant. Moreover, the dual-core screws had significantly higher bending strength and longer fatigue lives on each loading level when compared to cylindrical screws. During the quasi-static tests, all dual-core screws failed due to plastic deformation, whereas most of the cylindrical screws fractured in the proximal region of the threaded shaft. During dynamic tests, the fracture sites for both screw designs were observed either at the junction of the screw head and shaft or in the proximal region of the threaded shaft.

Additionally, a finite element analysis was carried out to compare the performance of both screw designs under static bending as well as to validate the quasi-static bending tests performed in the laboratory. The results of the analysis showed much lower stress values for a dual-core screw compared to a cylindrical design, under the same loading conditions.

The places of the maximum stress corresponded with fracture sites of the screws during the mechanical tests.

The study also included a visual assessment of failed, explanted cylindrical screws in order to identify the causes of their failure and to refer them to the results obtained during the mechanical tests. Visual assessment was performed by observing fracture surfaces of the broken screws using a low magnification stereomicroscope, as well as analysing X-ray images. Bending fatigue was identified as the main cause of screw failure. The failure sites were usually observed at the proximal part of the screw, at the junction of the screw head and shaft or at the threaded shaft, and corresponded to results obtained during mechanical tests and finite element analysis.

5.3   Future Work

The next stages of the CDyn device development would include further mechanical tests of the elastomeric material in order to verify its performance, especially in fatigue. It may be necessary to search for a new material in case of the fatigue failure. Once the final elastomeric material is determined the next step will involve manufacturing prototype implants from the final materials and subjecting them to a series of mechanical tests including wear tests and frictional torque performed using Bose spine simulator (Bose Corporation, ElectroForce Systems Group, Minnesota, USA) designed to carry out multi-directional motions. This would provide information about the tribological properties of the elastomeric core and the ball-on-socket connection. The new device is to be manufactured from PEEK; however, it would also be beneficial to test different materials. Stiffer materials such as PEEK reinforced with carbon fibres may allow for a lower thickness of parts and therefore larger dimensions of the elastomeric core. It would be also beneficial to evaluate the performance of a whole

assembly in a more complex simulated operating environment, where it could be incorporated into a fully defined cervical spinal segment and subjected to anatomical loads. Therefore, an FE model, including anatomical features such as ligaments, muscles and facet joints, would have to be created. The final step will include designing and prototyping dedicated tools for implanting the device, such as implant's inserter.

5.4   Conclusions

The overall conclusions of this thesis are as follows:

CDyn device

- A new design of the cervical disc replacement device combining the traditional ball-on-socket connection with the addition of an elastomeric core with viscoelastic properties has been modelled.

- The results of the FE analysis showed that, under the maximum compression of 1200 N, the stresses in the device are well below the compressive and fatigue strength of PEEK, the proposed material for the prototype of the new device. Therefore, the device will most likely withstand the expected loading conditions in the human cervical spine.

- The results of the FE analysis showed that the compressive force of 150 N, which is considered to be the average force found in the cervical segment in normal conditions, did not cause maximum compression of the elastomer (MED 4780) and thus maintained the ability of the device to compress axially.

- The results of quasi-static compression tests carried out on elastomeric materials showed that only MED 4780 met the initial requirements and could be qualified for further testing.

- Calculations of the likely working conditions of the ball-on-socket configuration carried out with Hertzian contact model showed that the clearance of 0.05 mm was the source of

low contact stresses. The theoretically predicted stress experienced by the contact surface of the device did not surpass the PEEK fatigue strength.

Pedicle screws study

- The dual-core screws had a higher pullout strength, in each PU foam, compared to cylindrical screws, however, the differences were not statistically significant.

- The double start thread provided shorter screw insertion time compared to a single thread, yet did not have a significant effect on pullout force.

- The dual-core screw had significantly higher bending strength and longer fatigue life, on each loading level, compared to the cylindrical type.

- During mechanical tests, the screw fracture occurred either at the head-shaft junction or in the proximal part of the threaded shaft. The fractures occurring at the threaded part of the shaft were initiated at the thread root.

- The FE analysis results showed lower stress values for the dual-core screw.

- The investigation of the explanted, failed pedicle screws has shown that the fatigue bending was the main cause of failure *in vivo*, and the failure sites corresponded to the results obtained during mechanical tests.

- The visual assessment of the broken screws based on the X-ray images, revealed that the likely causes of screw failure may not always be directly related to the hardware itself but to surgeon's wrong choice of the screw size.

Appendix A - Engineering Drawings

R5

R0.25

R0.25

4.50

$\phi 7$

All dimensions are in mm

TOLERANCES:
Tolerances unless otherwise stated:
whole numbers   0.25
one decimal place   0.1
two decimal places   0.05

MATERIAL: MED 4780

DRAWN BY: Alicja Kubiak

DATE: February 2018

TITLE: Elastomeric Core

SIZE
A4

SCALE: 10:1

Sheet 1 of 1

3rd Angle Projection

SECTION A-A

1.67
1.35
R5
R0.20
C

DETAIL C
SCALE 20 : 1

R0.25
0.11
R0.25

R0.75
R0.15
R8
A
A
4.70

Ø11

PROPRIETARY AND CONFIDENTIAL	All dimensions are in mm	MATERIAL: PEEK 450G	TITLE: Ball part		
The information contained in this drawing is sole property of A. Kubiak. Any reproduction in part or as whole without the written permission of A. Kubiak is prohibited.	TOLERANCES: Tolerances unless otherwise stated: whole numbers 0.25 one decimal place 0.1 two decimal places 0.05	DRAWN BY: Alicja Kubiak	SIZE A4	SCALE: 5:1	3rd Angle Projection
		DATE: February 2018		Sheet 1 of 1	

149

SECTION A-A

3.63
3.15
18°
2.50°
2.53
3.02

SECTION B-B

18°
R40
0.30
2.08

A
A

14
B
Ø7.30
Ø11
15
R2
R2
5.71°
4
B

MATERIAL: PEEK 450G	TITLE: Lower plate	
DRAWN BY: Alicja Kubiak	SIZE A4	SCALE: 5:1
DATE: February 2018		Sheet 1 of 1

All dimensions are in mm

TOLERANCES:
Tolerances unless otherwise stated:
whole numbers   0.25
one decimal place   0.1
two decimal places   0.05

PROPRIETARY AND CONFIDENTIAL
The information contained in this drawing
is sole property of A. Kubiak. Any reproduction
in part or as whole without the written
permission of A. Kubiak is prohibited.

3rd Angle Projection

3.30

2.01

5.90

R8

R20

R0.80

1.40

B

SECTION A-A

2.25

l

DETAIL B
SCALE 10 : 1

A

A

R20.44

R2

Ø11.41

Ø10.37

4

15

5.71°

14

PROPRIETARY AND CONFIDENTIAL		All dimensions are in mm		MATERIAL: PEEK 450G			TITLE:	Upper plate	

The information contained in this drawing is sole property of A. Kubiak. Any reproduction in part or as whole without the written permission of A. Kubiak is prohibited.

TOLERANCES:
Tolerances unless otherwise stated:
whole numbers 0.25
one decimal place 0.1
two decimal places 0.05

DRAWN BY: Alicja Kubiak

DATE: February 2018

SIZE **A4**

SCALE: 5:1

Sheet 1 of 1

3rd Angle Projection
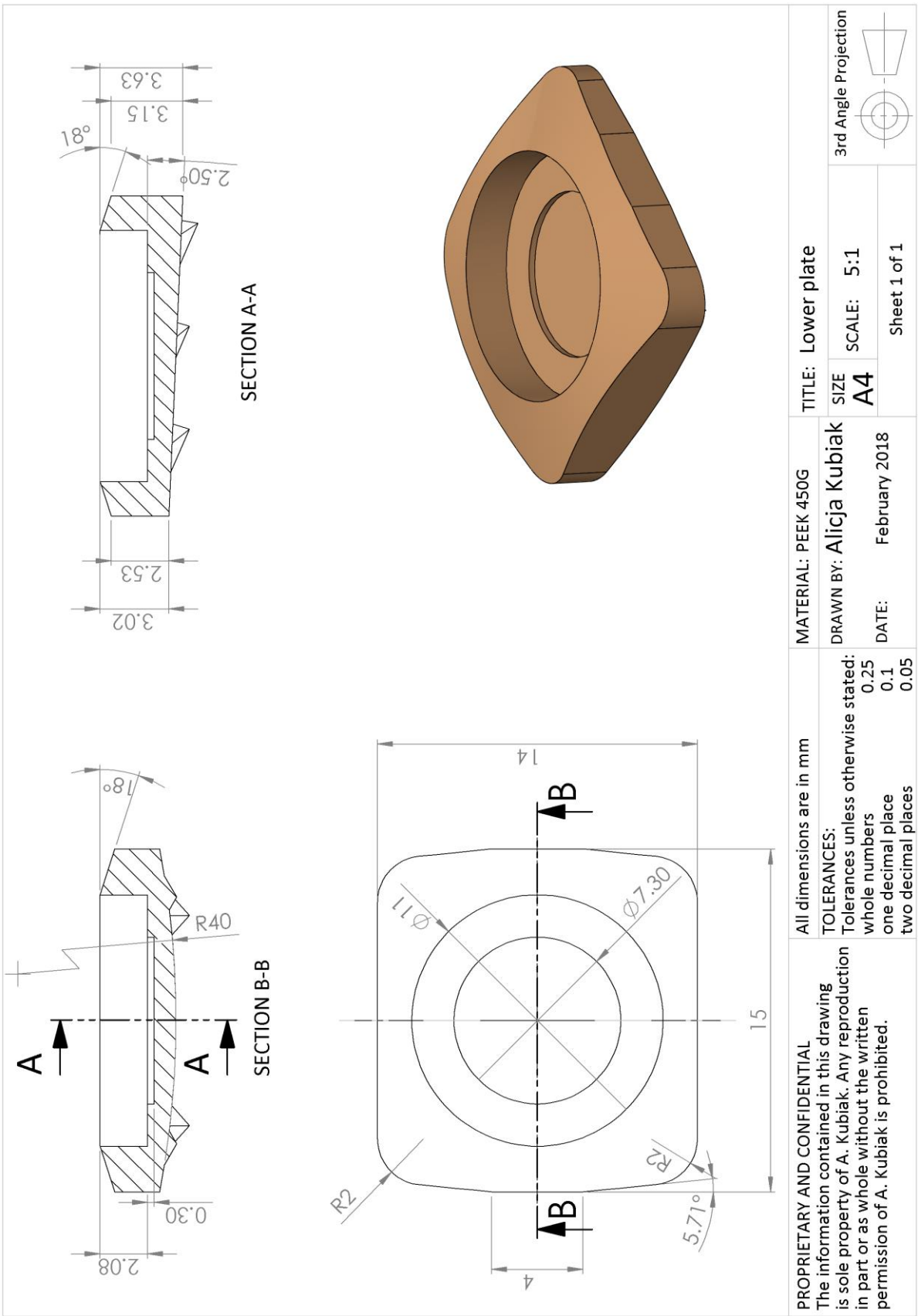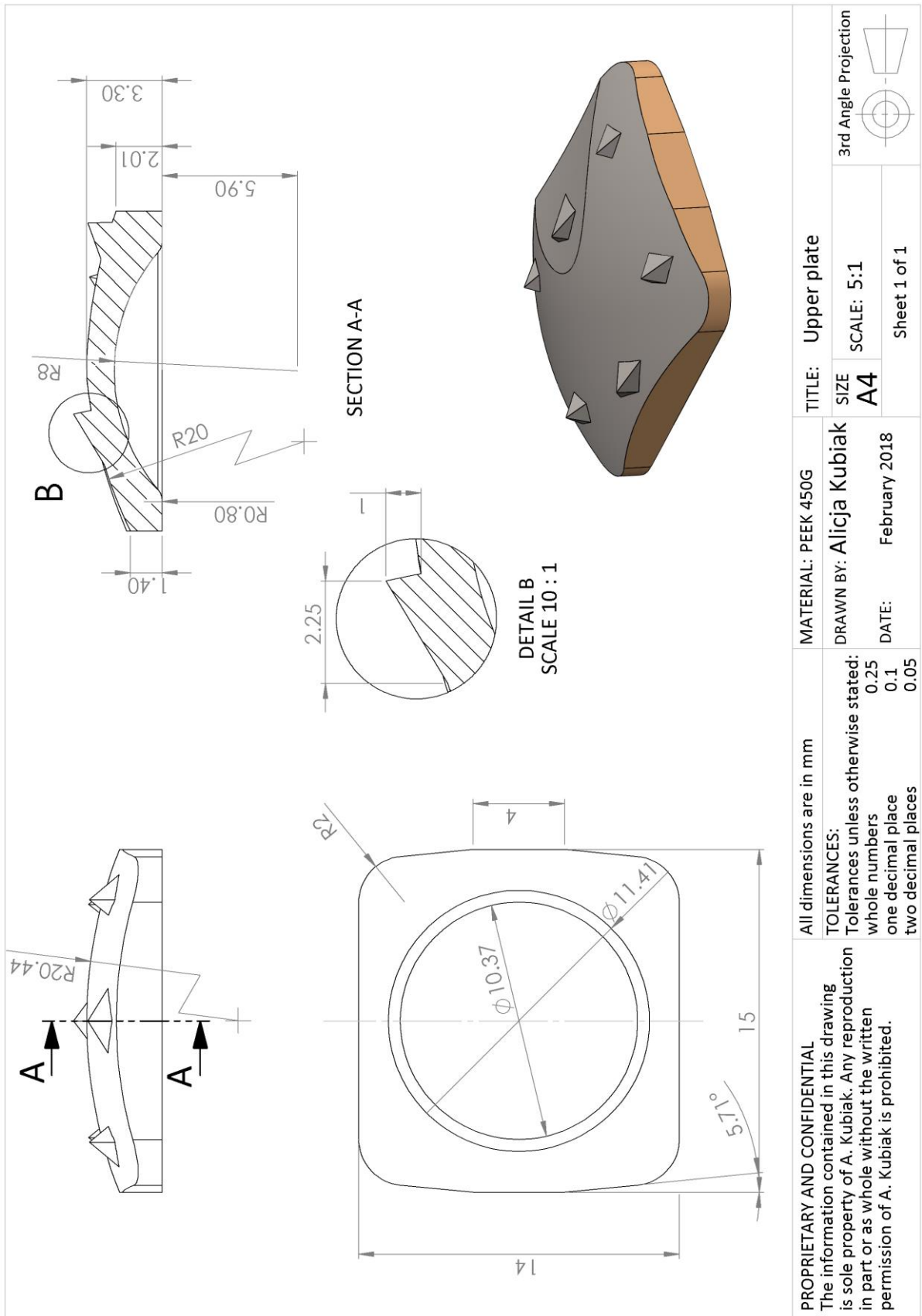
References

Abu Bakar, M. S. et al. 2003. "Tensile Properties, Tension-Tension Fatigue and Biological Response of Polyetheretherketone-Hydroxyapatite Composites for Load-Bearing Orthopedic Implants." *Biomaterials* 24(13): 2245–50.

Adams, Michael A. et al. 2000. "Mechanical Initiation of Intervertebral Disc Degeneration." *Spine* 25(13): 1625–36.

Altshuller, Genrich. 2004. *And Suddenly the Inventor Appeared. TRIZ, the Theory of Inventive Problem Solving*. ed. Lev Shulyak. Technical Innovation Center, Inc.

Alvin, Matthew D et al. 2014. "Cervical Arthroplasty: A Critical Review of the Literature." *The spine journal* 14(9): 2231–2245.

Alvin, Matthew D, and Thomas E Mroz. 2014. "The Mobi-C Cervical Disc for One-Level and Two-Level Cervical Disc Replacement : A Review of the Literature." *Medical Devices: Evidence and Research* 7: 397–403.

Amaritsakul, Yongyut, Ching Kong Chao, and Jinn Lin. 2014. "Biomechanical Evaluation of Bending Strength of Spinal Pedicle Screws, Including Cylindrical, Conical, Dual Core and Double Dual Core Designs Using Numerical Simulations and Mechanical Tests." *Medical Engineering and Physics* 36(9): 1218–23.

Anderson, Paul A., Steven M. Kurtz, and Jeffrey M. Toth. 2006. "Explant Analysis of Total Disc Replacement." *Seminars in Spine Surgery* 18(2): 109–16.

Anderson, Paul a., and Jeffrey P. Rouleau. 2004. "Intervertebral Disc Arthroplasty." *Spine* 29(23): 2779–86.

ASTM D695. 2011. "Standard Test Method for Compressive Properties of Rigid Plastics."

ASTM F136. 2013. "Standard Specification for Wrought Titanium-6Aluminum-4Vanadium ELI (Extra Low Interstitial) Alloy for Surgical Implant Applications."

ASTM F1839. 2012. "Standard Specification for Rigid Polyurethane Foam for Use as a Standard Material for Testing Orthopaedic Devices and Instruments."

ASTM F2193. 2014. "Standard Specifications and Test Methods for Components Used in the Surgical Fixation of the Spinal Skeletal System."

ASTM F543. 2013. "Standard Specification and Test Methods for Metallic Medical Bone Screws."

Auerbach, Joshua D et al. 2008. "The Prevalence of Indications and Contraindications to Cervical Total Disc Replacement." *The spine journal : official journal of the North American Spine Society* 8(5): 711–16.

AxioMed. 2012. *Durability Characterization of the Freedom Cervical Disc*. https://www.axiomed.com/pdf/WPaperDurabilityFCD.pdf.

Baltimore, Greater et al. 2013. "Cervical Total Disc Replacement with the Mobi-C Cervical Artificial Disc Compared with Anterior Discectomy and Fusion for Treatment of 2-Level Symptomatic Degenerative Disc Disease: A Prospective, Randomized, Controlled Multicenter Clinical Trial." 19(November): 532–45.

Barber, JW, SD Boden, T Ganey, and WC Hutton. 1998. "Biomechanical Study of Lumbar Pedicle Screws: Does Convergence Affect Axial Pullout Strength?" *J Spinal Disord* 11(3): 215–20.

Benmekhbi, M. et al. 2008. "Baguera Cervical Disc Prosthesis." *Interactive Surgery* 3(4): 201–4.

Bogduk, Nikolai. 2005. *Clinical Anatomy of the Lumbar Spine and Sacrum*. Elsevier Health Sciences.

Brasiliense, Leonardo B C et al. 2013. "Characteristics of Immediate and Fatigue Strength of a Dual-Threaded Pedicle Screw in Cadaveric Spines." *Spine Journal* 13(8): 947–56.

Brown, T, QB Bao, and HA Yuan. 2012. "The Use of PEEK in Spine Arthroplasty." In *Recent Advances in Arthroplasty*, , 211–34.

Brown, Tim, and Qi-Bin Bao. 2012. "The Use of Self-Mating PEEK as an Alternative Bearing Material for Cervical Disc Arthroplasty: A Comparison of Different Simulator Inputs and Tribological Environments." *European spine journal* 21 Suppl 5: S717-26.

BS EN 60812. 2006. "Analysis Techniques for System Reliability - Procedure for Failure Mode and Effects Analysis (FMEA)."

BS ISO 14630. 2012. "Non-Active Surgical Implants - General Requirements."

BS ISO 18192-1. 2011. "Implants for Surgery - Wear of Total Inervertebral Spinal Disc Prostheses - Part 1: Loading and Displacement Parameters for Wear Testing and Corresponding Environmental Condition for Test."

Caridi, John M., Matthias Pumberger, and Alexander P. Hughes. 2011. "Cervical Radiculopathy: A Review." *HSS Journal* 7(3): 265–72.

Chao, Ching-Kong, Ching-Chi Hsu, Jaw-Lin Wang, and Jinn Lin. 2008. "Increasing Bending Strength and Pullout Strength in Conical Pedicle Screws: Biomechanical Tests and Finite Element Analyses." *Journal of Spinal Disorders & Techniques* 21(2): 130–38.

Chao CK, Lin J, Putra ST, Hsu CC. 2010. "A Neurogenetic Approach to a Multiobjective Design Optimization of Spinal Pedicle Screws." *J Biomech Eng-T ASME* 132(9): 091006.

Chen, Chen Sheng et al. 2005. "Failure Analysis of Broken Pedicle Screws on Spinal Instrumentation." *Medical Engineering and Physics* 27(6): 487–96.

Chen, Qizhi, Shuling Liang, and George a. Thouas. 2013. "Elastomeric Biomaterials for Tissue Engineering." *Progress in Polymer Science* 38(3–4): 584–671.

Chen, S. I., R. M. Lin, and C. H. Chang. 2003. "Biomechanical Investigation of Pedicle Screw-Vertebrae Complex: A Finite Element Approach Using Bonded and Contact Interface Conditions." *Medical Engineering and Physics* 25(4): 275–82.

Cho, W, S K Cho, and C Wu. 2010. "The Biomechanics of Pedicle Screw-Based Instrumentation." *The Journal of bone and joint surgery. British volume* 92(8): 1061–65.

Christensen, F B et al. 2000. "Titanium-Alloy Enhances Bone-Pedicle Screw Fixation: Mechanical and Histomorphometrical Results of Titanium-Alloy versus Stainless Steel." *European spine journal* 9(2): 97–103.

Cramer, Gregory D, and Susan A Darby. 2013. *Clinical Anatomy of the Spine, Spinal Cord, and Ans (Third Edition)*. Elsevier Health Sciences.

Darden, Bruce V. 2012. "ProDisc-C Cervical Disk Arthroplasty." *Seminars in Spine Surgery* 24(1): 8–13.

David, Thierry. 2005. "Revision of a Charité Artificial Disc 9.5 Years in Vivo to a New Charité Artificial Disc: Case Report and Explant Analysis." *European Spine Journal* 14(5): 507–11.

Demir, Teyfik, and Cemile Basgül. 2015. *The Pullout Performance of Pedicle Screws*. Springer.

Dintwa, Edward, Engelbert Tijskens, and Herman Ramon. 2008. "On the Accuracy of the Hertz Model to Describe the Normal Contact of Soft Elastic Spheres." *Granular Matter* 10(3): 209–21.

Du, Junjie et al. 2011. "Early Follow-up Outcomes after Treatment of Degenerative Disc Disease with the Discover Cervical Disc Prosthesis." *The spine journal : official journal of the North American Spine Society* 11(4): 281–89.

Ebraheim, Nabil A., Robert E Rupp., Edward R. Savolaine, and Derek. Reinke. 1994. "Use of Titanium Implants in Pedicular Screw Fixation." *Journal of Spinal Disorders* 7(6): 478–86.

Faghihnejad, Ali, and Hongbo Zeng. 2013. "Chapter1: Introduction." In *Polymer Adhesion, Friction, and Lubrication*, ed. Hongbo Zeng. New Jersey: John Wiley & Sons Inc., 1–18.

Fogel, Guy R, Charles a Reitman, Weiqiang Liu, and Stephen I Esses. 2003. "Physical Characteristics of Polyaxial-Headed Pedicle Screws and Biomechanical Comparison of Load with Their Failure." *Spine* 28(5): 470–73.

Gadd, Karen. 2011. *TRIZ for Engineers: Enabling Inventive Problem Solving*. Wiley.

Gaines, R W. 2000. "The Use of Pedicle-Screw Internal Fixation for the Operative Treatment of Spinal Disorders." *The Journal of bone and joint surgery. American volume* 82–A(10): 1458–76.

Galbusera, Fabio, Chiara M Bellini, Marco Brayda-Bruno, and Maurizio Fornari. 2008. "Biomechanical Studies on Cervical Total Disc Arthroplasty: A Literature Review." *Clinical biomechanics (Bristol, Avon)* 23(9): 1095–1104.

Gere, James Monroe. 2008. "Mechanics of Materials." In *Mechanics of Materials*, , 913.

Ghori, Ahmer et al. 2016. "Long Term Societal Costs of Anterior Discectomy and Fusion (ACDF) versus Cervical Disc Arthroplasty (CDA) for Treatment of Cervical Radiculopathy." *International journal of spine surgery* 10: 8.

Giacaglia, Giorgio E O, and Wendell De Queiroz. 2015. "Pedicle Screw Rupture : A Case Study." *Case Studies in Engineering Failure Analysis* 4: 64–75.

Gillet, Philippe. 2003. "The Fate of the Adjacent Motion Segments after Lumbar Fusion." *Journal of Spinal Disorders and Techniques* 16(4): 338–45.

Golish, S Raymond, and Paul a Anderson. 2012. "Bearing Surfaces for Total Disc Arthroplasty: Metal-on-Metal versus Metal-on-Polyethylene and Other Biomaterials." *The spine journal : official journal of the North American Spine Society* 12(8): 693–701.

Goryacheva, G. 1998. *Contact Mechanics in Tribology*. Burlington: Kluwer Academic Publishers.

Griza, Sandro et al. 2012. "Case Study of Ti6Al4V Pedicle Screw Failures Due to Geometric and Microstructural Aspects." *Engineering Failure Analysis* 25: 133–43.

Grupp, Thomas M et al. 2010. "Alternative Bearing Materials for Intervertebral Disc Arthroplasty." *Biomaterials* 31(3): 523–31.

Haher Thomas R. and Valdevit Antonio. 2009. "Chapter 5 - Biomechanics of Spinal Instrumentation." In *Surgical Management of Spinal Deformities*, , 71–85.

Hallab, NJ. 2014. "Intervertebral Disc Joint Replacement Technology." In *Joint Replacement Technology*, Elsevier, 531–70.

Hibbeler, R.C. 2004. *Statics and Mechanics of Materials*. NJ: Upper Saddle River,: Pearson Prentice Hall.

Hickey, D S, and D W Hukins. 1980. "X-Ray Diffraction Studies of the Arrangement of Collagenous Fibres in Human Fetal Intervertebral Disc." *Journal of anatomy* 131: 81–90.

Holsgrove, Timothy Patrick. 2012. "A Dynamic Pre-Clinical Testing Protocol for Intervertebral Disc Replacement Devices." University of Bath.

Hsu, Ching Chi et al. 2005. "Increase of Pullout Strength of Spinal Pedicle Screws with Conical Core: Biomechanical Tests and Finite Element Analyses." *Journal of Orthopaedic Research* 23(4): 788–94.

Hughes, S P F et al. 2012. "The Pathogenesis of Degeneration of the Intervertebral Disc and Emerging Therapies in the Management of Back Pain." *The Journal of bone and joint surgery. British volume* 94(10): 1298–1304.

Hukins, David W. L., and Judith R. Meakin. 2000. "Relationship Between Structure and Mechanical Function of the Tissues of the Intervertebral Joint1." *American Zoologist* 40(1): 42–52.

Hukins, David W L, Johanna C Leahy, and Katharine J Mathias. 1999. "Selection of Replacement Materials." *Journal of Materials Chemistry* 3(d): 629–36.

Iyer, Sravisht, and Han Jo Kim. 2016. "Cervical Radiculopathy." *Current Reviews in Musculoskeletal Medicine* 9(3): 272–80.

Johansson, P, R Jimbo, and P Kjellin. 2014. "Biomechanical Evaluation and Surface Characterization of a Nano-Modified Surface on PeeK Implants: A Study in the Rabbit Tibia." *International journal of Nanomedicine* (9): 3903–11.

St. John, Kenneth R. 2014. "The Use of Polyurethane Materials in the Surgery of the Spine: A Review." *Spine Journal* 14(12): 3038–47.

Jutte, P. C., and R. M. Castelein. 2002. "Complications of Pedicle Screws in Lumbar and Lumbosacral Fusions in 105 Consecutive Primary Operations." *European Spine Journal* 11(6): 594–98.

Khoueir, Paul, K. Anthony Kim, and Michael Y. Wang. 2007. "Classification of Posterior Dynamic Stabilization Devices." *Neurosurgical Focus* 22(1): 1–8.

Kim, Young Yul, Woo Sung Choi, and Kee Won Rhyu. 2012. "Assessment of Pedicle Screw Pullout Strength Based on Various Screw Designs and Bone Densities - An Ex Vivo Biomechanical Study." *Spine Journal* 12(2): 164–68.

Krenn, Michael Hannes, Wolfgang Peter Piotrowski, Rainer Penzkofer, and Peter Augat. 2008. "Influence of Thread Design on Pedicle Screw Fixation. Laboratory Investigation." *Journal of neurosurgery. Spine* 9(1): 90–95.

Kurtz, Steven M. et al. 2007. "Polyethylene Wear and Rim Fracture in Total Disc Arthroplasty." *Spine Journal* 7(1): 12–21.

Kurtz, Steven M. 2011. "An Overview of PEEK Biomaterials." In *PEEK Biomaterials Handbook*, , 1–7.

Kurtz, Steven M, and John N Devine. 2007. "PEEK Biomaterials in Trauma, Orthopedic, and Spinal Implants." *Biomaterials* 28(32): 4845–69.

Kurtz, Steven M, and Avram A. Edidin. 2006. *Spine Technology Handbook*. London: Elsevier.

Kurtz, Steven M, Jeffrey M Toth, Ryan Siskey, and Lauren Ciccarelli. 2012. "The Latest Lessons Learned from Retrieval Analyses of Ultra-High Molecular Weight Polyethylene, Metal-on-Metal, and Alternative Bearing Total Disc Replacements." *Seminars in spine surgery* 24(1): 57–70.

Lauryssen, Carl et al. 2012. "Cervical Total Disc Replacement Using a Novel Compressible Prosthesis: Results from a Prospective Food and Drug Administration-Regulated Feasibility Study with 24-Month Follow-Up." *International journal of spine surgery* 6(1): 71–77.

Lawless, Bernard M., Spencer C. Barnes, Daniel M. Espino, and Duncan E.T. Shepherd. 2016. "Viscoelastic Properties of a Spinal Posterior Dynamic Stabilisation Device." *Journal of the Mechanical Behavior of Biomedical Materials* 59: 519–26.

Lazennec, Jean-Yves, Alain Aaron, Olivier Ricart, and Jean Patrick Rakover. 2016. "The Innovative Viscoelastic CP ESP Cervical Disk Prosthesis with Six Degrees of Freedom: Biomechanical Concepts, Development Program and Preliminary Clinical Experience." *European journal of orthopaedic surgery & traumatology : orthopédie traumatologie* 26(1): 9–19.

Lee, Casey K, and Vijay K Goel. 2004. "Artificial Disc Prosthesis: Design Concepts and Criteria." *The spine journal : official journal of the North American Spine Society* 4(6 Suppl): 209S–218S.

Leven, Dante, Joshua Meaike, Kris Radcliff, and Sheeraz Qureshi. 2017. "Cervical Disc Replacement Surgery: Indications, Technique, and Technical Pearls." *Current Reviews in Musculoskeletal Medicine* 10(2): 160–69.

Li, Yang, Guy R. Fogel, Zhenhua Liao, and Weiqiang Liu. 2017. "Finite Element Model Predicts the Biomechanical Performance of Cervical Disc Replacement and Fusion Hybrid Surgery with Various Geometry of Ball-and-Socket Artificial Disc." *International Journal of Computer Assisted Radiology and Surgery* 12(8): 1399–1409.

Lill, C. A. et al. 2006. "Mechanical Performance of Cylindrical and Dual Core Pedicle Screws in Calf and Human Vertebrae." *Archives of Orthopaedic and Trauma Surgery* 126(10): 686–94.

Lin, Chia-Ying et al. 2009. "Stress Analysis of the Interface between Cervical Vertebrae End Plates and the Bryan, Prestige LP, and ProDisc-C Cervical Disc Prostheses: An in Vivo Image-Based Finite Element Study." *Spine* 34(15): 1554–60.

Lou, Jigang et al. 2016. "Geometry of Inferior Endplates of the Cervical Spine." *Clinical neurology and neurosurgery* 142: 132–36.

Mcafee, Paul C. 2005. "Cervical and Lumbar Disc Replacement - The Ease of Revision." *Joint Replacement*: 38–42.

Misenhimer, G R et al. 1989. "Anatomic Analysis of Pedicle Cortical and Cancellous Diameter as Related to Screw Size." *Spine* 14(4): 367–72.

Mohi Eldin, Mohamed M., and Abdel Mohsen Arafa Ali. 2014. "Lumbar Transpedicular Implant Failure: A Clinical and Surgical Challenge and Its Radiological Assessment." *Asian Spine Journal* 8(3): 281–97.

Morishita, Y. 2008. "The Effects of the Degenerative Changes in the Functional Spine Unit on the Kinematics of the Cervical Spine." *Spine* 33(6): 178–82.

Mummaneni, Praveen V et al. 2002. "Biomechanical Evaluation of a Double-Threaded Pedicle Screw in Elderly Vertebrae." *Journal of spinal disorders & techniques* 15(1): 64–68.

Myshkin, Nikolai, and Alexander Kovalev. 2009. "Chapter 1: Adhesion and Friction of Polymers." In *Polymer Tribology*, London: Imperial College Press, 3–37.

Niinomi, Mitsuo. 1998. "Mechanical Properties of Biomedical Titanium Alloys." *Materials Science and Engineering: A* 243(1–2): 231–36.

Okuyama, K et al. 2000. "Can Insertional Torque Predict Screw Loosening and Related Failures? An in Vivo Study of Pedicle Screw Fixation Augmenting Posterior Lumbar Interbody Fusion." *Spine* 25(7): 858–64.

Van Ooij, A, F Oner, and A Verbout. 2003. "Complications of Artificial Disc Replacement." *Journal of Spinal Disorders & Techniques* 16(4): 369–83.

Panjabi, Manohar M. et al. 2001. "Mechanical Properties of the Human Cervical Spine as Shown by Three-Dimensional Load–Displacement Curves." *Spine* 26(24): 2692–2700.

Panjabi, Manohar M et al. 1998. "Critical Load of the Human Cervical Spine : An in Vitro Experimental Study." *Clinical Biomechanics* 13(1): 11–17.

Patel, Nr, and Pp Gohil. 2012. "A Review on Biomaterials: Scope, Applications & Human Anatomy Significance." *International Journal of Emerging Technology and Advanced Engineering* 2(4): 91–101.

Patel, Purvi. S D, Duncan. E T Shepherd, and David. W L Hukins. 2010. "The Effect of Screw Insertion Angle and Thread Type on the Pullout Strength of Bone Screws in Normal and Osteoporotic Cancellous Bone Models." *Medical Engineering and Physics* 32(8): 822–28.

Patel, Purvi S D, Duncan E.T. Shepherd, and David W.L. Hukins. 2013. "The Effect of 'Toggling' on the Pullout Strength of Bone Screws in Normal and Osteoporotic Bone Models." *The Open Mechanical Engineering Journal* 7: 35–39.

Patel, Purvi S D, Duncan E T Shepherd, and David W L Hukins. 2008. "Compressive Properties of Commercially Available Polyurethane Foams as Mechanical Models for Osteoporotic Human Cancellous Bone." *BMC musculoskeletal disorders* 9(1): 137.

Peng, Chan Wearn Benedict et al. 2011. "Intermediate Results of the Prestige LP Cervical Disc Replacement: Clinical and Radiological Analysis With Minimum Two-Year Follow-Up." *Spine* 36(2): E105-11.

Pihlajämaki, H, P Myllynen, and O Böstman. 1997. "Complications of Transpedicular Lumbosacral Fixation for Non-Traumatic Disorders." *The Journal of bone and joint surgery. British volume* 79(2): 183–89.

Pollintine, Phill, Patricia Dolan, Jon H Tobias, and Michael A Adams. 2004. "Intervertebral Disc Degeneration Can Lead to ' Stress-Shielding ' of the Anterior Vertebral Body A Cause of Osteoporotic Vertebral Fracture ?" 29(7): 774–82.

Popov, Valentin L et al. 2014. "Generalized Law of Friction between Elastomers and Differently Shaped Rough Bodies." *Scientific reports* 4: 3750.

Radhakrishnan K, Litchy WJ, O'Fallon WM, et al. 1994. "Epidemiology of Cervical Radiculopathy. A Population-Based Study from Rochester, Minnesota, 1976 through 1990." *Brain* 117(Pt 2): 325–35.

Renner, Susan M et al. 2004. "Augmentation of Pedicle Screw Fixation Strength Using an Injectable Calcium Phosphate Cement as a Function of Injection Timing and Method." *Spine* 29(11): E212-6.

Reyes-Sanchez, Alejandro et al. 2010. "Initial Clinical Experience with a Next-Generation Artificial Disc for the Treatment of Symptomatic Degenerative Cervical Radiculopathy." *SAS journal* 4(1): 9–15.

Rinde, J. A. 1970. "Poisson's Ratio for Rigid Plastic Foams." *Journal of Applied Polymer Science* 14(8): 1913–26.

Robotti, P, and G Zappini. 2011. "Thermal Plasma Spray Deposition of Titanium and Hydroxyapatite on Polyaryletheretherketone Implants." In *PEEK Biomaterials Handbook*, , 119–43.

Schoenfeld, A J, B McCriskin, M Hsiao, and R Burks. 2011. "Incidence and Epidemiology of Spinal Cord Injury within a Closed American Population: The United States Military (2000–2009)." *Spinal Cord* 49(8): 874–79.

Scholes, S.C., and A. Unsworth. 2010. "The Wear Performance of PEEK-OPTIMA Based Self-Mating Couples." *Wear* 268(3–4): 380–87.

Schroerlucke, Samuel R. et al. 2014. "How Does a Novel Monoplanar Pedicle Screw Perform Biomechanically Relative to Monoaxial and Polyaxial Designs?" *Clinical Orthopaedics and Related Research* 472(9): 2826–32.

Sekhon, L H S, and J R Ball. 2005. "Artificial Cervical Disc Replacement: Principles, Types and Techniques." *Neurology India* 53(4): 445–50.

Serhan, Hassan, Devdatt Mhatre, Henri Defossez, and Christopher M. Bono. 2011. "Motion-Preserving Technologies for Degenerative Lumbar Spine: The Past, Present, and Future Horizons." *SAS Journal* 5(3): 75–89.

Shea, Thomas M. et al. 2014. "Designs and Techniques That Improve the Pullout Strength of Pedicle Screws in Osteoporotic Vertebrae: Current Status." *BioMed Research International* 2014.

Shepherd, D E T, and A J Johnstone. 2005. "A New Design Concept for Wrist Arthroplasty." *Proceedings of the Institution of Mechanical Engineers, Part H: Journal of Engineering in Medicine* 219(1): 43–52.

Silbermann, J. et al. 2011. "Computer Tomography Assessment of Pedicle Screw Placement in Lumbar and Sacral Spine: Comparison between Free-Hand and O-Arm Based Navigation Techniques." *European Spine Journal* 20(6): 875–81.

Skeppholm, Martin et al. 2015. "The Discover Artificial Disc Replacement versus Fusion in Cervical Radiculopathy--a Randomized Controlled Outcome Trial with 2-Year Follow-Up." *The spine journal : official journal of the North American Spine Society* 15(6): 1284–94.

Smith, Lachlan J., and Nicola L. Fazzalari. 2009. "The Elastic Fibre Network of the Human Lumbar Anulus Fibrosus: Architecture, Mechanical Function and Potential Role in the Progression of Intervertebral Disc Degeneration." *European Spine Journal* 18(4): 439–48.

Souchkov, Valeri. 1999. "Accelerate Innovation with TRIZ." In *White Papers*, ICG training and consulting. http://www.xtriz.com/publications/AccelerateInnovationWithTRIZ.pdf.

Stanford, Ralph Edward, Andreas Herman Loefler, Philip Mark Stanford, and William R Walsh. 2004. "Multiaxial Pedicle Screw Designs: Static and Dynamic Mechanical Testing." *Spine* 29(4): 367–75.

Stokes, I. A F, and James C. Iatridis. 2004. "Mechanical Conditions That Accelerate Intervertebral Disc Degeneration: Overload versus Immobilization." *Spine* 29(23): 2724–32.

Suk S.I. and Kim W.J. 2016. "Biomechanics of Posterior Instrumentation for Spinal Arthrodesis." In *Biomechanics and Biomaterials in Orthopedics*, ed. Dominique G. Poitout. Springer-Verlag London, 437–66.

Taksali, Sudeep, Jonathan N Grauer, and Alexander R Vaccaro. 2004. "Material Considerations for Intervertebral Disc Replacement Implants." *The spine journal : official journal of the North American Spine Society* 4(6): 231S–238S.

Tang, S. M. et al. 2004. "Tension-Tension Fatigue Behavior of Hydroxyapatite Reinforced Polyetheretherketone Composites." *International Journal of Fatigue* 26(1): 49–57.

Thaler, Martin et al. 2013. "Footprint Mismatch in Total Cervical Disc Arthroplasty." *European spine journal* 22(4): 759–65.

Todd, Andrew G. 2011. "Cervical Spine: Degenerative Conditions." *Current reviews in musculoskeletal medicine* 4(4): 168–74.

Traynelis, Vincent C. 2006. "Cervical Arthroplasty." In *Clinical Neurosurgery*, , 203–7.

Vaccaro, Alexander et al. 2013. "Clinical Outcomes with Selectively Constrained SECURE-C Cervical Disc Arthroplasty: Two-Year Results from a Prospective, Randomized, Controlled, Multicenter Investigational Device Exemption Study." *Spine* 38(26): 2227–39.

Vaccaro, Alexander R. et al. 1998. "Early Failure of Long Segment Anterior Cervical Plate Fixation." *Journal of Spinal Disorders* 11(5): 410–15.

Vanichkachorn, Jed S., Alexander R. Vaccaro, Murray J. Cohen, and Jerome M. Cotler. 1997. "Potential Large Vessel Injury During Thoracolumbar Pedicle Screw Removal." *Spine* 22(1): 110–13.

Verlaan, Jorrit Jan, Wouter J A Dhert, and F. Cumhur Oner. 2013. "Intervertebral Disc Viability after Burst Fractures of the Thoracic and Lumbar Spine Treated with Pedicle Screw Fixation and Direct End-Plate Restoration." *Spine Journal* 13(3): 217–21.

Veruva, Sai Y et al. 2014. "Which Design and Biomaterial Factors Affect Clinical Wear Performance of Total Disc Replacements? A Systematic Review." *Clinical orthopaedics and related research* 472(12): 3759–69.

Vicars, R, R Hall, and J Fisher. 2011. "Wear: Total Intervertebral Disc Prostheses." In *Comprehensive Biomaterials*, Elsevier, 191–205.

Victrex plc. 2009. "Victrex ® PEEK 450G Datasheet." http://www.victrex.com/en/victrexlibrary/datasheets/datashee- ts.php.

Vital, J-M, and L Boissière. 2014. "Total Disc Replacement." *Orthopaedics & traumatology, surgery & research : OTSR* 100(1 Suppl): S1-14.

Wagner, S C, D G Kang, and M D Helgeson. 2016. "Traumatic Migration of the Bryan Cervical Disc Arthroplasty." *Global Spine J* 6(1): e15-20.

Wang, Jeffrey C., Paul W. McDonough, Kevin K. Endow, and Rick B. Delamarter. 2000. "Increased Fusion Rates with Cervical Plating for Two-Level Anterior Cervical Pas and Fusion." *Spine* 25(1): 41–45.

Wang, Xiaoyu, Carl Eric Aubin, Dennis Crandall, and Hubert Labelle. 2011. "Biomechanical Comparison of Force Levels in Spinal Instrumentation Using Monoaxial versus Multi Degree of Freedom Postloading Pedicle Screws." *Spine* 36(2): 95–104.

White, Augustus A., and Manohar M Panjabi. 1990. *Clinical Biomechanics of the Spine*. Second. Lippincott.

Williams, F.M.K., and P.N. Sambrook. 2011. "Neck and Back Pain and Intervertebral Disc Degeneration: Role of Occupational Factors." *Best Practice & Research Clinical Rheumatology* 25(1): 69–79.

Wittenberg, Ralf H., KYU-SUNG Lee, and M Shea. 1993. "Effect of Screw Diameter, Insertion Technique, and Bone Cement Augmentation of Pedicular Screw Fixation Strength." *Clinical Orthopaedics and Related Research* 296: 278–87.

Wu, Jau-Ching, Scott a. Meyer, Gurpreet Gandhoke, and Praveen V. Mummaneni. 2012. "PRESTIGE Cervical Arthroplasty: Past, Present, and Future." *Seminars in Spine Surgery* 24(1): 14–19.

Xin, H., D. E.T. Shepherd, and K. D. Dearn. 2013a. "Strength of Poly-Ether-Ether-Ketone: Effects of Sterilisation and Thermal Ageing." *Polymer Testing* 32(6): 1001–5.

Xin, H., D.E.T. Shepherd, and K.D. Dearn. 2013b. "A Tribological Assessment of a PEEK Based Self-Mating Total Cervical Disc Replacement." *Wear* 303(1–2): 473–79.

Xin, H, Det Shepherd, and Kd Dearn. 2012. "PEEK (Polyether-Ether-Ketone) Based Cervical Total Disc Arthroplasty: Contact Stress and Lubrication Analysis." *The open biomedical engineering journal* 6: 73–79.

Yaman, Onur et al. 2015. "The Comparison of Pullout Strengths of Various Pedicle Screw Designs on Synthetic Foams and Ovine Vertebrae." *Turkish Neurosurgery* 25(4): 532–38.

Yanagishita, Masaki. 1993. "Function of Proteoglycans in the Extracellular Matrix." *Pathology International* 43(6): 283–93.

Yerby, Scott A., John R. Ehteshami, and Robert F. McLain. 1997. "Loading of Pedicle Screws within the Vertebra." *Journal of Biomechanics* 30(9): 951–54.

Zhang, Qing Hang, Ee Chon Teo, Hong Wan Ng, and Vee Sin Lee. 2006. "Finite Element Analysis of Moment-Rotation Relationships for Human Cervical Spine." *Journal of Biomechanics* 39(1): 189–93.